DYNAMIC RESPONSE OF CAVITATING TURBOMACHINES

Thesis by

Sheung-Lip Ng

In Partial Fulfillment of the Requirements

For the Degree of

Doctor of Philosophy

California Institute of Technology

Pasadena, California

1976

(Submitted May 21, 1976)

ACKNOWLEDGMENTS

I would like to express my most sincere thanks to my advisor, Dr. A. J. Acosta, for giving me the opportunity to work on this project and for his constant guidance, encouragement and patience.

I also wish to thank Dr. C. Brennen for his close and indispensable assistance in the research. To Dr. R. Sabersky goes my deepest appreciation for his concern during my stay here.

For their technical consultations on the design of the facility, the help of Professor D. Welch, Dr. H. Shapiro and Mr. R. Rigley are acknowledged. I am grateful to Messrs. N. Keidel, E. Daly, V. Sodha and D. Laird for their technical assistance in the construction and assembly of the system.

Thanks go to Messrs. E. Adler, D. Braisted, C. Constantin, D. Carlson, J. DelValle, P. Mason and R. Higley for their valuable help in various phases of the experiment.

The financial support of this research came from NASA, George Marshall Space Flight Center, Huntsville, Alabama, Contract NAS 8-29313 and is gratefully acknowledged. Appreciation goes to Mr. L. Gross of NASA for his special interest in this program.

Special thanks are due Ms. B. Hawk, J. Sarkissian and M. Suggs in preparing this manuscript.

Finally, heartfelt thanks go to my parents for their extreme patience and understanding.

ABSTRACT

Stimulated by the pogo instability encountered in many liquid propellant rockets, the dynamic behavior of cavitating inducers is the subject of the present thesis. An experimental facility where the upstream and downstream flows of a cavitating inducer could be perturbed was constructed and tested. The upstream and downstream pressure and mass flow fluctuations were measured. Matrices representing the transfer functions across the inducer pump were calculated from these measurements and from the hydraulic system characteristics for two impellers in various states of cavitation. The transfer matrices when plotted against the perturbing frequency showed significant departure from steady state or quasi-steady predictions especially at higher frequencies.

TABLE OF CONTENTS

NOMENCLATURE

A_i	inlet area
C	compliance $\quad C = \dfrac{\tilde{Q}_d - \tilde{Q}_u}{-j\Omega \tilde{P}_u}$
DL	dimensionless inertance
DR	dimensionless pump resistance
gpm	gallon per minute
H	blade spacing
I	identity matrix
j	$\sqrt{-1}$
K_B	dimensionless compliance
K_{BI}	imaginary part of dimensionless compliance
L	inertance $\quad L = \dfrac{\tilde{P}_d - \tilde{P}_u}{-j\Omega \tilde{Q}_u}$
L_u, L_p, L_d	upstream section, pump and downstream section inertance
M_B	mass flow gain factor
M_{BI}	imaginary part of mass flow gain factor
NPSH	net positive suction head $\quad P_{-\infty} - P_v$
rpm	revolution per minute
R	pump resistance
ΔP	pressure rise across the pump
$P_{-\infty}$	upstream steady pressure
P_v	vapor pressure

$\tilde{P}$	fluctuating pressure
$\tilde{Q}$	fluctuating volumetric flow rate
p	dimensionless fluctuating pressure
m	dimensionless fluctuating mass flow rate
U_a	inlet axial velocity
U_{tip}	tip velocity
Y	Z + I matrix
Z	total transfer matrix between measuring stations
ZD	downstream section transfer matrix
ZP	pump transfer matrix
ZU	upstream section transfer matrix
ψ	head coefficient $\frac{\Delta P}{\rho U_{tip}^2}$
ρ	density of fluid
σ	cavitation number $\frac{P_{-\infty} - P_v}{\frac{1}{2}\rho U_{tip}^2}$
φ	flow coefficient $\frac{U_a}{U_{tip}}$
ω	dimensionless frequency
Ω	fluctuating frequency

Subscripts

u	upstream
d	downstream

LIST OF FIGURES

I. INTRODUCTION

1.1 Background

Formerly, the designers of many hydraulic systems were concerned solely with the steady state performance of the system since this was the only information available. In recent times, the added complexity has resulted in stability problems which calls for the study of the unsteady performance. This added complexity may be due to an improved and more sophisticated component which will give a more complicated performance as in the case of a turbomachine or may simply be due to additional network system. The instability may be a transient problem like the case of boiler feed system (see Liao and Leung 1972, and Liao 1974) or may be like the periodic oscillation encountered in hydropower installations (see Jaeger 1963 and Streeter and Wylie 1974). The oscillatory type of problem is the one to be studied here.

Many hydraulic systems suffer a vibrational problem which may be severe if a natural resonance frequency is excited. The resonance frequency may come from a structure vibration mode or may be solely hydraulic in nature or a combination of both. This may happen when a small excitation disturbs the system to operate away from its steady state condition. The response of the system may be transient and decay gradually back to the steady state or the response may be a cyclic oscillation growing in amplitude until it causes the shut down of the system. Such vibrational problems are attracting new attention as increasing complexity is built into hydraulic systems; the added

complexity creates an increasing number of excitable resonance modes. Of all the hydraulic components involved in this vibration, the most complex and least understood is the role played by the turbomachine. Whereas other components may be passive in nature, the turbomachine is active in the sense that it is designed to impart energy to the fluid as in a pump or extract energy from it as in a turbine. Because of this, the turbomachine may play a dominant role in the dynamics of the whole system.

The steady performance which relates flow rate and pressure rise of a pump for a given speed is well understood. But if a small fluctuation in flow rate is superimposed on the steady state flow, there is little available information about the effect of this on the fluctuating pressure rise across the pump. This problem is further complicated by the fact that some turbomachines operate with a two phase fluid. Besides the analysis of the two individual fluid flows, the interaction between them has to be considered. This is exemplified by the growing concern about the influence on the structural vibrational instability of the cavitating sodium pump used in nuclear power stations (see Gibbs and Oliver 1973). Another example occurs in the liquid propellant pump of a rocket engine where high pump speed causes the propellant to cavitate; this example motivates the present work and will be discussed in detail in the following section.

1.2 Pogo Instability

Occasionally, during the launching of some liquid propellant rockets and space vehicles, a large amplitude longitudinal vibration

may gradually occur (see NASA SP-8055). This is called the "POGO" instability. Although in most of the cases this vibration may decay after about 10 - 40 seconds, severe damage to the structure and instruments can occur besides discomfort and even bodily injury to astronauts. This may also happen in a multistage rocket such as in the second stage of Saturn engine where the occurrence of pogo has caused the premature shut down of an engine. In some extreme cases of pogo, the vibration can attain an acceleration level of 17 g's with frequency of 5 - 60 Hertz (see NASA SP-8055). Recent data show that pogo is a very frequently encountered phenomenon and also is a very severe problem (see Fig. 1.1). Analysis indicates that each of these frequencies coincides with a longitudinal vibrational mode of the rocket structure.

The cause of pogo is a closed loop feedback coupling of the propulsion system and the structure. In short, a small longitudinal disturbance in the propellant tank creates an unsteady flow rate in the feed line leading to the turbopump. The turbopump experiences an upstream fluctuation of pressure and flow rate and in turn creates its own characteristic downstream pressure and flow rate fluctuations. The unsteady supply of propellants to the combustion chamber leads to an unsteady propellant burning rate which in turn produces an unsteady thrust. The loop is closed when this fluctuating thrust causes amplification of the longitudinal vibration of the structure.

Presently, there is no sure way to completely eliminate the pogo problem besides suppressing it by minor modifications to the propulsion feed system. These methods try to alter the resonance

frequencies of the propellant feed system. For instance, if the resonance frequencies of the propellant feed system and structure are known in advance, some means can be found to change the frequency of the feed system such that they are decoupled. This includes, for example, the injection of gas into the feed line or the incorporation of a tuned gas accumulator upstream of the pump (see Norquist, Marcus, Ruscio 1969). Since the gas contained in a gas accumulator can easily be adjusted to any designed volume and pressure this device is the main way of pogo suppression employed in most existing liquid propellant rockets.

There is a possibility that the Space Shuttle may be even more prone to pogo instability than previous rockets. The propellant pump system in this case employs two physically separated pumps for each propellant (see Rothe 1974). Besides the normal propulsion system and structural system interaction, there is the additional possibility of a sympathetic oscillation between the two pumps. Furthermore, the Space Shuttle has a multibody, non-axisymmetric structure with many vibrational modes; hence the pogo analysis is more complex. Along with the investigation on the use of the conventional passive tuned gas accumulator (see Lock and Rubin 1974), the feasibility of using a more elaborate active suppression system (see Farrel and Fenwick 1973) has also been explored; this method attempts to control the pressure fluctuation upstream of the pump using a very complicated electronic hydraulic servo feedback system.

All the approaches just mentioned are corrective in nature and consist of modifications to the existing system in the absence of sufficient dynamic information. Detailed analysis of the

pogo instability encounters difficulty because of the lack of enough information about the turbopump. The study of turbopumps under fluctuating conditions is the theme of the present study.

1.3 Cavitation in an Inducer Pump

To save weight and volume carried by liquid propellant rockets and to yield similar savings of material in hydraulic systems in general, the design of a turbopump within a system is optimized to operate at the maximum attainable speed (see NASA-8052). This introduces a high velocity at the outer tip of the pump impeller which in turn creates a low pressure region there as indicated by the Bernoulli equation. As liquids cannot withstand too high tension, the liquid undergoes a phase change into vapor phase (see Knapp, Daily and Hammitt 1970). Furthermore, any other gas previously dissolved in the liquid may also come out of solution. This phenomenon is termed cavitation and it can lead to excessive noise, erosion damage to the material surface and degradation of the pump performance. Increasing the upstream supply pressure may suppress this cavitation but this requires the additional strengthening of the container tank and thus decreases the payload of the rocket. The degradation of pump performance due to cavitation can be minimized by careful design of a first stage axial flow inducer pump (see Stripling and Acosta 1962, Acosta 1958, King 1970 and NASA SP-8052). This first stage inducer pump will be designed to operate under cavitating conditions but give enough pressure rise to eliminate cavitation in the subsequent stages which are often of a mixed flow or centrifugal type.

The development of cavitation on the axial flow inducer pump is described by a parameter, the cavitation number. The cavitation number is the ratio of the static pressure head above vapor pressure of the fluid to the dynamic head (for definition see nomenclature). As the cavitation number is gradually reduced either by lowering the upstream pressure or by raising the rotative speed, cavitation starts at the tip clearance space, enveloping the outer blade passages of the inducer; this is referred to as tip clearance cavitation. If the flow coefficient (for definition, see nomenclature) is low enough, the downstream pressure will force the tip clearance cavitation to flow upstream forming "back flow" cavitation. As the cavitation number is further reduced, small pockets of cavitation bubbles first build up on the blade surface starting at the leading edge, spreading towards the trailing edge until they eventually cover the whole blade surface. This changes the angle of attack between the blade and flow direction preventing the blade from putting mechanical work into the fluid. At this point, the performance of the pump begins to deteriorate. Finally, if the cavitation number is further reduced, the cavitation grows in size and partially blocks the flow passage which leads to complete performance breakdown.

The cavitation performance of a typical pump is illustrated in Fig. 1.2 where the pump head rise is plotted against net positive suction head for a constant flow rate and constant rotational speed. The net positive suction head (NPSH) is the difference between absolute pressure upstream of the inducer and the vapor pressure of the fluid. As the upstream pressure is reduced between A and B on the graph,

the head rise is unchanged. Actually the head rise increases a little due to the reduced viscous drag when the cavitation covers the blade surfaces. As the NPSH is further reduced between B and C, the performance of the inducer breaks down and the head rise decreases drastically.

Turbopump inducers usually operate at a stage of cavitation just before breakdown with large amounts of cavitation. When flow rate and pressure fluctuations are imposed upstream of the inducer, the cavities collapse and grow, thus inducing downstream mass flow and pressure fluctuations. During a fluctuating cycle, the extremes of the operating point may move into the region of performance breakdown. Such complex phenomena can alone lead to the instability of a hydraulic system.

1.4 Lumped Parameter Model of a Turbomachine

It is essential at this moment to discuss how these complex phenomena can be represented. The basic interest is a way to represent the fluctuating or oscillating output when a hydraulic system is subjected to a given oscillating input. In the present context we are concerned with fluctuating quantities that are small departures from a mean steady state. Conventionally the dynamics of hydraulic systems have been treated in terms of lumped parameter models.

The lumped parameter model assumes that the distributed physical effects between two measuring stations can be represented by a lumped constant. This assumption is valid when the hydraulic system is relatively simple and when the physical lengths of the system are shorter than the acoustic wavelength at the frequencies of

interest. For example, the inertial effect of fluid between the two ends of a long pipe can be represented by an inertial constant known in hydraulics as the inertance obtained by dividing the force (which is the pressure drop multiplied by the area) by the acceleration (which is simply the time derivative of the velocity). Similarly a compliance value can be assigned to a pipe with a flexible wall by dividing the change of fluctuating volumetric flow rate by the fluctuating pressure. To clarify this, it is useful to use an electrical analogy. If we replace the pressure by a voltage and the mass flow rate by an electrical current, then the electrical analogies of inertance and compliance terms are an inductance term and a capacitance which is connected to ground. Further, if the pressure and volumetric flow rates are sinusoidal oscillations, the equations relating these to the inertance and compliance are

$$\tilde{P}_d - \tilde{P}_u = -j\Omega L\tilde{Q}_u \tag{1.1}$$

$$\tilde{Q}_d - \tilde{Q}_u = -j\Omega C\tilde{P}_u \tag{1.2}$$

where $\tilde{P}_d$, $\tilde{P}_u$ and $\tilde{Q}_d$, $\tilde{Q}_u$ are the downstream and upstream fluctuating pressure and downstream and upstream fluctuating volumetric flow rate, L and C are the inertance and compliance and Ω is the frequency of oscillation. These two examples are quoted because they will be used to analyze some of the results in a later chapter.

Previous lumped parameter models of the dynamic of pumps were based on the steady state performance. The upstream and downstream quantities were connected by terms like "compliance", "dynamic gain factor" and "pump resistance" (see Rubin 1966, Vaage

Fidler and Zehnle 1972). The pump performance curve which plots the steady pressure rise across a pump against mass flow rate for a constant rotational speed is shown in Fig. 1.3. The "pump resistance" during flow oscillation is simply assumed to be the negative local gradient of the steady pump performance curve, i.e., the slope of the total pressure rise with mass flow rate. The cavitating performance of a pump was discussed and shown in Fig. 1.2. The "dynamic pump gain factor" is defined to be the fluctuating change of total pressure rise across the pump with the fluctuating change of upstream pressure. The dynamic model assumes that this can be taken to be the slope of the cavitation performance curve. The "compliance" in these analyses measures the change of cavitation volume with the change of upstream pressure and is a most important parameter for dynamic analysis. A basic simplification was made that the compliance could be represented by a large "bubble" located at the pump inlet in quasi-steady equilibrium and this simulation gives rise to a "bubble spring constant". Values of the bubble spring constant and thus the compliance were based on static firing tests of the engine as will be mentioned in Section 1.5.

Analytical calculations of compliance based on quasi-steady blade cavitation flow were made by Brennen and Acosta (1973). These calculations assume that the instantaneous cavitation size is determined by the instantaneous upstream pressure and these are related by their steady state calculation. The result of this calculation yielded a value much lower than experiment (see next section). Calculation of compliance contribution from other types of cavitation also

exist in the literature. These include the effect of backflow cavitation by Ghahremani (1970) and bubble cavitation by Brennen (1973).

The characterization of the cavitating inducer pump can be broadened by the introduction of one more quantity, "the mass flow gain factor" which is defined as the difference in the fluctuating mass flow rates for a change in the upstream flow rate. A quasi-steady calculation to find the mass flow gain factor from blade cavitation flow was done by Brennen and Acosta (1975). The change of upstream mass flow rates gives rise to a change of angle of attack on the blade thus changing the cavitation volume and this change of cavitation volume was calculated from steady state performance. This quantity which was assumed zero in all previous analysis was found to give a contribution to the dynamic characteristics comparable with that of the compliance term and bridged the discrepancy between compliance calculation and measurement (see Fig. 1.4).

However, all of these analyses are quasi-steady in nature thus are only valid at low frequency. At higher frequencies all these quantities may have a more complicated behavior and may be complex. A more general but incomplete calculation on the dynamic response of a cavitating cascade has been presented by Kim and Acosta (1974). All these calculations need to be verified by a carefully controlled experiment where all the important variables could be directly measured.

In order to understand, predict, and hopefully, to eliminate the occurrence of the pogo instability, lumped parameter models of space vehicle dynamics have been constructed (see Rubin 1966, Rubin,

Wagner and Payne 1973). Such analyses are based on transfer functions for each component involved in pogo. These include: the structure, fuel tank, feed lines, pump and combustion chamber. The transfer functions relate the input and output of each component when the input is a sinusoidal oscillation of a certain frequency. The input and output can be acceleration in the case of structure or the pressure in the case of a feed line, etc. These transfer functions are connected into a mathematical feedback loop and the stability criterion of the loop is investigated. The transfer functions for the pumps consisted of terms like the pump resistance, compliance and pump gain factor. However, the results of these analysis were not completely satisfactory because of insufficient information about the values of the pump resistance etc. under dynamic cavitating conditions.

Similar calculations to investigate the system oscillations associated with cavitating inducers in a hydraulic loop were performed by Sack and Nottage (1965). In their study, the instantaneous size and shape of the cavities were calculated from steady state analyses. Fanelli (1972) studied a similar problem concerning the dynamic behavior of large hydraulic power turbines with no cavitation. In his calculation, he used the oscillating single airfoil result with a modification factor which was used to correlate the single airfoil and cascade steady state performance. However, these calculations were incomplete and lacked an exact description of the dynamic behavior of the fluid flow.

1.5 Experimental Work

Three main categories of experiments on the dynamic behavior

of turbomachines exist in the literature. These experiments included cavitating and fully wetted conditions. The first type of experiment (see Natanzon, et al 1974 and Kamijyo and Suzuki 1973) consists of operating a cavitating inducer pump in a closed hydraulic circuit. Cavitation number, flow conditions and physical dimensions of the circuit were varied until a self-sustaining hydraulic oscillation occurred in the system. Although there were fluctuating pressure measurements, no fluctuating flow measurements were taken so that only a limited quantitative analysis of the experiment could be undertaken. These experiments confirmed that there was a strong interaction between the cavitating inducer pump and the rest of the hydraulic system. In the pogo problem the interaction is provided by the combustion chamber, structure, etc. The experiments also showed that the pump could be the source of energy which maintained this kind of oscillation.

The second category of experiments attempted to measure the compliance of a cavitating inducer pump by perturbed inlet engine tests. These tests measured a perturbation pressure transfer function of the feed system by measuring the perturbed inlet and outlet pressure of the pump caused by pulsing the suction flow rate. The pulsation was provided by a hydraulically activated piston operating at various frequencies. This transfer function when plotted against frequency gave the first fundamental frequency of the inlet pump system. The dynamic characteristics of the feed system were modeled like a spring and mass system. The mass value was given by the known inertia of the feed line. The spring constant was derived from the observed fundamental

frequency. This calculated spring constant or compliance consisted of contributions from cavitation and expansion of the feed line and the value was taken to be the compliance of the pump, (see Rocketdyne 1969, Vaage, Fidler and Zehnle 1972). The results of such tests have been used in the pogo analysis of rocket engines.

Past efforts to measure the compliance with this type of method showed a wide data scatter for different engines (see Fig. 1.5). This is perhaps due to the oversimplification of the whole process. The representation of the whole complex cavitation effect by only a single lumped parameter, the compliance, was not justified. Furthermore, the tests could not differentiate between the individual contributions from bubble compliance, the compliance of the structure or the cavitation effect due solely to the pump; also no account was taken of the influence of the fluid flow conditions or the different forms of cavitation that could occur in a pump. The perturbed inflow engine tests also revealed one interesting fact; namely that the pump gain did not retain its steady state value under dynamic conditions (see Rubin 1966 and Wagner 1971).

The third kind of experiment actually tried to measure directly the fluctuating quantities. Anderson et al (1971) (see also Stevans and Blade 1971) attempted to measure the response of a radial bladed pump under sinusoidal upstream disturbance with no cavitation. In their experiments, the fluctuating pressures and mass flow rates were measured but only one quantity, the pump impedance, which was defined as the difference in oscillating pressure rise over the oscillating exit flow rate, was analyzed. The results showed a wide scatter. This is probably

due to the lack of reliable oscillatory mass flow measurements and because only one quantity was used to describe the pump dynamic performance, namely the pump impedance. The pump impedance so derived also contains some uncertainty since this method of calculation depends on the impedance downstream of the pump.

Two mass flow systems were employed in Anderson's experiment. One involved measuring the oscillatory pressure drop across a multiholed orifice in the discharge flow. Since the dynamic measurement of an orifice is not a simple extension of its steady calibration the dynamic response of an orifice was calculated theoretically and this was used for the calibration. No actual dynamic calibration was attempted. The principle of the upstream mass flow meter was to measure the acoustic wave velocity in the moving fluid. The measurement was done in a long pipe upstream of the pump. Since the acoustic velocity depends on the air bubble content, any unknown amount of air in the flow affects the measurement. This effect is more severe for cavitating tests where there may be substantial quantities of gas entrained in the upstream section. The main problem encountered in the measurement of dynamic flow systems hinges on the development of a reliable dynamic mass flow measuring system.

1.6 Pump Transfer Matrices

It was reasoned that the analytical representation of a cavitating inducer pump executing small periodic excursions about its mean condition could be represented by groups like dynamic pump gain factor, compliance, pump resistance and mass flow gain factor. This

naturally led to an even more complete and general representation, the ZP pump transfer matrix (see Brennen and Acosta, 1975) defined as

$$\begin{bmatrix} p_d - p_u \\ m_d - m_u \end{bmatrix} = \begin{bmatrix} ZP_{11} & ZP_{12} \\ ZP_{21} & ZP_{22} \end{bmatrix} \begin{bmatrix} p_u \\ m_u \end{bmatrix} \tag{1.3}$$

where p_u and p_d are the dimensionless upstream and downstream fluctuating pressures and m_u and m_d are the dimensionless upstream and downstream mass flow rates. These quantities are non-dimensionalized by the following equations

$$p_{\substack{u \\ d}} = \frac{\tilde{P}_{\substack{u \\ d}}}{\frac{1}{2}\rho U_{tip}^2} \tag{1.4}$$

$$m_{\substack{u \\ d}} = \frac{\tilde{Q}_{\substack{u \\ d}}}{A_i U_{tip}} \tag{1.5}$$

where $\tilde{P}_{\substack{u \\ d}}$ and $\tilde{Q}_{\substack{u \\ d}}$ are the upstream and downstream pressure and volumetric fluctuation, ρ is the density of the fluid, U_{tip} is the tip speed of the pump and A_i is the inlet flow area. Therefore, if small cyclic perturbations of a certain frequency are imposed upstream of the inducer, the downstream oscillatory state can be calculated from a ZP-matrix if this was known. Since there may be phase differences between all the four pressure and mass flow quantities, the elements of the ZP-matrix are complex in general. This representation is only valid for small fluctuating pressures and mass flows and assumes a linear relation between these quantities. An even more complete representation should include the effect of pump rotational speed also (see

Rubin, Wagner and Payne 1973), but this effect is small in many applications as demonstrated by Brennen and Acosta (1975) based on quasi-steady blade cavitation calculations.

It is necessary at this point to interpret the ZP-matrix in terms of the lumped parameter analysis as mentioned in Section 1.4. Since ZP_{11} is the ratio of fluctuating pressure rise to fluctuating upstream pressure, this term will be called the pump gain term. The real part is simply the dynamic pump gain factor, as defined in Section 1.4; but there is no simple parallel for the imaginary part. This will be referred to as the imaginary pump gain factor. The ZP_{12} is a ratio of the fluctuating head rise to the fluctuating upstream flow rate. This term will be referred to as the negative of a pump impedance. The negative sign is introduced here such that it will be consistent with the pump resistance defined earlier. The real part of ZP_{12} is therefore the negative of a dimensionless pump resistance DR as follows

$$\text{Re } ZP_{12} = - DR \quad . \tag{1.6}$$

The relationship between this and the dimensional pump resistance, R is given by

$$DR = R \frac{2A_i}{\rho U_{tip}} \quad . \tag{1.7}$$

The imaginary part of ZP_{12} is analogous to an inertial term. A dimensionless inertance DL is defined in terms of the imaginary ZP_{12} by the following equation

$$\text{Im } ZP_{12} = -\omega DL \tag{1.8}$$

where ω is a dimensionless frequency defined as

$$\omega = \frac{\Omega H}{U_{tip}} \quad . \tag{1.9}$$

In this equation H is the tip spacing of the inducer pump. The relationship between the dimensionless inertance DL and dimensional inertance L is given by

$$DL = L \frac{2A_i}{\rho U_{tip}} \quad . \tag{1.10}$$

Similarly a dimensionless compliance K_B can be defined in terms of ZP_{21} by

$$\text{Im } ZP_{21} = -\omega K_B \tag{1.11}$$

where K_B is related to dimensional compliance C through

$$K_B = C \times \frac{U_{tip}^2 \rho}{2HA_i} \quad . \tag{1.12}$$

No simple analogy can be drawn for the real part of ZP_{21}. Therefore, this will be referred to simply as the real compliance term. Finally, the imaginary part of ZP_{22} is related to the mass flow gain factor M_B through

$$\text{Im } ZP_{22} = -\omega M_B \tag{1.13}$$

as introduced by Brennen and Acosta (1975). Again there is no simple physical interpretation for the real part of ZP_{22} and this will be referred to as the real mass flow gain factor term.

All the dimensionless groups defined in the last paragraph through the ZP-matrix are not direct analogies to the lumped

parameter groups discussed in Section 1.4. For example, the pump resistance term in ZP_{12} from Eq. (1.3) will be an exact analogy to the pump resistance as defined in Section 1.4 only if the pump gain factor term that appears in ZP_{11} is identically zero and vice versa. A similar argument applies to the compliance and mass flow gain factor terms.

Experimental evaluation of the components of the ZP-matrix requires that all the fluctuating pressures and mass flows be measured. After all the fluctuating pressures and mass flows are measured, the ZP-matrix can be obtained by inverting Eq. (1.1). However, since the matrix is of order two, two linearly independent sets of data are needed. In other words, to solve for four complex unknown numbers, we need four complex linearly independent equations. Each data set gives two equations and thus two data sets are needed. In the present experimental study, more than two linearly independent data sets were obtained and a special least square fit procedure was used to extract the ZP-matrix.

In the present experiment, an inducer pump was installed in a closed hydraulic loop and fluctuations were imposed upstream of the pump. Linearly independent data sets could have been obtained by changing the physical parameters such as the hydraulic length or resistance elements of the system. An alternative way was to provide pulsation downstream of the pump by a second fluctuator. By varying the amplitudes of fluctuation and the relative phase between the two fluctuators, more than two linearly independent data sets could be obtained and this was the scheme used in the present study.

1.7 Goals of the Research

The object of the present research was to measure the dynamic response of inducer pumps under different cavitating conditions, the result being represented by ZP-matrices as described in Section 1.6. The elements of the ZP-matrix are expressed as functions of frequency.

A test impeller was required along with means to vary the system pressure for cavitation conditions and some way to change the steady flow condition must also be provided. Two specially designed valves were needed to provide the disturbances to the mean flow at a given frequency. Oscillatory pressure and mass flow rate measurements were made upstream and downstream of the pump and from these transfer matrices were calculated. The difficulty of measuring the fluctuating mass flow rate encountered in previous experiments was overcome with the advent of laser doppler velocimeter. Since the measuring stations were not immediately upstream and downstream of the pump, the matrix thus calculated included some dynamic effects due to the intervening hydraulic components. These system effects were subtracted out to give the required ZP-matrix.

In the following chapters, we will discuss how such a facility and its associated instrumentation were designed, constructed, tested and used. This will be followed by a description of how the data were processed and system effects removed. Finally, the experimental measurements will be presented and discussed in the light of what is known about unsteady flows through pumps.

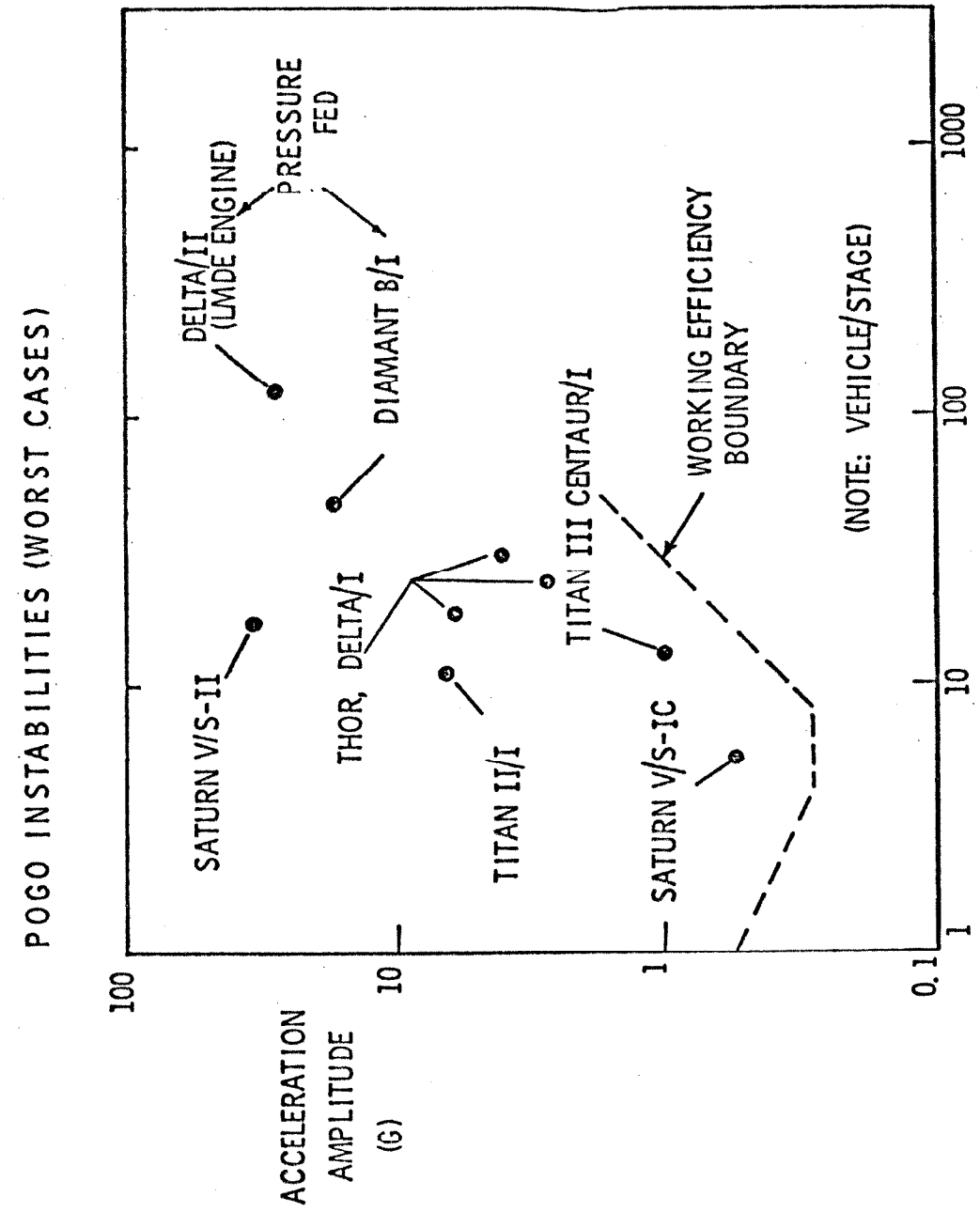

Fig. 1.1 Occurrence of pogo instability.

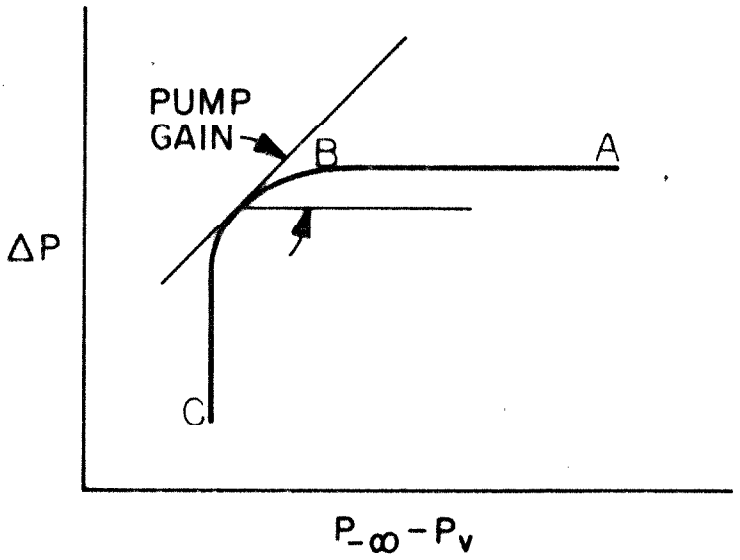

Fig. 1.2 Typical cavitation performance of pumps.

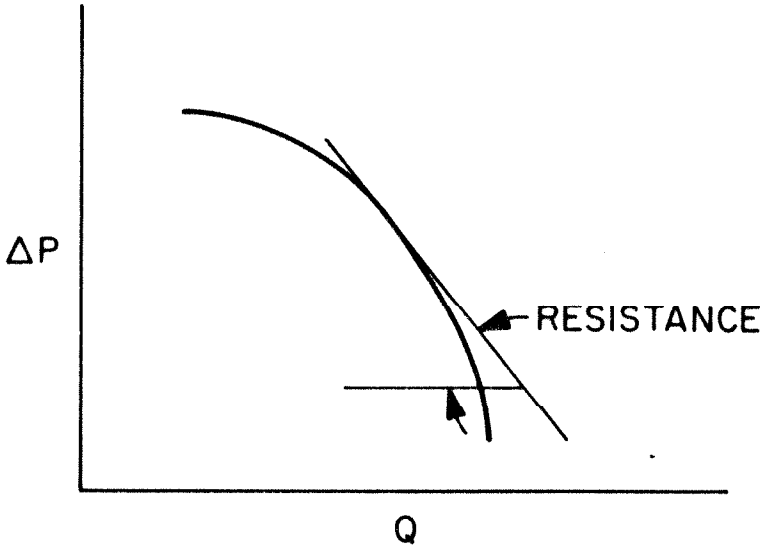

Fig. 1.3 Typical fully-wetted pump performance curve.

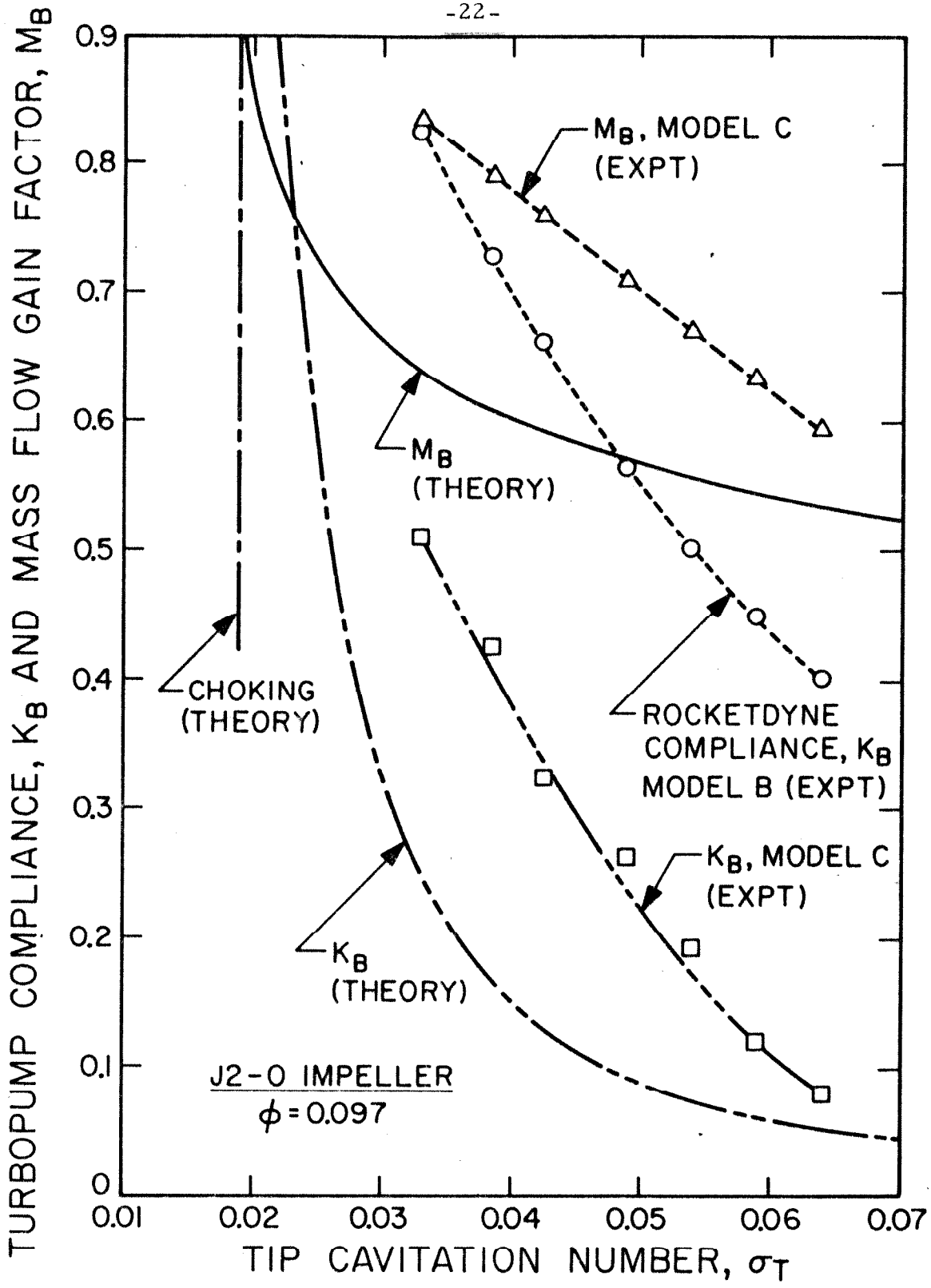

Fig. 1.4 Theoretical and experimental comparisons of compliance and mass flow gain factor.

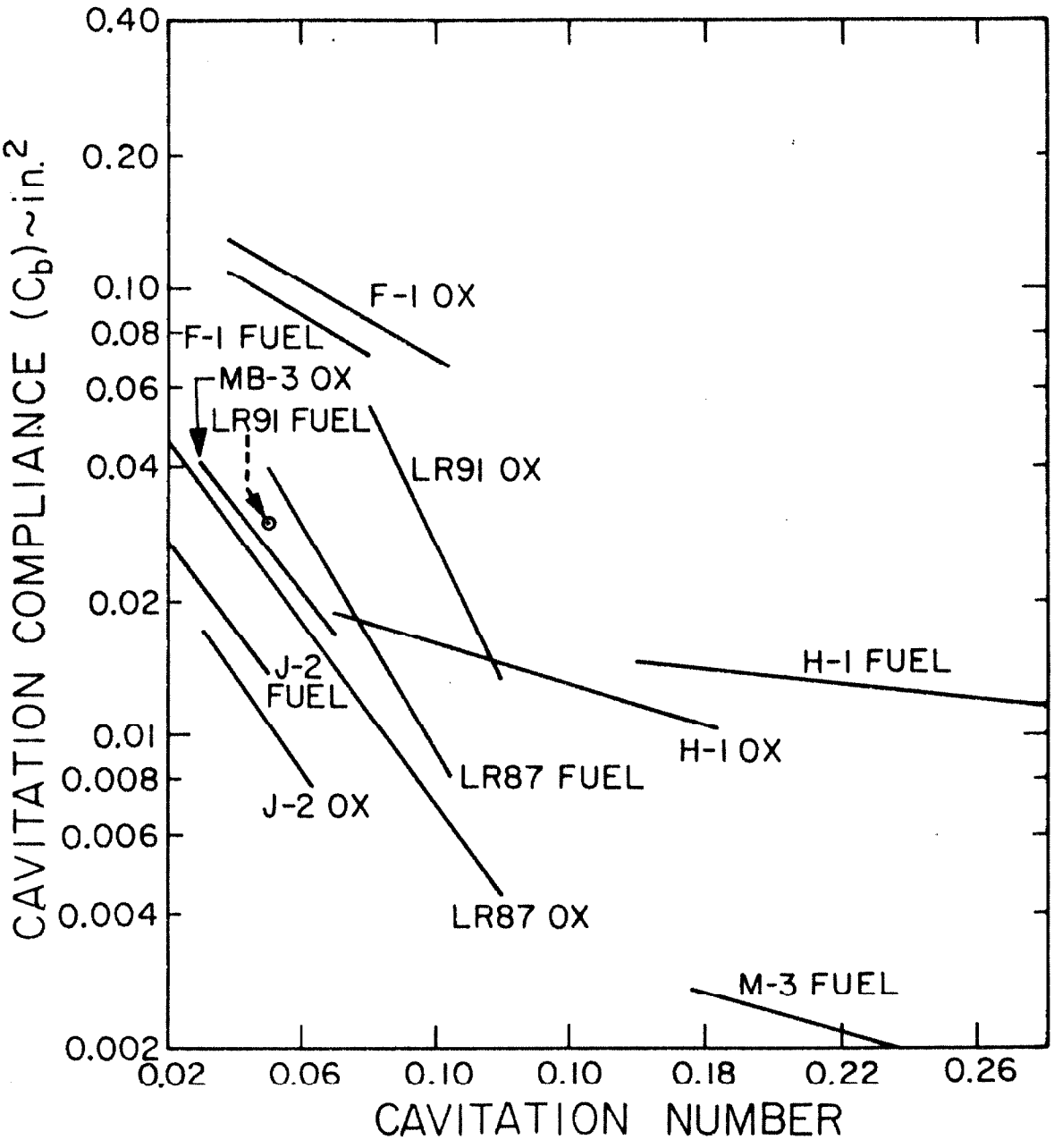

Fig. 1.5 Cavitation compliance as measured from perturbed inlet engine test.

II. SYSTEM DESIGN

2.1 Design Requirements and Problems

As mentioned in the introduction, the present study was directed toward representing the dynamics of cavitating inducers by a ZP-matrix. In order to measure this ZP-matrix for a pump, the minimum number of fluctuating quantities to be measured are upstream and downstream pressure and upstream and downstream mass flow rate. These are needed together with the steady state information to calculate the required matrix. The two most important design considerations were the fluctuating mass flow measurements and some kind of fluctuators to impose the fluctuation.

An important consideration was the amplitude of the fluctuating mass flow rate. This magnitude is dictated by the linearity assumption requirements that the mass flow rate fluctuation will be allowed to reach a maximum of five or six percent of the mean flow rate. Of course, a lower value is more desirable in fulfilling the linearity restrictions; but this would decrease the signal to noise ratio. The discharge of the pump is a highly rotational and a very turbulent flow. It was expected that the turbulence level could be reduced to a minimum of approximately 1.0 to 0.5 percent by passing through turbulence reducing devices. This would give a maximum signal to noise level of about 5 to 10. Of the signal analyzers available in the market at that time, the most suitable one being considered for purchase required a minimum signal to noise ratio of one (see Section 2.5.8). Thus a signal to noise ratio of about 5 is adequate for this purpose.

Three mass flow measuring systems were considered keeping in mind that the main task was to measure a fluctuating mass flow rate. These were, a small pilot tube connected to a strain gauge pressure transducer, a hot film anemometer and a laser doppler velocimeter (see Appendix A). After considerable evaluation, the laser doppler velocimeter was chosen. The reason for not using the pilot tube was a result of the large phase shift and pressure loss due to the compliance of the connecting line. The hot film anemometer was abandoned due to its need for frequent calibrations and the need for a fluctuating calibration, in any case, to retain phase reference. The laser doppler velocimeter was regarded as the most suitable choice at the time because it was non-intrusive to the flow and measured the absolute velocity. However, the laser velocimeter was still not completely satisfactory because it only measured the velocity at one point of the flow which does not truly represent the mass flow rate. The true mass flow rate, as calculated by the laser velocimeter reading, can be given by locating the measuring station to be at the end of a converging nozzle to give a flat velocity profile. This also reduces the turbulence level that is needed for a better data processing. The converging nozzle will be augmented by a smoothing chamber designed to give a low turbulence level. This proposed scheme was tested in the preliminary setup described in Section 2.2.2.

We needed some means to generate the five to six percent mass flow fluctuation at a given frequency as mentioned above. The ideal velocity profile against time is a sine wave, but a periodic wave form with a high fundamental frequency content was acceptable. As explained previously, the signals were analyzed by a signal analyzer which

required a minimum signal to noise ratio of one, any other harmonics being treated as noise. In the design of the fluctuator, special care was taken that no high velocities region existed in the fluctuator. High velocity would create low pressure areas that would drive the dissolved air out of the solution and influence the measurement.

Several designs were considered. These included, for example, the periodic squeezing of a piece of rubber with longitudinal holes through it by a servo-hydraulic system or the linear displacement between two slotted throttling plates similar to the design by Anderson etc. (1971). These were abandoned because they were too costly and difficult to fabricate. Finally, a variation of Anderson's design using two concentric slotted cylinders, one rotating inside a stationary one, to provide the variable throttling was decided upon.

The first proposal was to use two sintered metal cylinders one inside the other. The cylinders were to have longitudinal bands in which the pores were blocked either by machining on the surface or filling with epoxy resin. The rotation of one cylinder with respect to the other would provide the necessary modulation. The selection of sintered metal was made because the throttling effect would be wholly viscous and high velocity regions would be minimized. This approach was abandoned because great difficulties were encountered during attempts to manufacture the bands on the sintered metal.

A final design based on the foregoing principle was used. This design consisted of two slotted concentric cylinders with the inside one made of bronze rotating within the outside stationary one, which was

made of stainless steel. The different metals were used to avoid binding. A piece of sintered bronze cylinder was situated coaxially and next to the slotted cylinders providing a bypass to the flow when the slots were momentarily closed completely. The varying amplitude of fluctuation was provided by a cylindrical sleeve which slid axially to cover either the slotted cylinders and/or the sintered metal cylinder. The amplitude of fluctuations was proportional to the relative amount of area covered by the sleeve. This sintered bronze throttling bypass was intended to provide a viscous resistance and to minimize the air being driven out of the solution. This arrangement was called the "siren valve". The design does have some drawbacks because it produces a square-wave kind of fluctuation and the abrupt cutoff and opening of the flow path causes high velocity regions. An arrangement as described above was made and tested in the preliminary set-up described in the next section.

2.2 Preliminary Experimental Setup

To develop the laser doppler velocimeter and the "siren valve" fluctuator, a small pump test loop was constructed. This system consisted of a 7 hp centrifugal pump, the fluctuator, a silent valve for the steady state throttling (for details of this valve, see Section 2.4.6), transparent windows for the laser to pass through and a one hundred gallon storage tank. These were connected by a 4 in. diameter plastic pipe. The fluctuator shaft was driven by a one hp variable speed motor. Figure 2.1 shows a schematic of the setup.

Keeping in mind the requirements put forth in Section 2.1, the

components of this setup were tested and re-designed to give the optimum performance. This included the detailed design of the siren valve, the turbulence reducing components inside the smoothing chamber and the shape and fabrication of the laser doppler velocimeter windows. After many modifications, a satisfying design was arrived at and adopted in the final pump loop design with very slight changes. Thus only a brief description of the important lessons learned will be given below.

2.2.1 Fluctuator Valve.

Figure 2.2 shows a functional schematic of this valve. The siren valve arrangement which has a diameter of 6 in., was housed in a 12 inch diameter and one foot long chamber. The flow was brought in through a side entrance. After it passed through either the rotating slotted path or the sintered bypass path, the flow exited through the center of the fluctuator chamber into the smoothing chamber. Two lessons were learned from this setup.

(i). The original slotted cylinders were made too thin causing these parts to bend slightly and this eventually led to jamming of the valve. The final design used cylinders with a thickness of 1/4 in.

(ii) The open area on both slotted cylinders was made equal in area to the solid surface. This design gave periodic spike fluctuations instead of the square wave intended. The design was revised to make the inner one three-quarter solid surface and one-quarter open and the outer cylinder remained half open and half solid area. This design subsequently gave a satisfactory square wave fluctuation.

For a detailed design of this valve, see Section 2.4.7.

2.2.2 Laser Doppler Velocimeter System and Smoothing Chamber Design

Two transparent windows were needed to let the laser beam pass and be focused in the channel. This channel had a circular cross section of 4 in. internal diameter. It was calculated that with this channel size, the flow velocity inside the channel would be between 2 to 10 ft/sec and this was a convenient velocity to be measured by the laser doppler velocimeter both in this preliminary setup and eventually in the final design. Two acrylic windows were installed in a viewing section to provide the laser beam access to the flow. It was found that the surfaces of the windows had to be very flat and free of scratches to avoid multiple scattering of the laser beam. This multiple scattering of the beam would increase the noise level measured by the laser velocimeter by several folds.

To reduce the turbulence level of the flow, the flow from the siren valve passed through a smoothing chamber and a convergent nozzle before it entered the laser viewing channel. This smoothing chamber contained perforated metal plates, honeycomb material and screens installed perpendicular to the flow to aim for a turbulence level of less than 1 percent. To give such a low turbulence level, the water emerging from the siren valve was first slowed down to less than 0.5 ft/sec by the increased area of the 12 in. diameter chamber. Inside the chamber, it first passed through two plates of perforated metal to cut down the large scale eddies, then passed through the

honeycomb to reduce the lateral direction turbulence. The water further went through a series of screens to reduce any leftover small scale turbulence and finally it went through a distance of about 12 in. of straight chamber for further damping before it was brought to the 9 to 1 area converging nozzle. Different shapes, sizes and arrangements were tested before the final decision was made on the configuration. This was incorporated into the final design and will be given in the Section 2.4.5.

2.3 Analytical Model

After it was established that we could furnish the necessary mass flow measurement system and design of the fluctuator, we began the design of the final pump facility. It was decided that the inducer pump would be housed in a closed hydraulic loop. The essential parts of this loop consisted of the inducer pump, two fluctuators (one upstream and one downstream) and an isolation tank between the fluctuators. The main purpose of this isolation tank was to dynamically uncouple the two fluctuators. All these parts were connected by hydraulic pipes.

If the dynamic behavior of the inducer could be represented by the ZP-matrix as mentioned in the introduction, the fluctuating quantities upstream and downstream of the pump as excited by the fluctuators would depend on the dynamic behavior of the rest of the hydraulic system. The dynamic response of the hydraulic loop depended mainly on its physical dimension. In order to have some idea of the physical

dimensions allowable, a mathematical model of the pump loop was constructed using one-dimensional linear theory. The constraints of this mathematical model were the requirements that

(a) The percentage mass flow fluctuation should be at least one to two percent of the mean. This percentage was the lowest allowable limit which could be measured by the laser doppler velocimeter.

(b) The amplitudes of the fluctuating quantities should be large enough that a compliance value ranging from 0.01 to 0.001 $ft.^2$ could be measured accurately. Although we intend to measure the ZP-matrix, there was no estimation on the values of this matrix thus a compliance value taken from engine tests as described in introduction was used as a design evaluation parameter.

(c) The pressure fluctuations upstream of the inducer should not cause the cavitation number to vary more than 30 percent. A lower value of the variation would be more desirable but this implied smaller mass flow fluctuation and this opposed the intention (a).

The mathematical model had four main elements; these were, the cavitating pump, two variable throttling valves and an "isolation tank" between the two valves (see Fig. 2.3). These elements were connected by hydraulic pipe lines. It was intended to calculate the dynamic response of this mathematical pump loop when the throttling valves were varied about their mean value at a given frequency. The characteristics of the individual elements are as follows:

(i) The pump — One of the impellers intended to be installed

in the final pump loop was a larger three in. diameter model of the nine degree helical inducer described by Acosta (1958). The steady performance of the mathematical pump was taken to be that of this nine degree inducer. The fluctuating performance of the pump was composed of two parts; a pump resistance which was taken to be the gradient of its steady state performance as in the model by Rubin and an assigned compliance value which related the fluctuating mass flow difference to the fluctuating upstream pressure. During the calculation, different compliance values were used covering the range from 0.01 to 0.00001 $ft.^2$ No direct relationship between compliance values and cavitation number was assumed. This is because the information from engine tests (see Fig. 1.5) shows wide data scatter and the mathematical model in this case covered all the possibilities.

(ii) The two valves — The reasons for using two valves for the required fluctuations were mentioned in the introduction and will not be repeated here. These valves were assumed to have a steady resistance which defined the steady operating point of the pump loop and a fractional sinusoidal variation about the mean to give the fluctuating action at a selected frequency. The fluctuating amplitude of the valves could be varied independently and they could be operated with an arbitrary phase difference. The exact values used for these resistances were actually determined after the steady operating states were chosen.

(iii) The isolation tank — This tank was situated between the two fluctuating valves. It was assumed that the tank contained a large

volume of air which had a large compliance value thus isolated the two fluctuators. The absolute pressure of the air volume also defined the datum pressure of the system and thus controlled the cavitation number of the pump.

(iv) Hydraulic pipes – The four components mentioned above were connected by hydraulic pipes. The pressure drop across these pipes was assumed to consist of frictional losses as well as inertial effects. The lengths of the pipes were varied during each calculation but the size of the pipe was taken to be constant and equal to four in. diameter.

A computer program for this mathematical model was devised. This computer program was given the steady state operating point of the system with some value of the total pipe length. Then based on the assumed dynamic characteristics of the components, the mass flow fluctuations and pressure fluctuations at various stations in the circuit were calculated for frequencies of excitation between 0 and 50 Hertz. Different lengths of pipe sections were used and the whole process was repeated for different values of compliance. Only solutions within the required amplitude of mass flow fluctuation and within the limits of the variation of the cavitation number were subsequently considered.

A typical result of the calculation is shown in Fig. 2.4. It can be seen that for a certain amplitude of mass flow fluctuation, the upstream pressure fluctuation which is equivalent to cavitation number fluctuation increases as the pipe length increases. This is because in order to create the same amplitude of mass flow fluctuation, more

pressure will be needed for the increased inertia due to longer pipes. To limit the cavitation number fluctuation, it is then best to minimize the total length of the hydraulic pipes. This was the most important guideline learned in this analytical pump loop model and will be applied to the final design of the pump test facility.

2.4 Final Design of the Dynamic Pump Test Facility

The design of a pump test facility to measure the dynamic transfer characteristics of a cavitating pump was based on the confidence and experiences gained from the preliminary experimental setup and mathematical model. For a schematic drawing of the facility see Fig. 2.5, and Fig. 2.6 shows photographs of it. The focus of the facility was an impeller pump driven by a dc electric motor through a step up gear box. Before the flow entered the pump, it passed through a mass flow measuring arrangement. This arrangement consisted of a smoothing chamber to reduce the turbulence level, a convergent nozzle to give a flat velocity profile as well as accelerating the velocity to a suitable velocity to be measured by the laser doppler velocimeter. A similar mass flow measuring arrangement existed downstream of the pump. Following the downstream laser doppler velocimeter station was a "silent" throttling valve to control the steady state operation of the hydraulic flow. The flow passed through a turbine flowmeter for mean flow calibration before it entered the downstream fluctuator. The flow then passed through an isolation tank, an upstream fluctuator then finally flowed into the upstream smoothing

chamber. The two fluctuators were driven by a phase lock dc motor through an 8 ft. long connecting shaft. The whole hydraulic flow circuit was located on top of an eight in. I-beam frame supported on five legs bolted to the floor. The system was supplemented by auxiliary systems namely a deaeration system, an air bleed system and a heat exchanger to condition the water used in the system.

As for instrumentation, a reference signal from a signal analyzer commanded the fluctuator motor to rotate very precisely at the selected frequency. Sensors like the pressure transducers, accelerometers and laser doppler velocimeters located upstream and downstream of the pump measured the respective fluctuating quantities. The output voltage signals of these instruments consisted of mean values which were taken during experiment and fluctuating values which were amplified, low pass filtered and finally recorded in analog instrument recorders to be processed later. The detailed description of the components follows:

2.4.1 The Impellers

(i) Impeller III[1] – This was a three bladed nine degree helical impeller with 2.985 in. outer diameter. The solidity which is defined as the ratio of blade length to blade spacing was 1.75 and the hub ratio which is a ratio of hub diameter to tip diameter was 0.4. The design

---

[1] This impeller was fabricated by
M. C. Bidwell Co.
71 No. San Gabriel Blvd.
Pasadena, California 91107

was based on a similar impeller used by Acosta (1958). A drawing of Impeller III is shown in Fig. 2.7 and a photograph is included as Fig. 2.8. This impeller was made of aluminum with the surface hard anodized.

The tip clearance between the impeller tip and housing was 0.005 in. A radial clearance of 0.002 in. was used at first but this close clearance caused scratches on the acrylic housing and it was decided to increase the clearance. The impeller had a straight, sharp leading edge thus causing a high stress concentration on the root of the leading edge. After about one year of testing during which time the impeller had gone through 6 million fluctuating cycles and about 70 million rotating cycles, it had a fatigue fracture at the blade root (see Fig. 2.9). A similar impeller, Impeller V, was made to replace this one.

(ii) Impeller IV[2] - This is a one-quarter scale model of the first stage low pressure oxidizer pump of the Space Shuttle main engine. See Fig. 2.10 for a drawing and Fig. 2.11 for a photograph of this impeller. The inducer consisted of a four blade helical section of seven degree tip angle followed by a tandem row of twelve highly loaded blades. The outer diameter was 2.983 in. and had a radial clearance of 0.004 in. A scaled model of the stator stage was also fabricated. The impeller was made of aluminum which made it structurally as well as hydraulically similar to the prototype impeller.

---

[2] Fabricated by Contrua Inc.
430 No. Berry St.
Brea, California 92621

After this impeller had been operated under cavitating conditions for about eight hours, there was some cavitation damage to the leading edge at the tip where the surface was found to be pitted. This was repaired by filing off the uneven part and the blade surface was reanodized.

(iii) Impeller V[3] - This was designed and constructed after the fatigue failure of Impeller III. This impeller had the same basic design as Impeller III except for a thicker root and a swept back leading edge. It was made of 304 stainless steel and was thus stronger structurally than Impeller III. Figure 2.12 is a drawing and Fig. 2.13 is a photograph of this impeller.

2.4.2 Acrylic Impeller Housing

This was a 6 in. × 6 in. × 8 in. laminated block of acrylic with a 3.002 in. bore. Part of this bore was enlarged to house the stator when using Impeller IV. The transparent acrylic made it possible to view and photograph the cavitating impeller.

2.4.3 Pump Volute

The downstream of the acrylic housing was joined to a volute to turn the flow through a right angle. The central part of this volute contained the bearing cartridge which will be described in 2.4.4. Guide vanes were installed at the volute exit to reduce the rotation of the flow. Figure 2.14 is a diagram of the aluminum volute casting.

---

[3] M. C. Bidwell Company

2.4.4 Motor, Gear Box and Bearing Cartridge

Preliminary calculations based on estimated performance characteristics of the impellers indicated that the power required at 50 percent efficiency would be about 20 hp. The calculation was based on a top pump speed of 12000 rpm which was believed to give a suitably low cavitation number. A 20 hp open loop SCR variable speed dc motor was purchased (Sabina Electric)[4]. This motor had a top speed of 1750 rpm.

The rotation speed was increased via a straight, parallel gear box[5] with a step up ratio of 6.86. This brought the maximum rotation speed to 12000 rpm. Originally, a set of spur gears were used which gave excessive chatter, vibration and noise. These were replaced by a set of helical gears which reduced the noise to a tolerable level. The output shaft of the gear box was connected to the impeller shaft via a one foot long intermediate light aluminum connecting shaft. This shaft is very stiff in the torsional direction but soft in bending.

The impeller shaft which was made of stainless steel was housed in a bearing cartridge. During fluctuating flow experiments, any axial movement of the shaft would constitute additional motion between the impeller and fluid flow and this was to be avoided. The design of the bearing system needed to be very stiff in the axial direction but free to rotate. As an estimation of the shaft axial displacement effect

---

[4] Sabina Electric and Engineering, 1196 Batavia St., Orange, Ca.

[5] Vi-Star Gear Co., Inc., 7312 Jefferson Street, Paramount, Ca.

we may note that a typical axial fluid velocity of 10 ft/sec with a two percent mass flow fluctuation at 40 Hertz will have a 5 percent error if the axial displacement of the shaft is as little as 0.0005 in. Thus, a maximum value of 0.0005 in. axial displacement was allowed in the design of the stiffness of the bearings.

The bearing design consisted of a set of two class A7 precision angular contact bearings back to back located near the middle of the shaft to restrain axial motion. This duplex bearing set had no free end play nor radial run out and had in addition a very high spring constant in the axial direction. The driven end of the shaft was supported by a deep groove precision ball bearing. The bearings were air mist lubricated. A mechanical seal having a stationary carbon face rubbing against a 440 C seal ring was installed outboard of the duplex bearings to seal the bearing cavity. Provision was made for an additional slinger and drain port so that the air mist flow would tend to purge any small water leakage into a drain pot. The impeller shaft was connected to the light intermediate drive shaft via a steel plate that had sixty teeth machined on its circumference. A magnetic pickup provided a frequency output equal to the pump rotational speed in rpm. These details are shown in the assembly drawing of Fig. 2.15.

2.4.5 Smoothing Chambers and Convergent Nozzles

In order to minimize the turbulence level of the flow to be measured by the laser doppler velocimeter, the two laser beam measuring ports were preceded by smoothing chamber and a nine to one area ratio convergent nozzle. The general description was given

in Section 2.2.1 and the details will follow.

The smoothing chamber had a diameter of 12 in. and a length of 24 in. It was made of aluminum with surface anodized. The flow entering the chamber first met two perforated metal plates in series to break up any large scale eddies. The perforated metal plates were 1/4 in. thick with 30 percent opening area of hole size 3/16 in. This was followed by a piece of aluminum honeycomb material 2 in. thick and 1/8 in. cell size. The honeycomb section damped down the lateral turbulence velocity. The flow finally passed through two mesh 22 fine wire screens into approximately 12 in. of straight chamber. The fine wire screens broke up any left over small scale turbulence and the straight chamber provided enough length for any small scale turbulence to be reduced by internal viscous damping. The flow passed through a nine to one convergent nozzle then entered the laser velocimeter measuring port as mentioned above. A schematic of the smoothing chamber is shown in Fig. 2.16.

2.4.6 Silent Valve[6]

This provided the steady state throttling action. The important part of the valve is a block of elastomer which is 8 in. long and 6 in. in diameter containing about 200 longitudinal holes. This elastomer block was placed inside a stainless stell cylindrical housing and was squeezed axially between two matching steel end plates. A hydraulic cylinder applied force at one end to reduce the hole size thus

[6] Supplied through the courtesy of Mr. C. A. Gongwer.

providing extra resistance to the flow. The hydraulic loss is predominantly viscous making the operation of the valve very quiet; hence the name "silent valve" and a schematic is shown in Fig. 2.17.

The oil pressure to the hydraulic cylinder was supplied by a hydraulic oil pump via a servo valve. The servo valve was controlled by an electronic feedback system governed by the output of the turbine flowmeter. The steady flow rate could thus be preset by adjusting a reference voltage input to the feedback amplifier. This elaborate feedback system was needed because readjustment of the fluctuator for fluctuation amplitude was liable to change the steady state operation of the system. Schematic diagrams of the feedback system and hydraulic pressure system are shown in Figs. 2.18 and 2.19.

2.4.7 Siren Valve

The general description and function of this valve were discussed in Sections 2.1 and 2.2. Only the essential dimensions will be given here.

The bronze rotating armature and stainless steel cage were about 5 in. in diameter and 6 in. in length with a thickness of 1/4 in. The number of slots manufactured was nine. The sintered bronze cylinder used was 5 in. in diameter, 6 in. in length and 1/4 in. thick with bead sizes of about 0.03 in. It was found out later that the pressure drop across the sintered bronze was too high. Fifteen holes of 3/8 in. diameter were then drilled in the sintered bronze piece to reduce the resistance. The slotted cylinders and the sintered bronze

pieces were situated at the center of a 12 in. long and 12 in. diameter chamber.

The two fluctuators, one upstream and one downstream, were of the same design but had opposite flow direction. The two fluctuators were driven by a synchronized speed dc motor as will be discussed in Section 2.4.8 and the connection between the dc motor and the fluctuators was provided by three couplings and a 6 ft. long and 1 in. diameter hollow shaft between the fluctuators. The actual right angle connection between the siren armature and the shaft was by a nine to one reducing worm gear and this was the reason for using nine slots in the siren valve. Figure 2.20 shows an assembly drawing of the valve.

2.4.8 Fluctuator Motor[7]

The signal analysis by the Bafco required that the fluctuating measurements of velocity, pressure and acceleration be phase referenced to the reference output signal. The connection for this phase reference was through the fluctuator motor that drives the siren valve to produce the fluctuating flows.

The electric motor was a one horse power dc motor with SCR dc power supply. The rotational speed was controlled by the reference

---

[7] Electric Motor — Sabina Electric and Engineering, 1196 Batavia Street, Orange, California 92667

Feedback Electronic Design — Shapiro Scientific Instruments, 3500 East Coast Highway, Corona Del Mar, California 92625

signal from the Bafco and the maximum speed of the motor was about 2500 rpm. To provide the phase reference locking, an optical encoder was installed at the free end of the motor to provide a feedback loop for the speed control. A two way dial indicated the speed of the motor relative to the signal. Zero dial reading indicated that the motor speed had achieved synchrony with the reference signal.

2.4.9 Isolation Tank

The chief function of the isolation tank was to prevent interactions between the two fluctuators in returning the flow to the inlet side. This was accomplished by a plastic bladder containing about one cubic foot of air. Control of the pressure inside the bladder also fixed the static datum pressure of the system. The tank was made of galvanized steel with a side port to house the plastic bladder. It had a large cross sectional area providing a low flow velocity region where any air bubbles carried by the water would float to the top and be bled away. A coiled copper tubing heat exchanger inside the tank was connected to the house chilled water system to absorb the heat generated from the pumping action to maintain a constant temperature of the water.

2.4.10 Foundation and Foundation Bracing

The whole hydraulic system was supported on an 8 in. wide flange I beam welded framework supported by five columns formed of six in. steel pipe. These columns had welded flanges which could be bolted to the concrete floor. This foundation was originally bolted to

the floor firmly to minimize the vibration of the system. During the experiment, noise and vibrations from the electric motor, gear box and pulsations from the cavitating flow were transmitted through the steel supports to the floor and subsequently transmitted to the whole building. This noise and vibration disturbed the comfort of the community within the building. To isolate the system, the bolts holding the foundation to the floor were loosened and rubber insulation pads were placed between the support and the floor.

However, during this phase of the experiment, there was growing concern over the vibrational level of the frame as a sufficiently large amplitude vibration of the hydraulic structure would produce a faulty reading of the LDV velocity reading. Accelerometer measurements of the I beam framework were subsequently observed to be too high (in some cases about one half the velocity signal) and therefore the foundation was again bolted tight to the floor. Further accelerometer readings of the structure at the LDV measuring stations revealed that even in this case the foundation was not completely satisfactory. These tests at various locations of the foundation found that there existed internal vibrational modes due to the bending of the I-beams and supporting columns. This unwanted effect was greatly reduced by adding three diagonal braces between the I beam and the vertical columns constucted of six in. pipe. Figure 2.21 shows the locations of the cross members and Figs. 2.22 and 2.23 show the vibrational level in two directions above the LDV viewing windows before and after the bracing of cross members.

2.4.11 Air Bleed System

At the highest point of each section in the circuit, connections were made to a water accumulator of a vacuum system. The water accumulator was simply a small tank connected to a vacuum pump and a drain valve at the bottom. Its function was to trap any water that was entrained in the vacuum line and prevent this water from entering the vacuum pump.

2.4.12 Water Treatment

Distilled water was used in the system. Because of the many different metals used in the system, the water was treated chemically to prevent corrosion by maintaining a chromate ion concentration of about .06 percent by weight and maintaining a minimum ph of 8. The water was deaereated for about three days before each experiment and cooled to about 70°F. during experiments.

2.4.13 Deaeration System

This was a system to recycle the air between a vacuum tank and a storage tank such that the water could be deaeration. The water was pumped into the vacuum tank and sprayed inside via a set of nozzles forming small droplets. The increased relative surface area and small volume enable the dissolved air to diffuse through the water and be removed by the vacuum pump. The water droplet itself fell to the bottom of the tank and was pumped into the storage tank. The vacuum tank was elevated about 5 ft. above the ground giving a better suction performance to the transfer pump pumping water into the storage tank. The capacity of the storage tank was about 300 gallons and had a layer of small plastic plates floating on the water surface to inhibit air from

dissolving back into the water. The vacuum was provided by a Nash 3 hp vacuum pump. Figure 2.24 shows a schematic of the deaeration system.

2.5 Instrumentation

This section contains a detailed description of the instrumentation. The interrelationships between these instruments are shown in the signal flow diagram of Fig. 2.25.

2.5.1 Laser Doppler Velocimeter (LDV) and Mounting Systems

For a preliminary description of this instrument, see Section 2.2.1 and for the theory, see Appendix A. In the final version of the LDV system adopted for the facility, a 50 cm focal length lens caused the two laser beams to cross at the center of the measuring sections. These sections had four in. diameter cross-section and followed the nine to one converging nozzles. The laser beams passed through one in. thick flat lucite windows on each side of the sections. A collimating stop consisting of a piece of cardboard with a small hole let only the weak beam pass into the photomultiplier. The photomultiplier tube was mounted about two feet away from this window. It was found that the dirt existing in the water provided enough light reflecting particles for the LDV to function properly.

Originally, the lasers and the photomultipliers were mounted on a light aluminum channel attached to the main beam of the foundation. This arrangement proved to be unacceptable due to the vibration of the LDV mounting frame. The resonant frequency of this frame was found to be only 25 Hertz which was well within the experimental frequency range of excitation. This source of error was avoided by mounting the lasers

and photomultipliers on a sturdy massive steel structure constructed of 2 x 6 in. channels welded into a box beam suspended from the ceiling. The natural frequency of this suspension system was found to be about one half Hertz and during subsequent tests no velocity excitations of this mounting framework approached one percent of the fluid velocity perturbations measured by the LDV systems. All flow velocity measurements are then referred to this "inertia" frame.

As can be seen from Appendix A, the ratio between the measured velocity and doppler frequency depends on the angle between the two laser beams. This angle is very small and very difficult to measure precisely. Coupled with the fact that the actual measurement required was the volumetric flow rate and not velocity at a single point, the turbine flowmeter signal was used to calibrate the output of LDV in volumetric flow rate.

By operating the pump loop with a small fluctuation and observing the signals on the oscilloscope, it was found that the laser doppler velocimeter could measure velocity fluctuations down to one percent of the mean flow. But the signal as measured by the upstream LDV had a different fluctuating amplitude and phase than the downstream one even when the flow was fully wetted and great care was taken to exclude the possibility of air bubbles in the system. There then appeared to be two questions that needed answering; first, were the two velocimeters actually working identically and secondly, was the observed difference between the two signals due to structural compliance. In the present context assurance as to the first question was needed for the program to continue. The second is addressed in the subsequent chapters.

In order to investigate possible differences in the operation of the two LDV systems, the two LDV photomultipliers were located side-by-side and fed by the same laser beam with the aid of a beam splitter. One would expect two identical velocity signals. It was found that there was a small phase shift between the two systems. Since the LDV processor electronics were both designed with a high frequency response, the only time shifting component could come from the two similar but not identical frequency-to-voltage convertors. (One of them was actually purchased at a later date and turned out to be a slightly different version; see Appendix A). It was believed to be necessary then to measure the transfer function of the combined LDV processor systems including the frequency-to-voltage convertor. This was accomplished by replacing the photomultiplier input with a frequency-modulated carrier frequency generator[8]. In this test the frequency generator fed the LDV processor a signal with a main carrier frequency of about 80 - 150 k Hertz which was the normal doppler frequency. This frequency was changed by an amount of 2-5 percent at a frequency of 5-50 Hertz. This latter modulating signal was provided by the Bafco signal analyzer reference signal. By this means it was possible to simulate the behavior of a real photomultiplier signal of a mean flow with 2-5 percent fluctuation. The output of the entire LDV system was then analyzed by the Bafco return signal analyzer from which the amplitude and phase shift response of each LDV system could be determined. These are shown as a function of frequency in Fig. 2.26

[8] Wavetek 164

One very important point that should be mentioned here is that the upstream LDV did not work when the leading edges of the impeller blades are highly loaded. This highly loaded condition causes a tip clearance backflow vortex to intrude into the upstream viewing windows and this higher turbulent flow blurs the phase locking mechanism of the LDV system. This experimental limitation happens when the flow coefficient is 0.07 for the Impeller V and 0.05 for Impeller IV.

2.5.2 Pressure Transducers

Three Entran[9] miniature strain gauge pressure transducers were purchased. These had a 1/8 in. diameter pressure sensitive surface and could be flush mounted on the wall of the system. These proved to be a complete failure due to the following reasons. The first problem encountered was the thermal effect of the flow on the transducer. It was found that thermal transients due to fluctuating fluid velocity also changed the resistance of the sensing elements thus giving a faulty measurement of fluctuating pressure. This effect which is not unsimilar to the hot wire effect is amplified due to the small thermal mass of these transducers. Further problems were encountered when mounting these delicate transducers to the system. Although great care had been taken during mounting, small releasing or tightening of the mounting mechanism changed the transducer balance and thus required frequent rebalancing of the transducers. Finally, all these miniature transducers were completely damaged beyond repair due to this mounting difficulty and were discarded.

---

[9] Entran Devices Inc., 145 Paterson Ave., Little Falls, New Jersey

Two Statham[10] 0-100 psia pressure transducers were purchased to replace the Entran transducers. These pressure transducers were chosen to have a natural resonance frequency of 10,000 Hertz. This value was many orders higher than the frequency range of interest in the present experiment. In this design, the pressure sensitive diaphragm was recessed in a tube fitted with a 1/8 female pipe thread. These transducers were connected to the smoothing chambers via short, 1/2 in. long, plastic tubings. The short plastic tube helped to isolate the transducer from the vibrations of the structure. The compliance effect of the short plastic tubing was calculated to be small. Provisions to bleed any air trapped in the pipe connection or in the transducer were made. The signal conditioning systems used for these transducers were home-made balancing resistance bridges and Burr-Brown[11] 3620L/16 operational amplifiers.

2.5.3 Accelerometers

From Section 2.4.10 on foundations and Section 2.5.1 on LDV it can be seen that it is necessary to monitor the vibration of the structure at the point of mass flow measurement. Two ±4g Statham accelerometers were installed directly above the LDV viewing windows. The accelerometer's balancing units were similar to the pressure transducers system and the amplifiers used were two Burr-Brown 3640 operational amplifiers. Velocities calculated from the readings of

---

[10] Statham Instruments Inc., 2230 Statham Blvd., Oxnard, Calif.

[11] Burr-Brown Research Corp., International Airport Industrial Pk., Tuscon, Arizona

these accelerometers were subtracted from the LDV readings to give the velocity of flow relative to the structure. A typical value of the structure vibration gave a typical velocity correction of less than 5 percent.

2.5.4 Turbine Flowmeter

To calibrate the volumetric mass flow rate of the LDV, a turbine flowmeter was installed in the circuit just upstream of the downstream fluctuator. It should be noticed that this turbine flowmeter could not measure the fluctuating velocity because the response of the turbine was too slow to give any fluctuating reading.

The particular turbine flowmeter[12] was originally used on a J2 engine and its calibration curve is shown in Fig. 2.27. The output is a periodic voltage with frequency proportional to the flow rate. This frequency signal was converted to a dc voltage by a frequency to voltage convertor[13] with a conversion ratio of .1 volt/100 GPM.

2.5.5 Pump Speed Magnetic Pickup

To measure the pump speed, a magnetic pickup transducer was situated 1/8 in. from a sixty tooth steel wheel mounted on the pump shaft. The number of voltage pulses per second is equal to the speed in rpm and this voltage pulse is counted by a HP 5302A frequency counter.

In order to measure the variation of speed during the experiment, these voltage pulses were fed into a frequency to voltage convertor. The output of this frequency to voltage convertor was a dc

[12] Potter Aero Company

[13] Teledyne Philbrick (Model 4702), Dedham, Massachusetts

voltage output adjusted to 1 volt/1000 rpm and any variation of the fluctuating frequency in the pump speed would appear as small ripples of the dc output (see also Section 5.4).

2.5.6 Axial Motion Proximity Transducer

To measure the axial displacement of the pump shaft during fluctuating experiments, a Karman[14] proximity transducer was purchased and located on the pump volute with its sensing surface facing the flat surface of the geared wheel. Any axial movement between the volute and the shaft would appear as a voltage proportional to the displacement which was due to the slight yielding of the precision bearing cartridge. This voltage output was connected to the Bafco signal analyzer to measure the fluctuating displacement. No readings were observed during a typical two percent upstream mass flow rate experiment using these instruments. Since the resolution for the displacement transducer and analyzer combination was 0.0005 in., this meant that the axial displacement of the shaft relative to the volute is less than 0.0005 in. which was within the design requirement of the bearing.

2.5.7 Amplifier and Filter Bank

The original signals like LDV output and pressure transducer output were usually in the form of a small ac signal riding on a large dc voltage. These signals also had a high noise content with values comparable to the ac signals. It was intended to record these signals

[14] Karman Sciences Corporation, P. O. Box 7463, Colorado Springs, Colorado.

by instrumentation tape recorders (see Section 2. 5. 10) and analyze by the Bafco signal analyzer. This presented difficulties as the tape recording accuracy of the small ac was limited by the dynamic range of the recorders. The accompanying recording of the large dc voltage allowed only a low amplifying factor on the tape recorder. The Bafco analyzer (see Section 2. 5. 9) also encountered difficulties as this analyzer had to filter out the large dc component and reject the high noise.

To improve the situation, the dc component was rejected and the ac signal was amplified to a higher level such that the recorder would not be saturated by the dc but instead record a high level of ac signal. Since the dc values were not recorded, the values were displayed on an integrating voltmeter (see Section 2. 5. 9) and written on data sheets. Furthermore, the noise was filtered by a low pass filter. The dc rejection, ac amplification and noise filtering were accomplished by a bank of ac filters followed by a bank of low pass filters. Six ac amplifiers made from conventional 741 operational amplifiers and six two stage, four pole butterworth filters with a cut-off frequency of about 80 Hertz were fabricated to condition the six signals. The six signals were upstream and downstream velocities, upstream and downstream pressures and upstream and downstream accelerations.

However, these amplifiers and filters had their own characteristic dynamic response thus contributing an amplitude and phase change at different frequencies. To measure these amplitude and phase changes, a given ac voltage signal was connected to the individual combined amplifier and filter input and the ac output signal was measured at various input frequencies. The ratio of input and output amplitude

was calculated. These, together with ratio and the phase change, were plotted on graph paper. A curve derived from the filter characteristic formula was fitted to these data points and a typical curve is given in Fig. 2.28. The fitted curves of the combined low pass filter and amplifier were used in the data reduction procedure to calculate the original signals.

2.5.8 Bafco 910 Signal Analyzer[15]

This instrument is the most important one in the equipment. It gives out a precise sine wave as reference at a pre-set frequency to drive the fluctuator motor. Any fluctuating signal to be analyzed is connected to the input end. The Bafco measures the in-phase and quadrature component of the fluctuating signal rejecting the noise present in the signal. The in-phase and quadrature voltages are displaced on two taut band meters. For easier reading, rear panel outputs of the in-phase and quadrature voltages were connected to two digital panel meters and readings were taken from these.

The above description is for real time analysis of the signal. For recording playback, an additional tracking unit was needed. This tracking signal accepts the playback reference signal and sets the Bafco to exactly the same frequency so that there is phase reference between the Bafco and the signal to be analyzed. The signal to be analyzed is connected to the normal input terminal of the Bafco.

Forty db of noise and harmonic rejection were obtained by using this analyzer. The performance was guaranteed at a signal to noise level of one to one with a one percent accuracy on the measured

[15] Bafco Inc., 717 Mearns Road, Warminster, Pennsylvania

in-phase and quadrature measurements. This value dominates the accuracy of the final results.

2.5.9 Integrating Voltmeter

To measure the mean dc component, an ordinary dc voltmeter was not suitable because most voltmeters measure an instantaneous voltage or measure the mean within a very short time interval and this would not give a true mean voltage because of the low frequency used in this experiment.

A NLS[16] integrating voltmeter was incorporated into the system and all the mean dc voltages were measured using an integrating time of one second. The one second integrating time averaged out all the small fluctuating ac components.

2.5.10 Recorders

The real time data analysis by the Bafco analyzer was time consuming and the data were subjected to error due to the slowly drifting of the mean operating state and the accumulation of air between measuring stations during cavitating tests. Two HP-3960[17] instrumentation time tape recorders were provided to record the signals during the experiment. The recordings were played back at leisure after the experiment.

Each of the tape recorders had 4 channels and the recordings were accomplished by always recording the reference signal on the

---

[16] Non-linear Systems, Inc., Model No. 2900, Del Mar, California

[17] Hewlett Packard Company, 690 East Middlefield Road, Mountain View, California

first channel and fluctuating signals on the second, third and fourth channels. The six recorded signals were two LDV signals, two pressure transducer signals and two accelerometer signals. These tape recorders were FM recorders with a cut-off frequency at about 300 Hertz and the recorders were checked to insure that there was negligible phase shift between the individual recorded data channels.

Since the recordings were simultaneous for all channels, the playback analyzed the signals for the same recorded time. This method thus only demanded a shorter time for experiment and reduced the time exposure of the inducer to the cavitation damage. Futhermore, shorter experimental time meant that the drifting of mean state and air accumulation in the system was minimized.

During playback, the playback reference signal had occasional high frequency spikes and these spikes disturbed the tracking mechanism of the Bafco tracking unit. A low pass filter with a cut-off frequency of about 500 Hertz was installed between the tape recorder reference output and the tracking unit. Although this low pass filter introduced a phase shift, this was the same for all the channels and hence was not corrected for in the analysis since we were only interested in the relative phase between all the fluctuating signals.

2.5.11 Selection Switch and Panel

All the outputs of the instruments were connected to a central panel where BNC connections were provided in the front. These signals were connected to the filters and ac amplifiers. The outputs of the amplifiers were brought back to the panel and connected to

another set of BNC connections. A selection switch was installed on the panel such that any signal on the panel could be connected to the Bafco analyzer and dc integrating voltmeter by turning a selection dial. (See the flow diagram, Fig. 2.25).

2.5.12 Manometers and Pressure Gauges

Pressure gauges and water over mercury manometers were connected to the pressure transducer locations for two purposes. The first purpose was to provide the static calibration of the pressure transducers. For this a precision Bourdon pressure gauge provided the calibration above atmospheric pressure and the manometers provided calibration for pressures below an atmosphere. The second purpose was to measure the static pressure during experiments. This may be redundant but proved necessary to ensure that the pressure transducers were functioning properly.

2.5.13 Stroboscope Synchronizer

A stroboscope synchronized drive was constructed to keep the inducer blades stationary visually. This device takes the pulsed signal from the pump speed magnetic pickup, divides it by sixty to give one pulse per revolution and the divided pulse train is used to drive the stroboscope. Provisions were made on the driver such that a phase lag can be imparted to the driving signal and the inducer can be viewed from another angle.

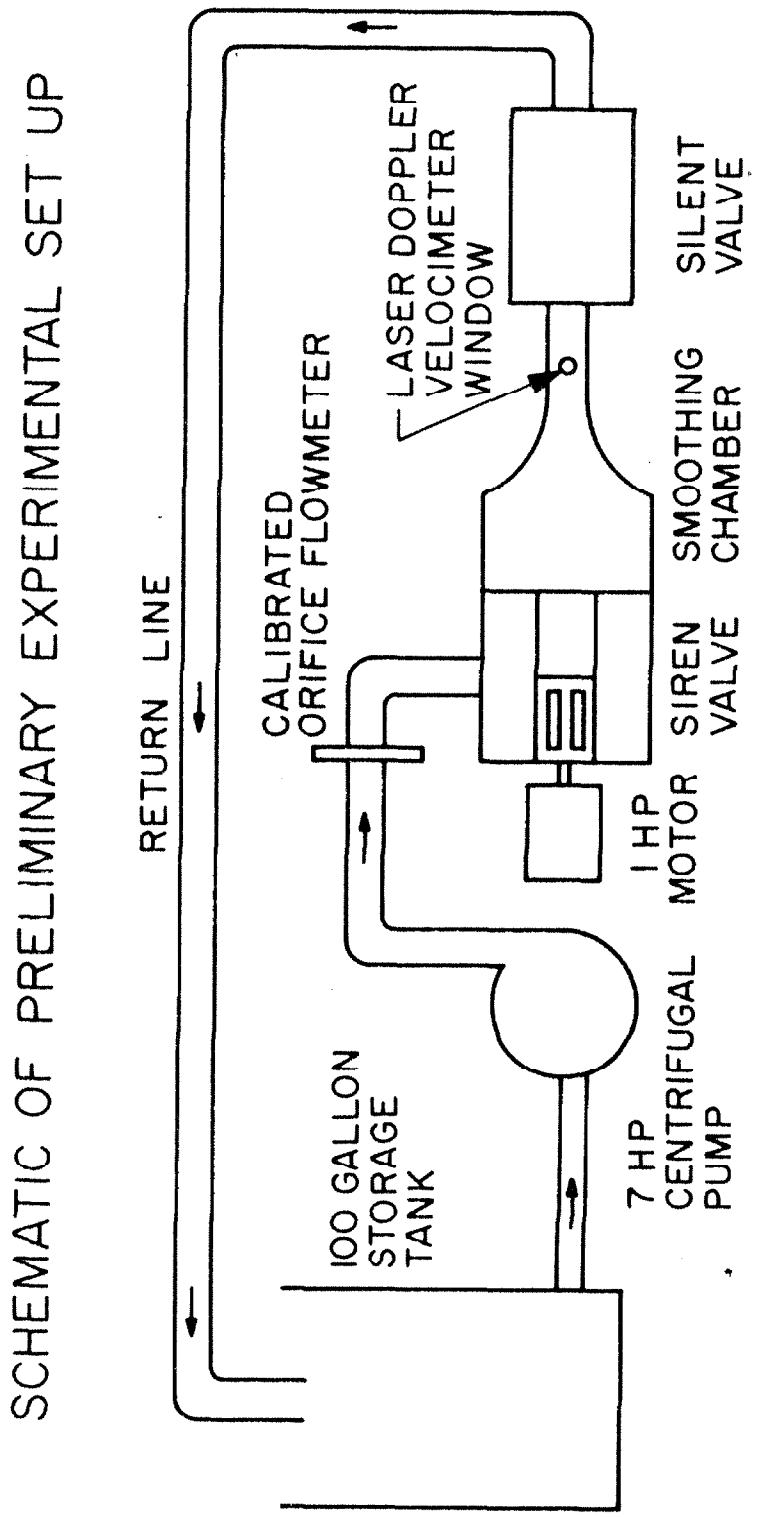

Fig. 2.1 Schematic of preliminary experimental setup.

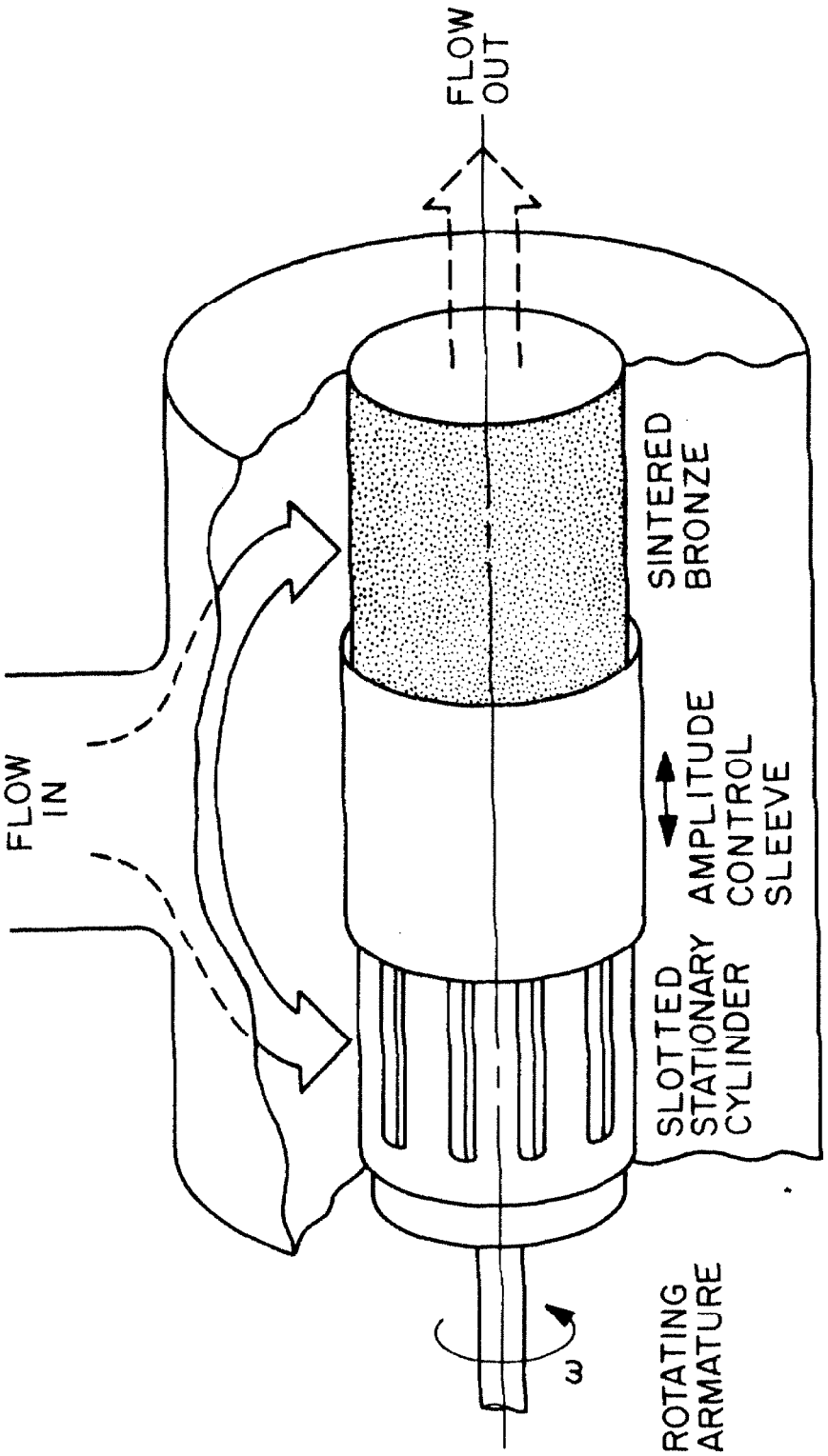

Fig. 2.2 Functional schematic of the fluctuator valve.

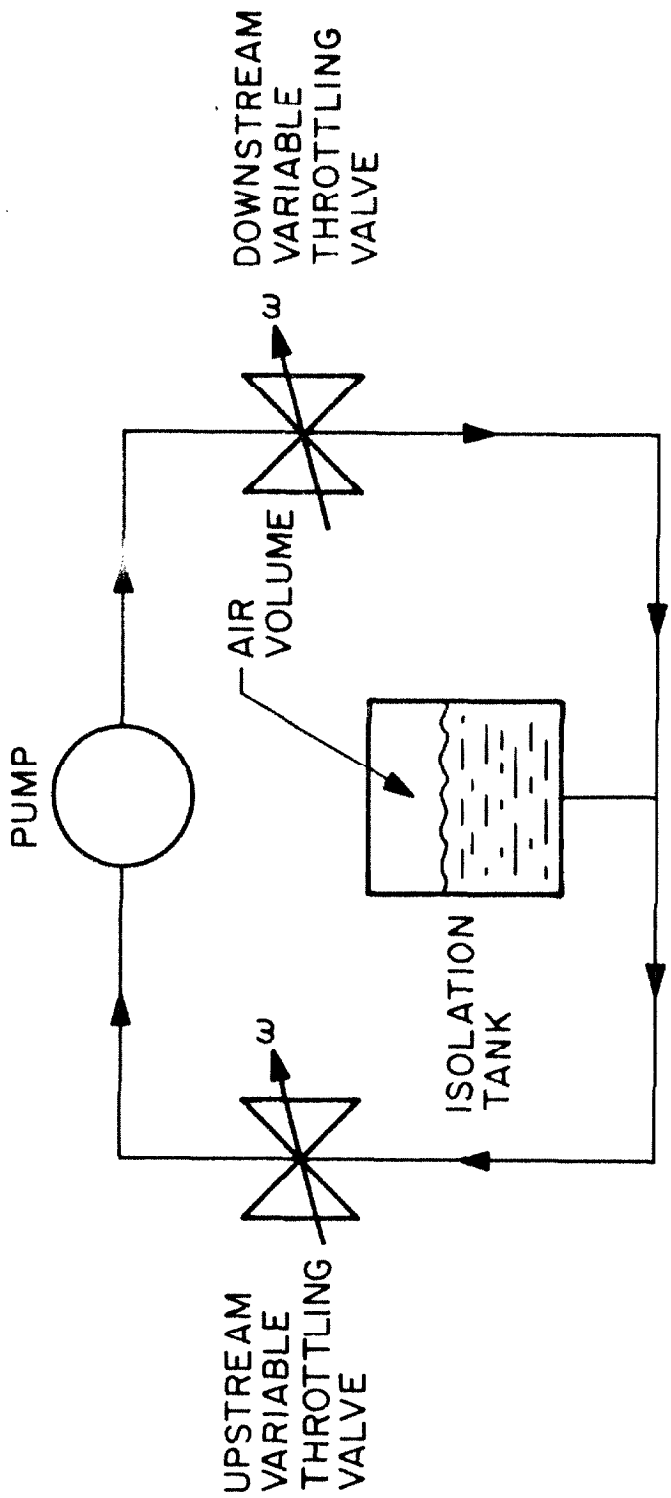

Fig. 2.3 Schematic diagram of the mathematical pump loop.

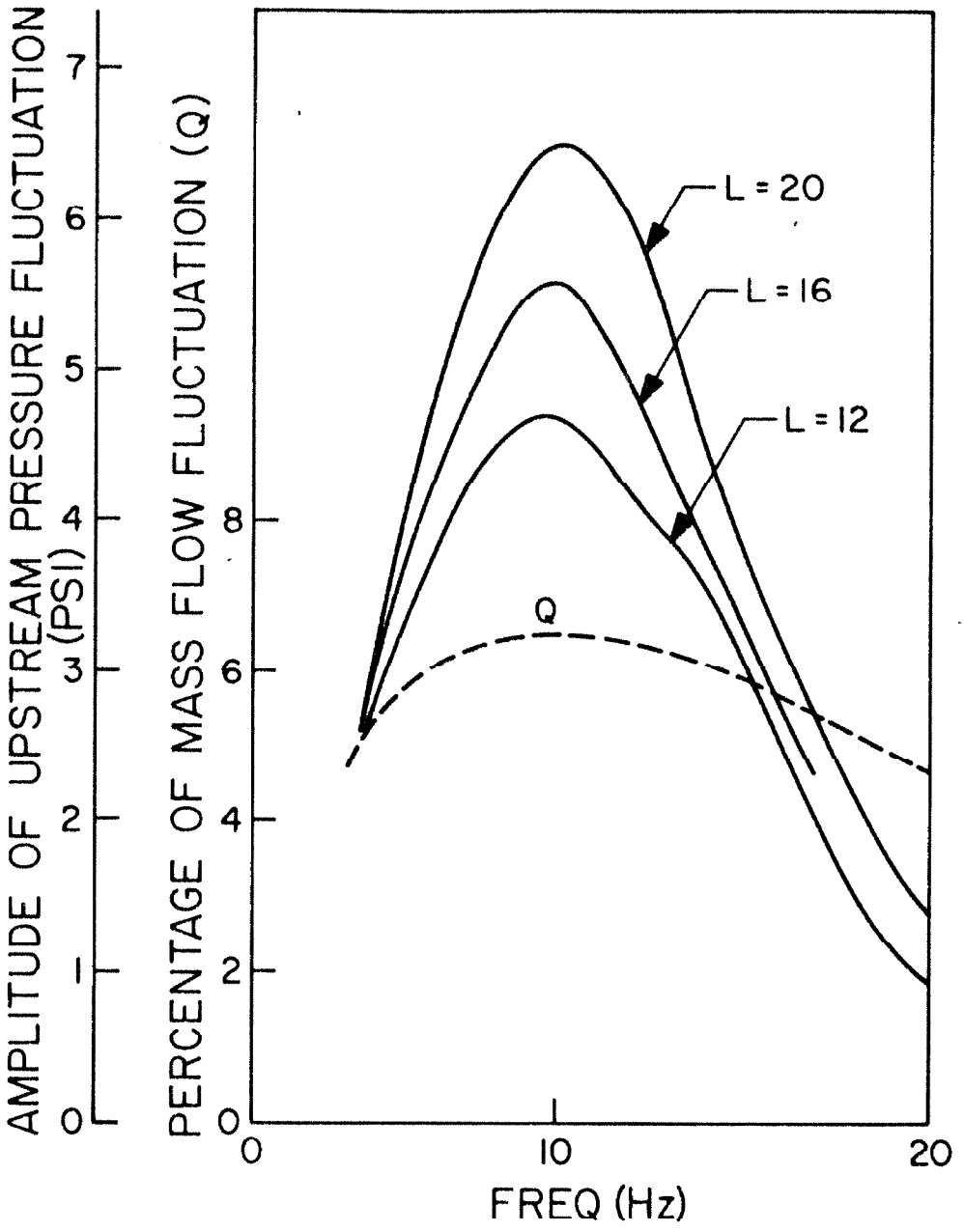

Fig. 2.4 Results of the mathematical pump loop showing amplitude of upstream pressure fluctuation for the same upstream mass flow fluctuation. The curves were calculated from various total hydraulic pipe lengths in feet when the pipe diameter is 4 in.

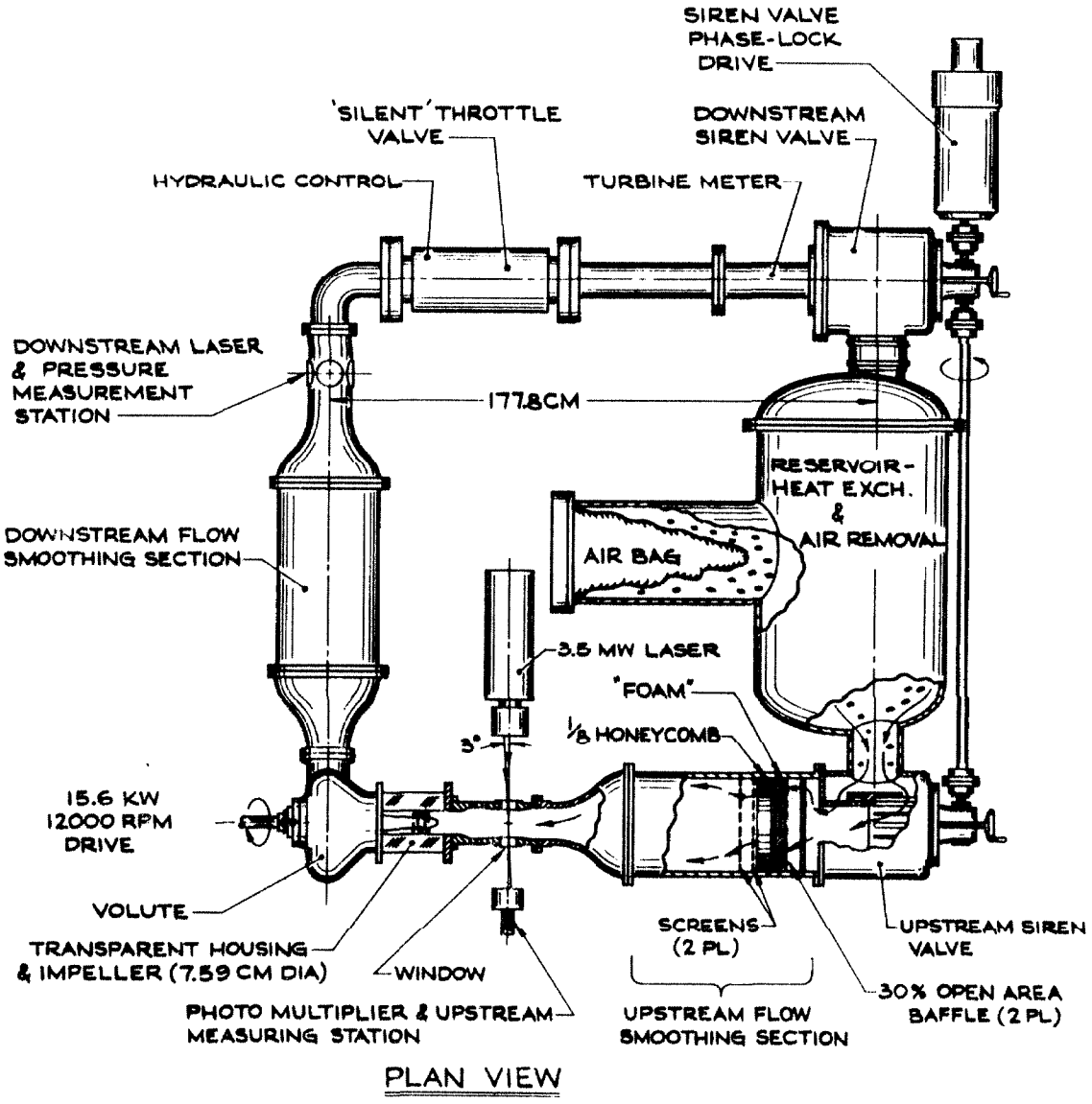

Fig. 2.5 Schematic drawing of the dynamic pump test facility.

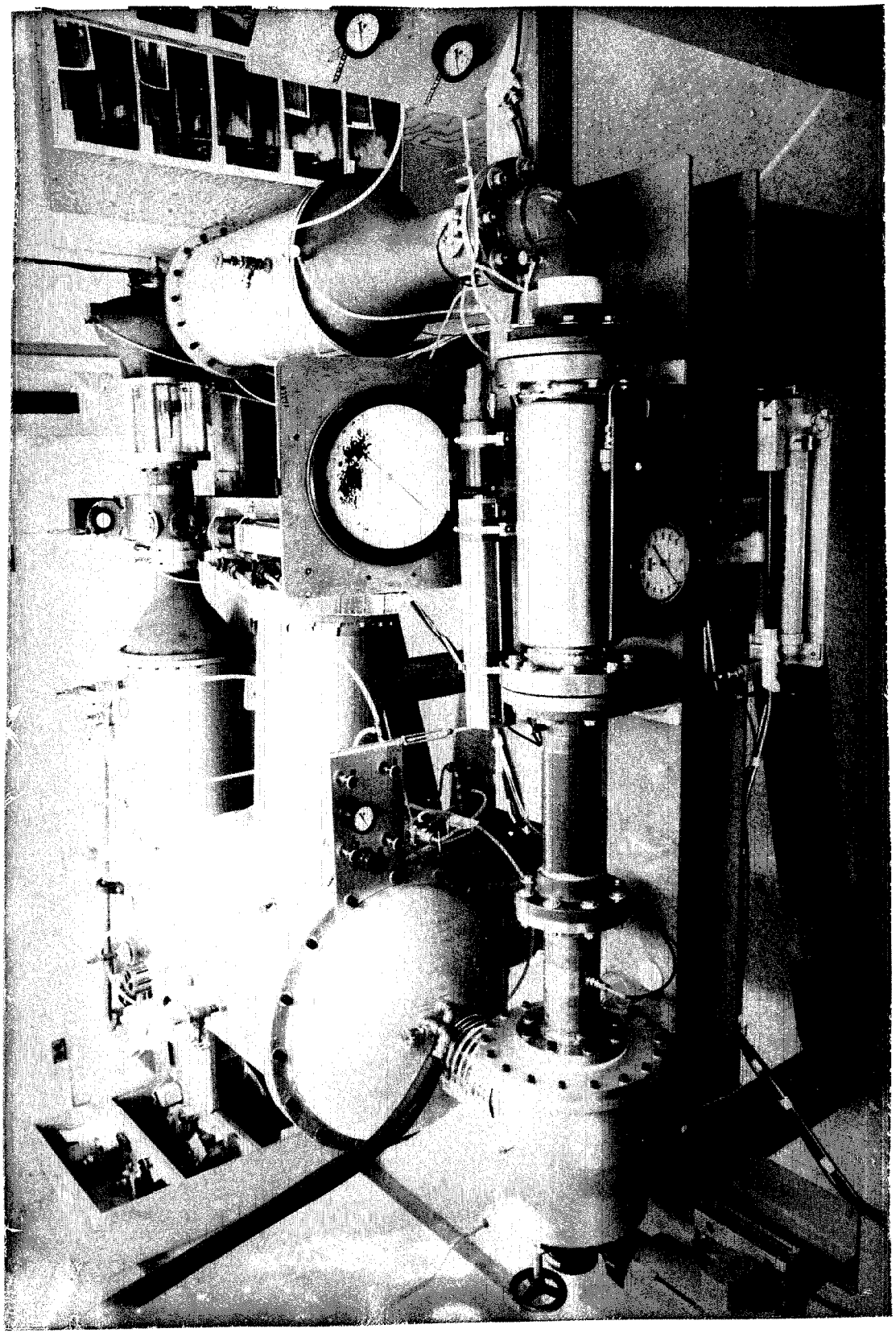

Fig. 2.6 Photograph of the dynamic pump test facility.

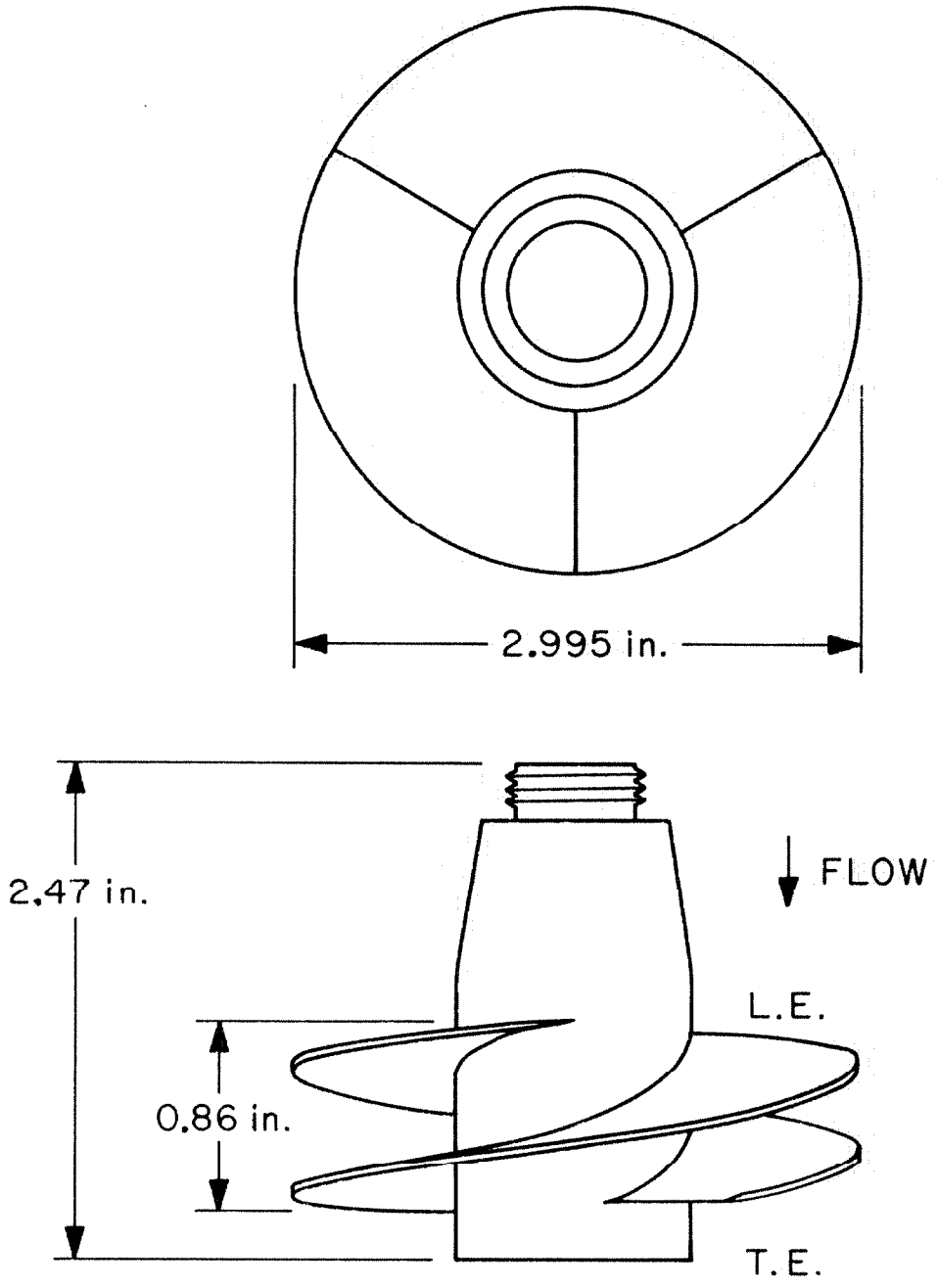

Fig. 2.7 Schematic drawing of Impeller JJ.

Fig. 2.8 Photograph of Impeller III.

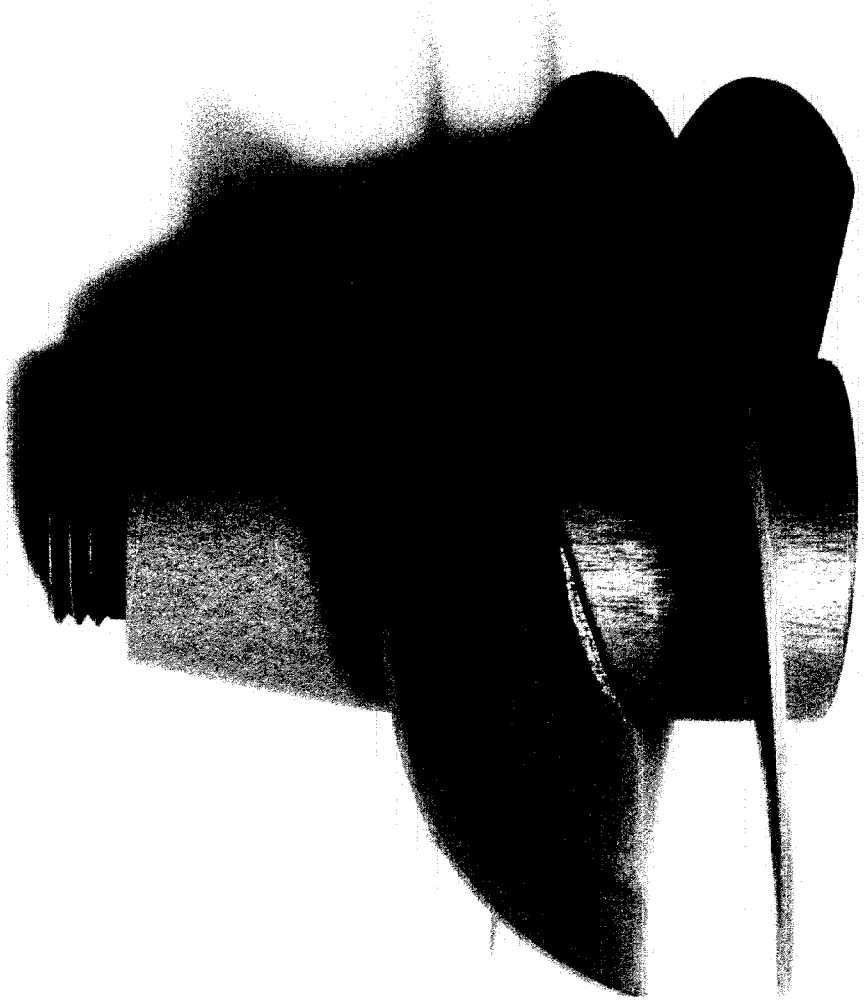

Fig. 2.9 Photograph showing fatigue fracture of Impeller #1.

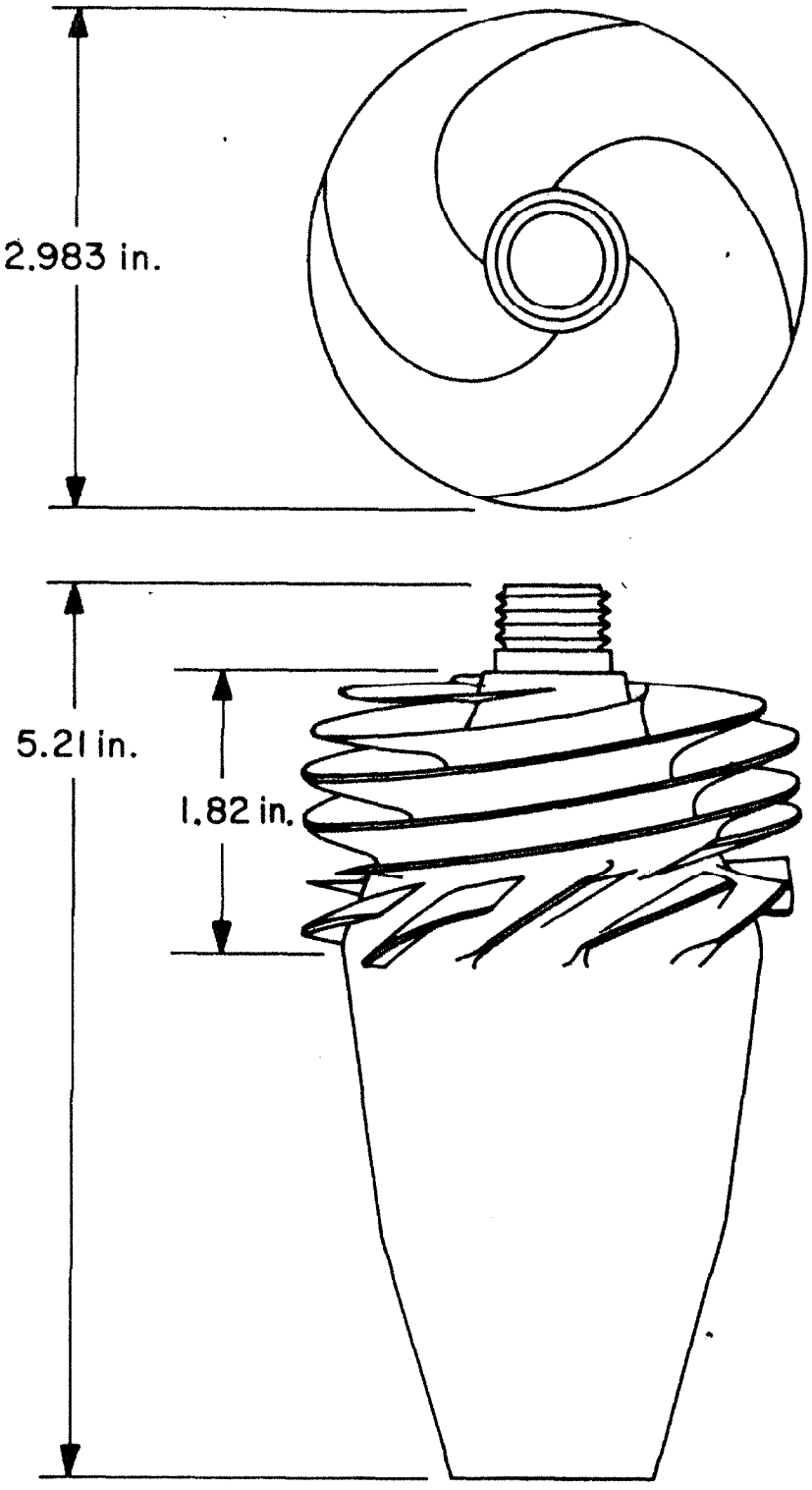

Fig. 2.10 Schematic drawing of Impeller IV.

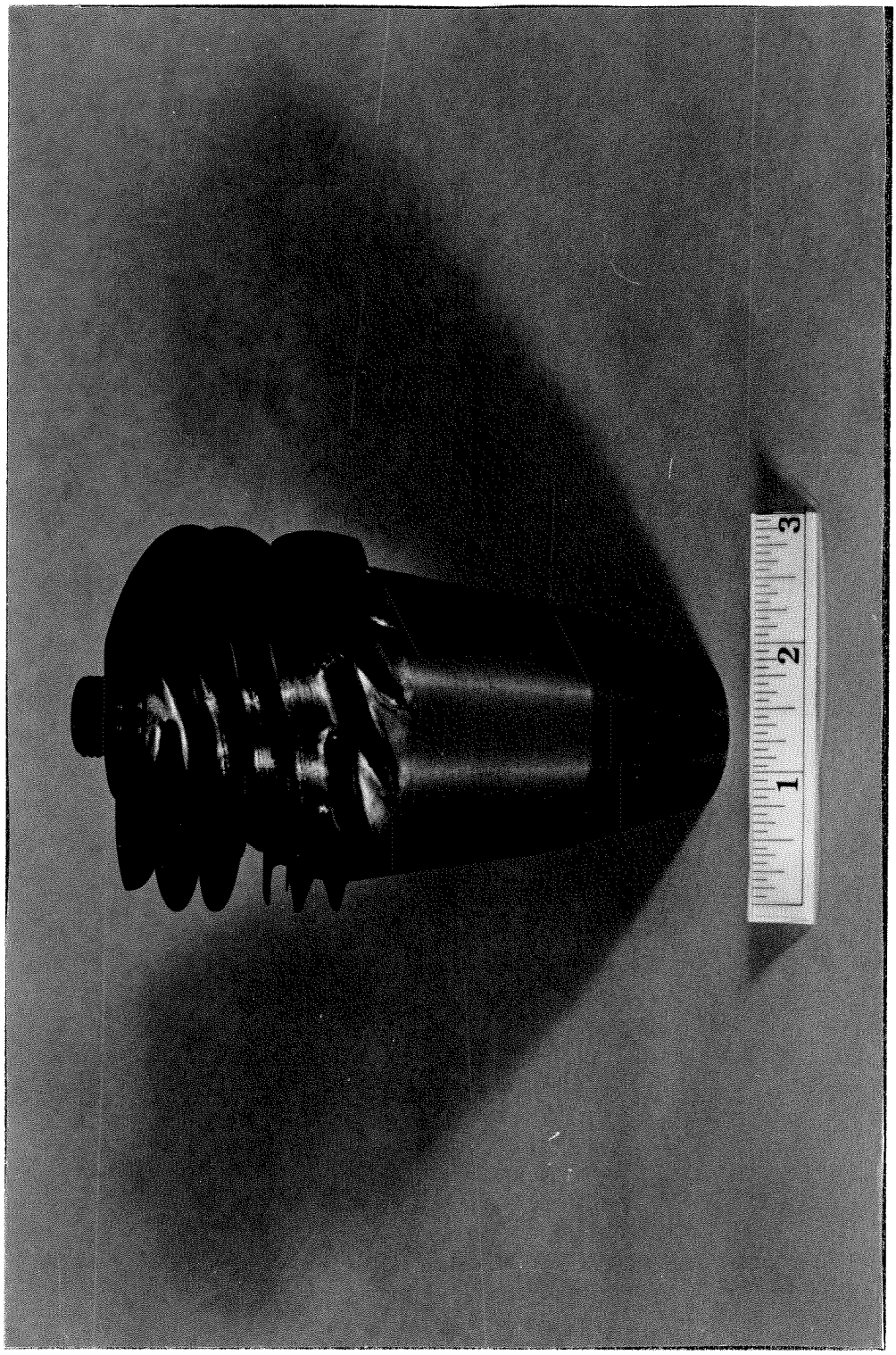

Fig. 2.11 Photograph of Impeller IV.

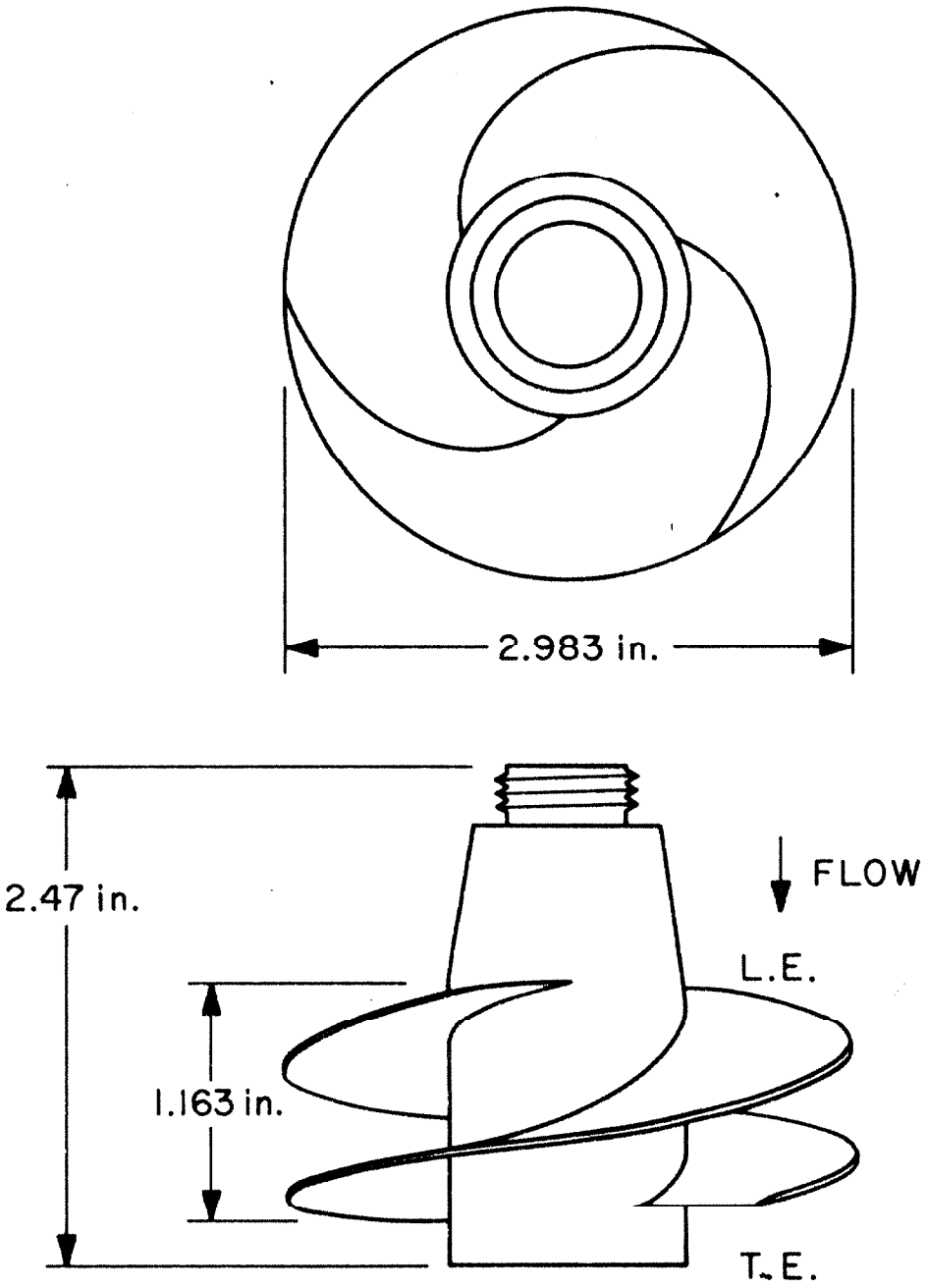

Fig. 2.12 Schematic drawing of Impeller V.

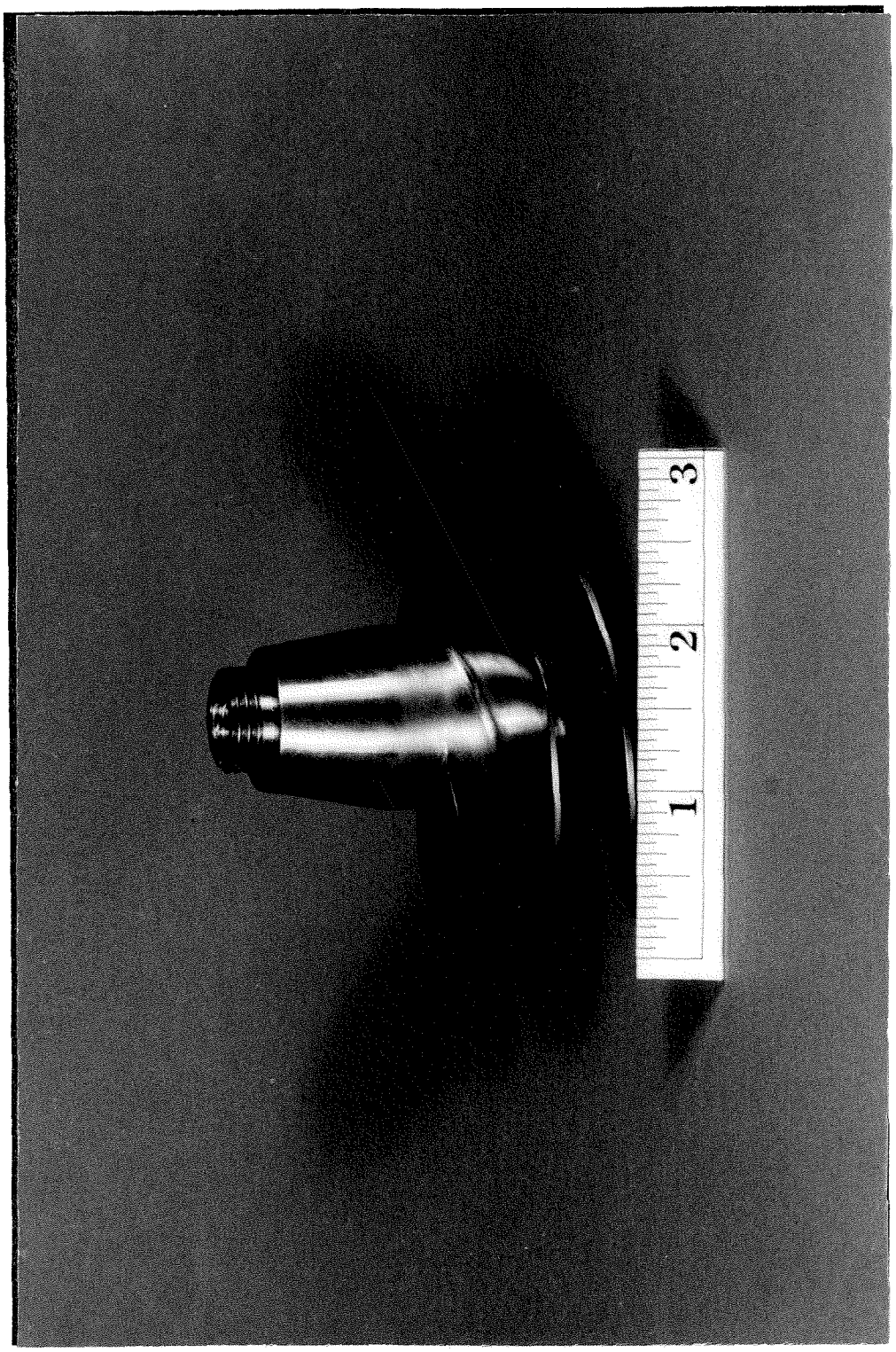

Fig. 2.13 Photograph of Impeller V.

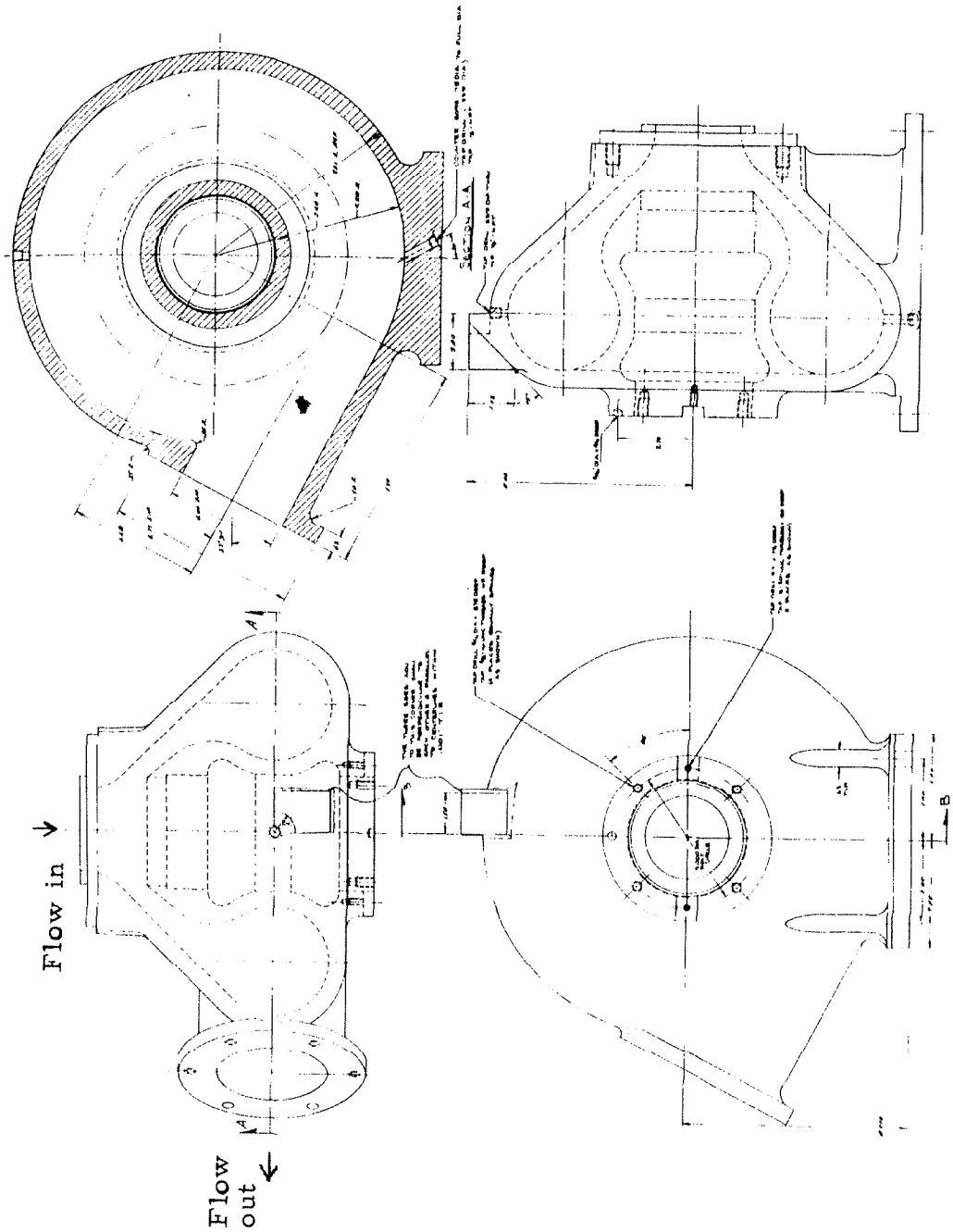

Fig. 2.14 Drawing of the pump volute.

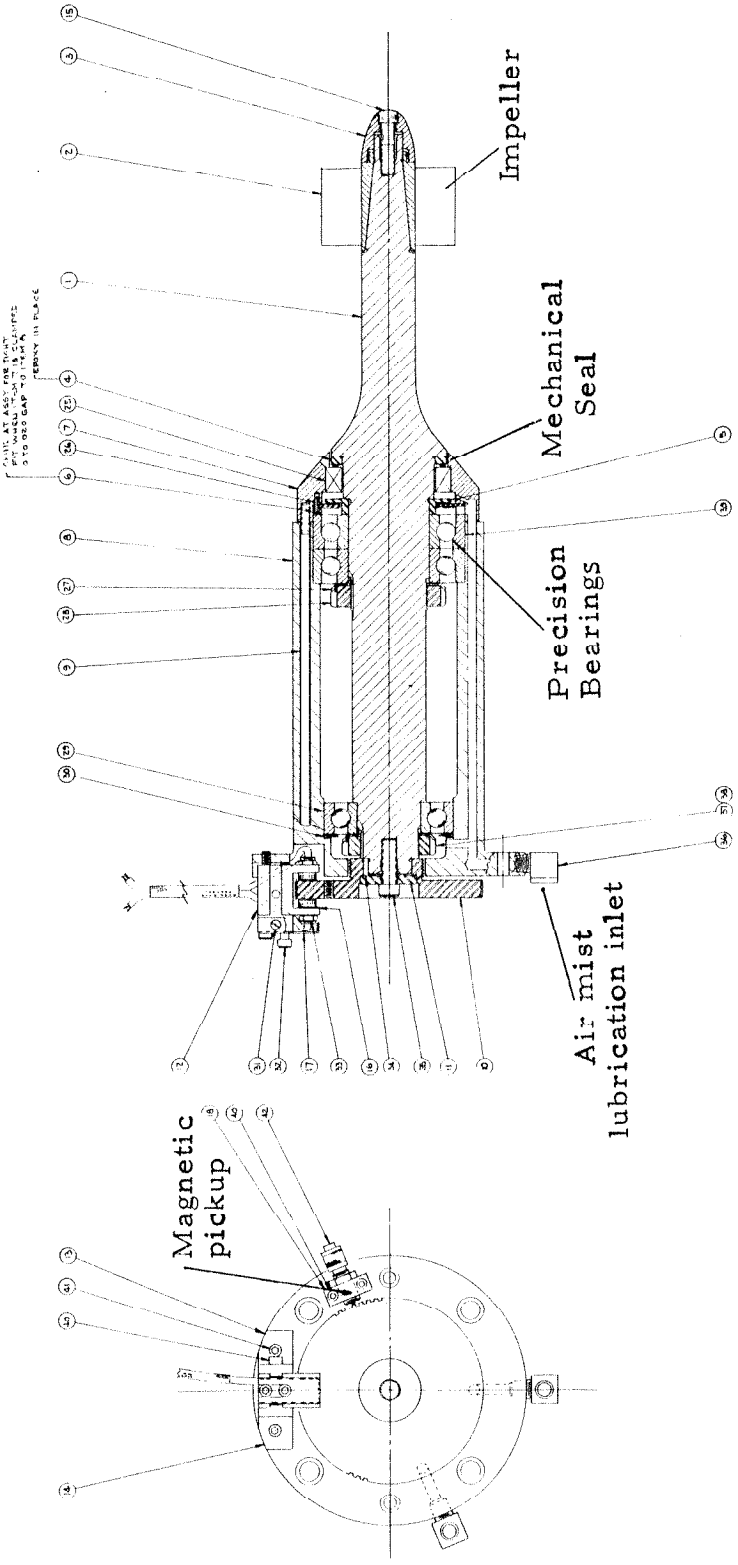

Fig. 2.15 Assembly drawing of the bearing cartridge.

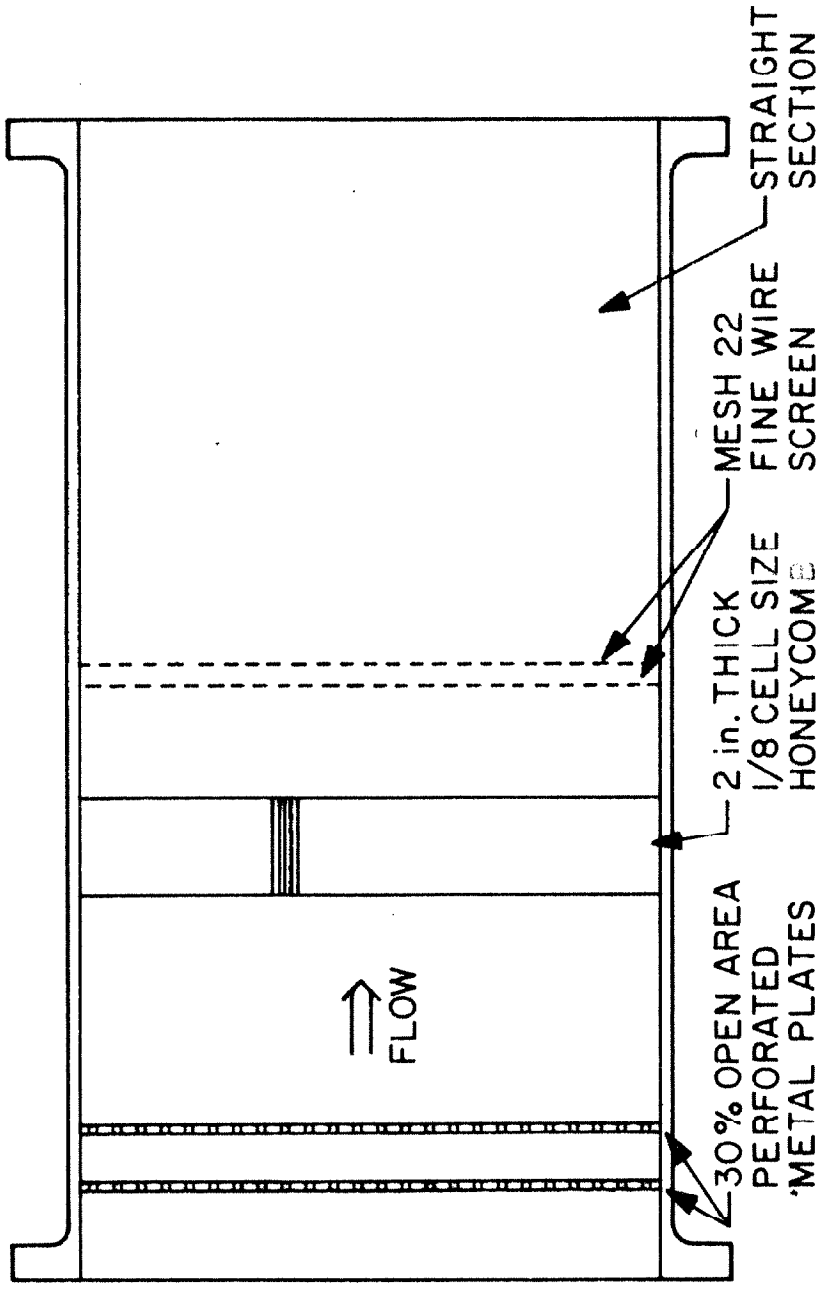

Fig. 2.16 Schematic drawing of the smoothing chamber.

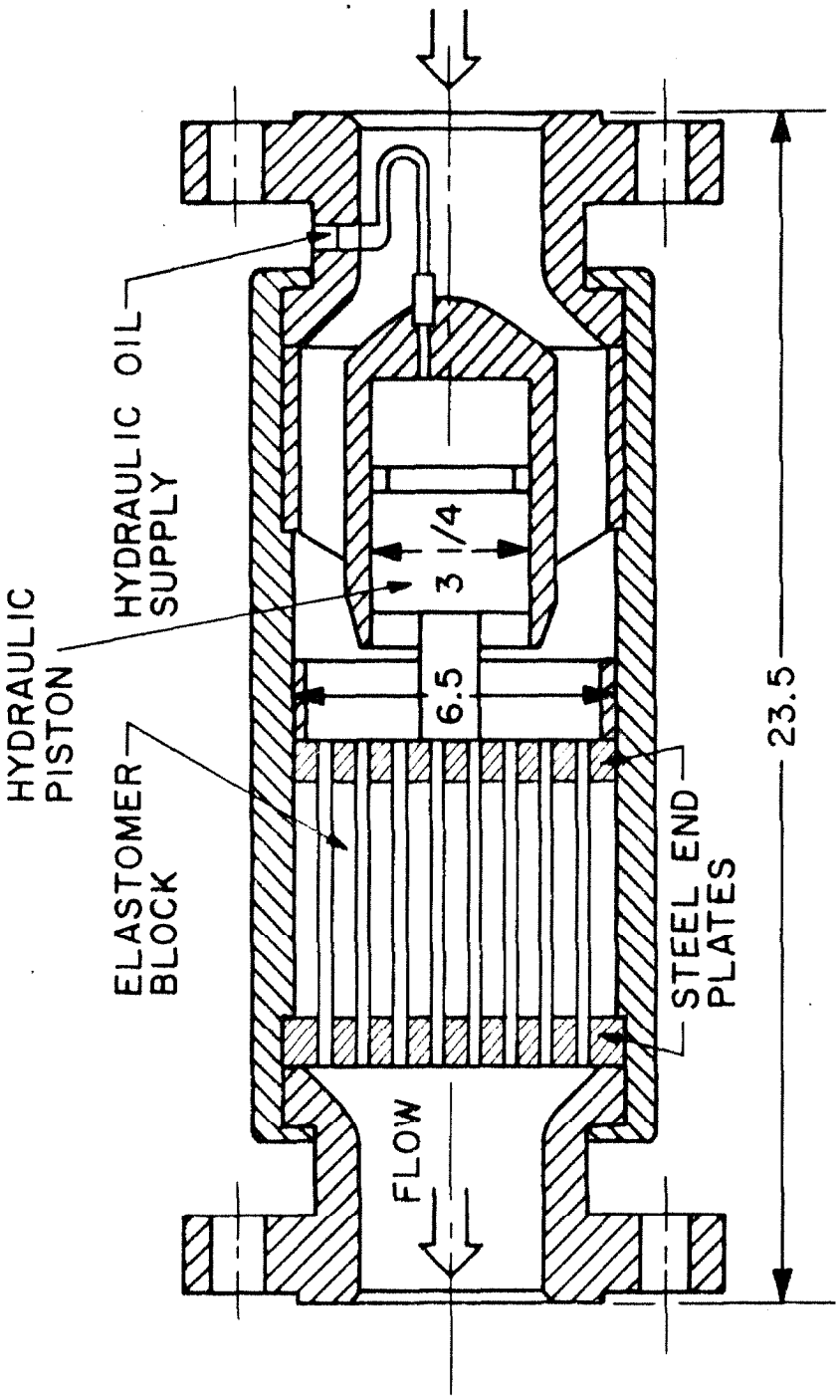

Fig. 2.17 Schematic drawing of the silent valve.

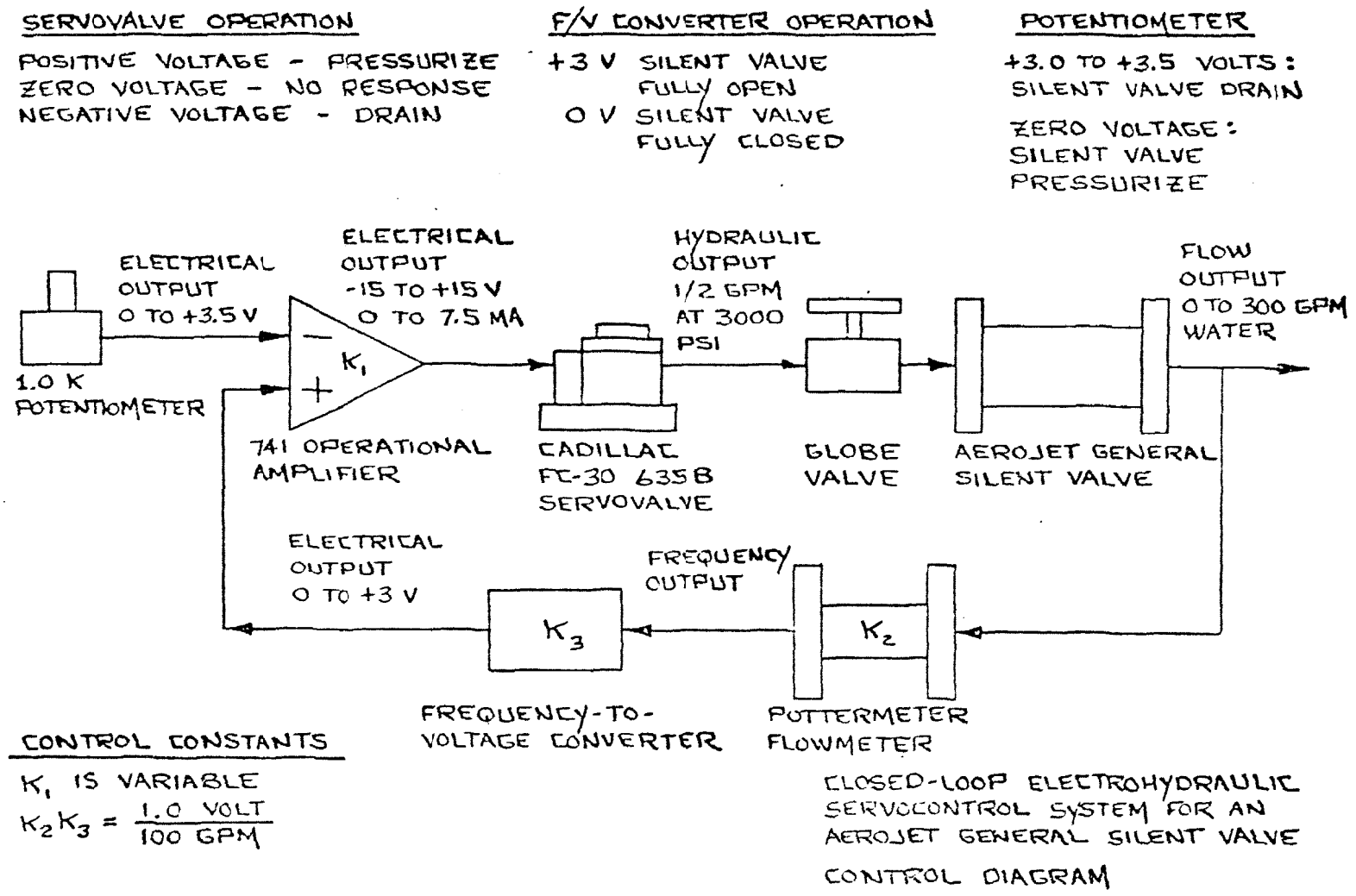

Fig. 2.18 Electronic feedback system of the silent valve.

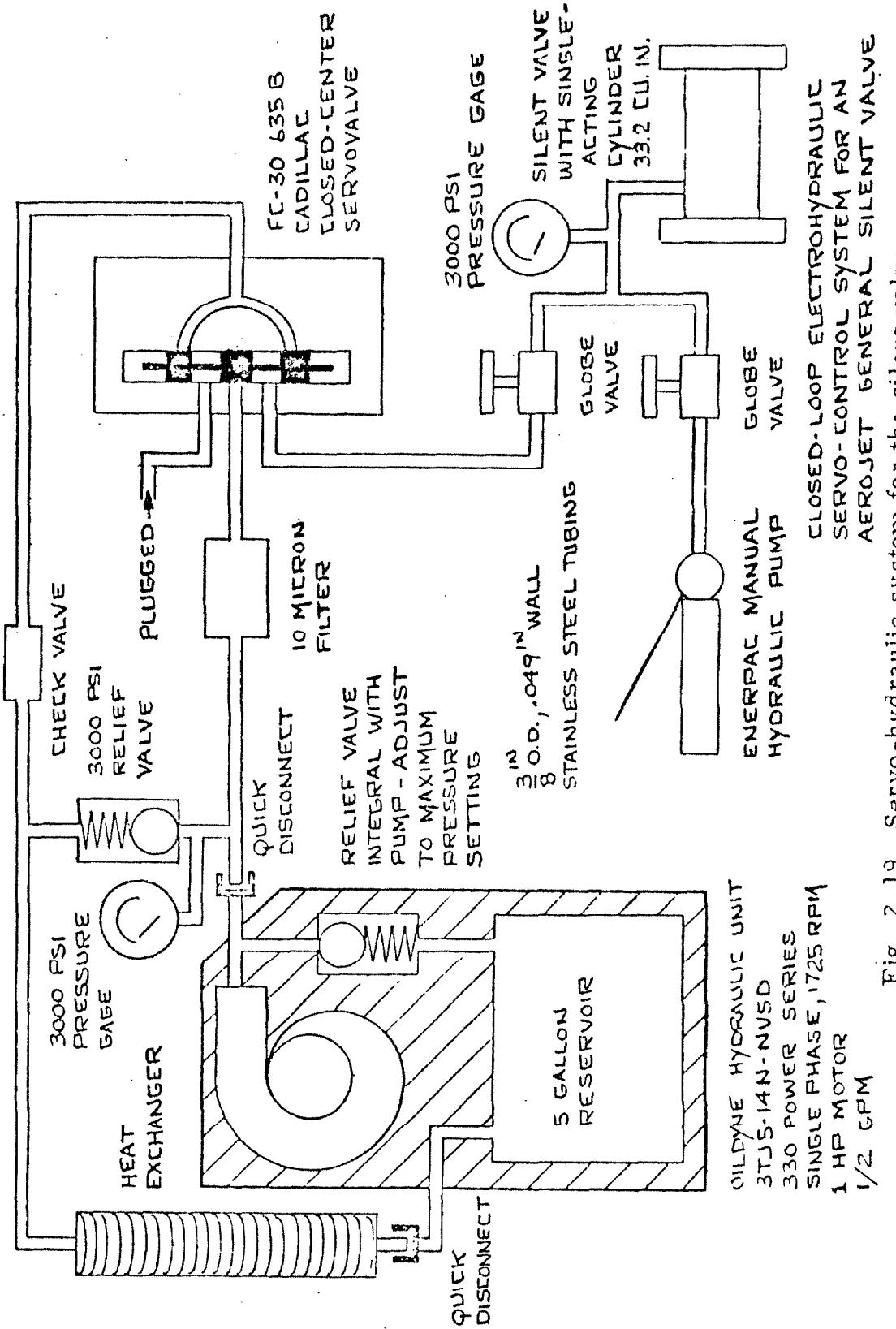

Fig. 2.19 Servo-hydraulic system for the silent valve.

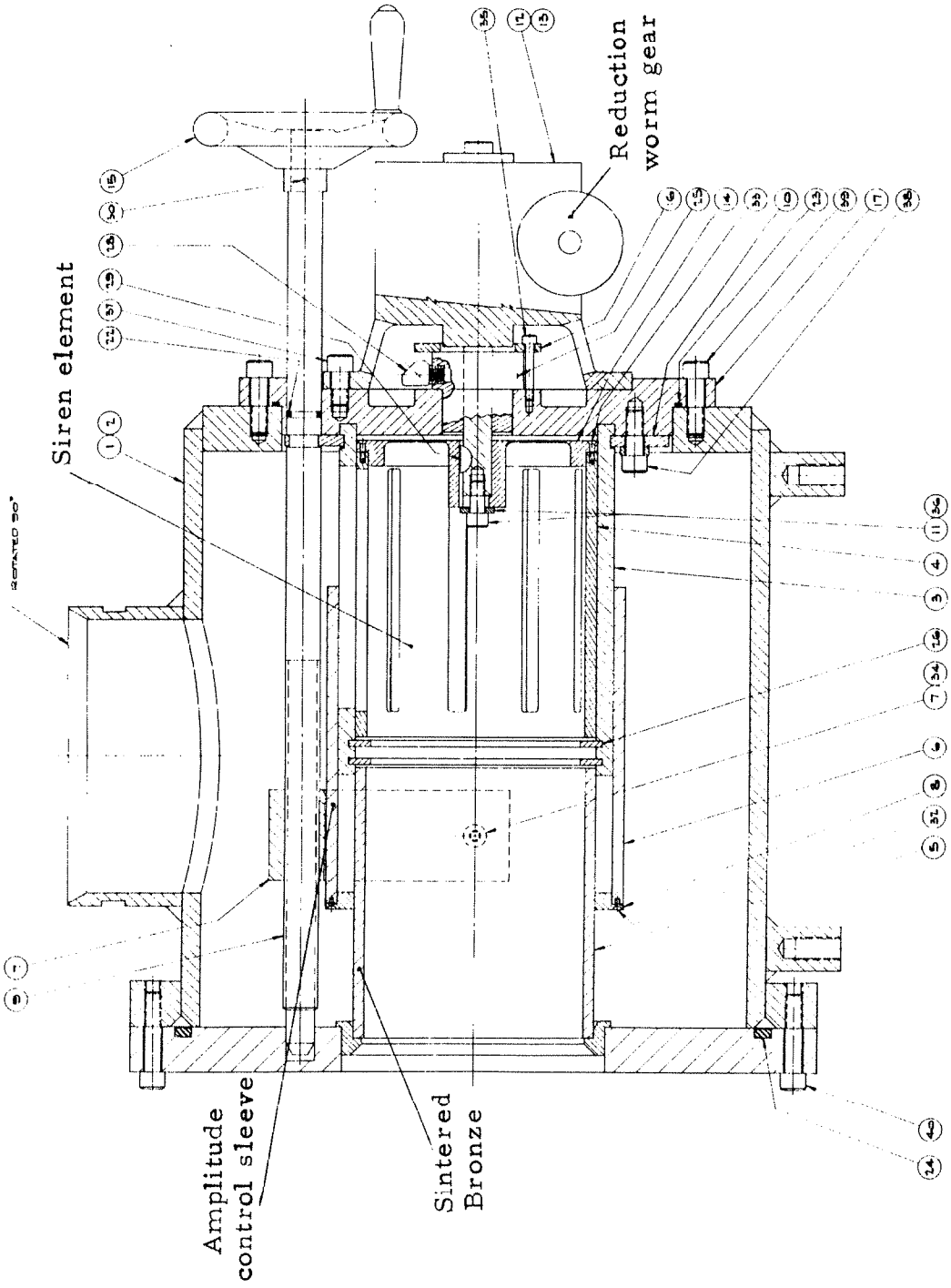

Fig. 2.20 Cross section of the fluctuator valve.

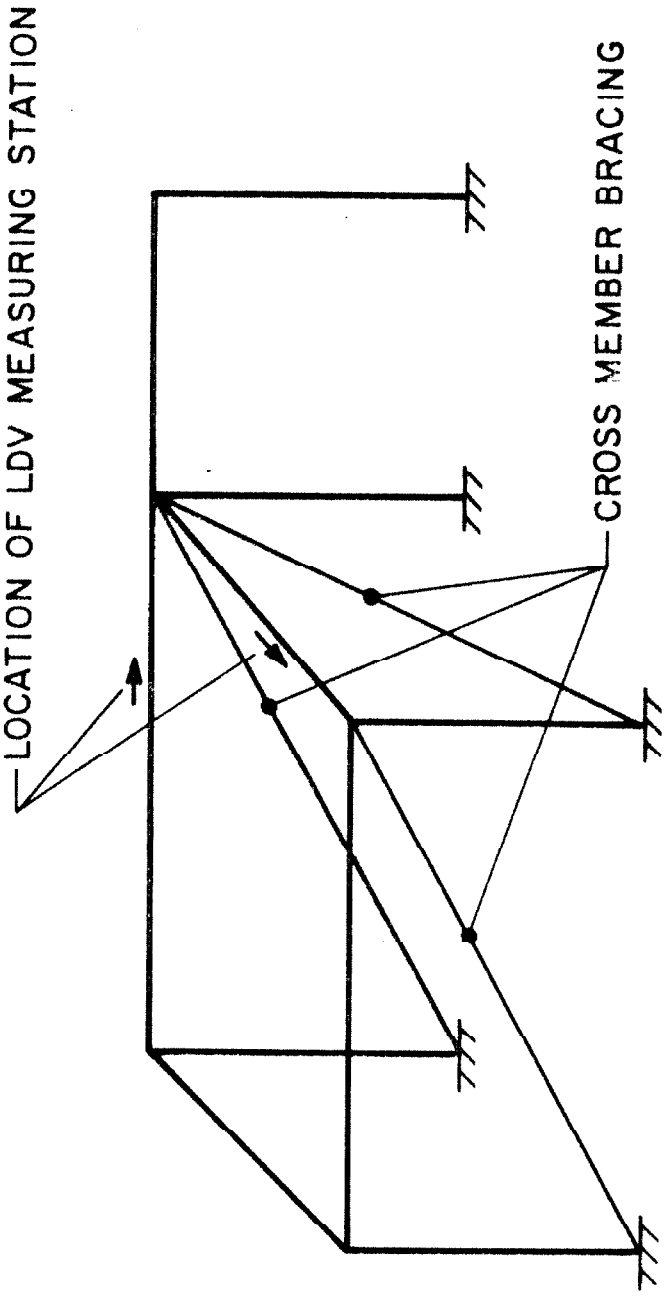

Fig. 2.21 Locations for the cross member bracing of the foundation.

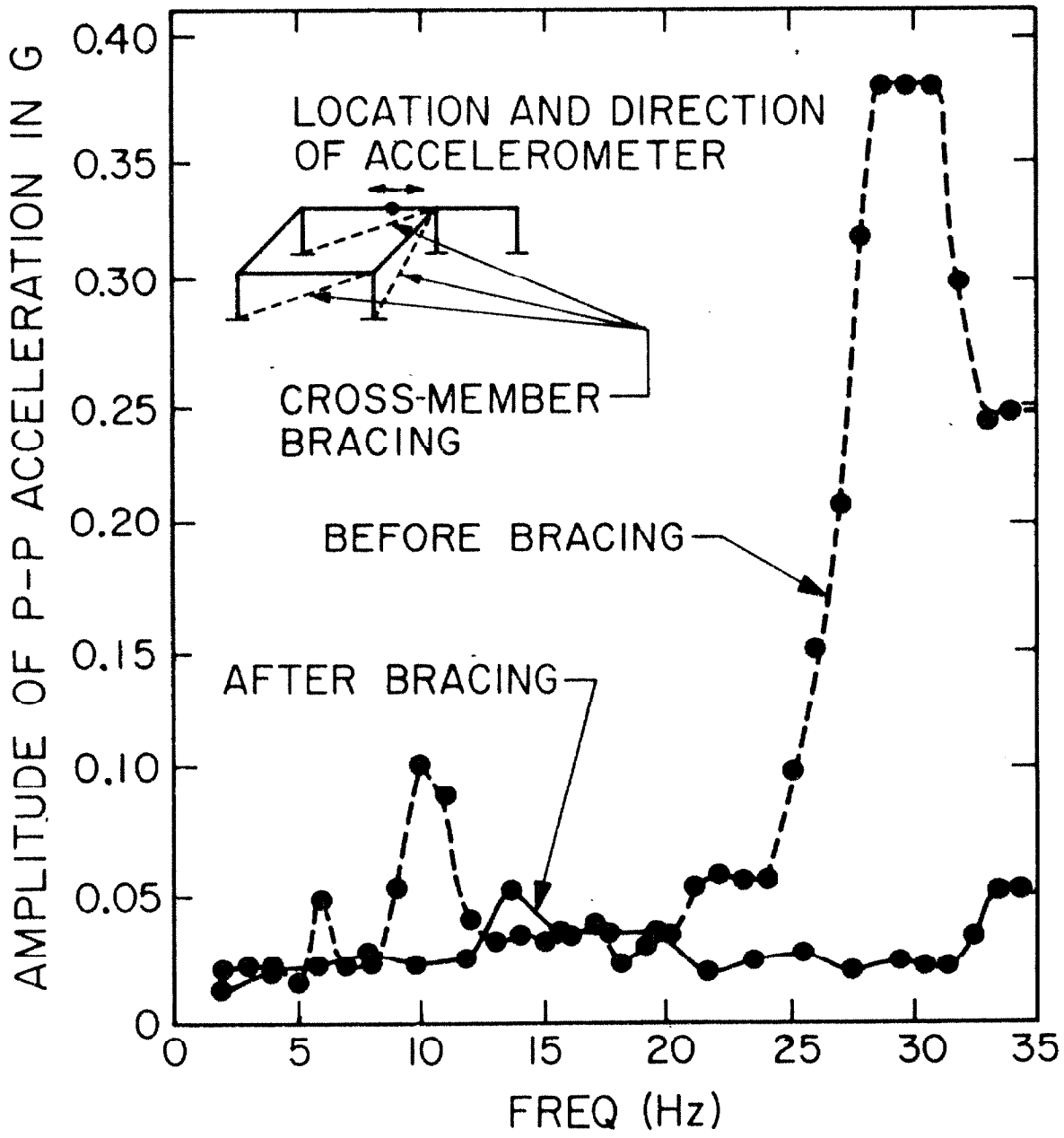

Fig. 2.22 Vibration level of the foundation in direction parallel to the pump axis.

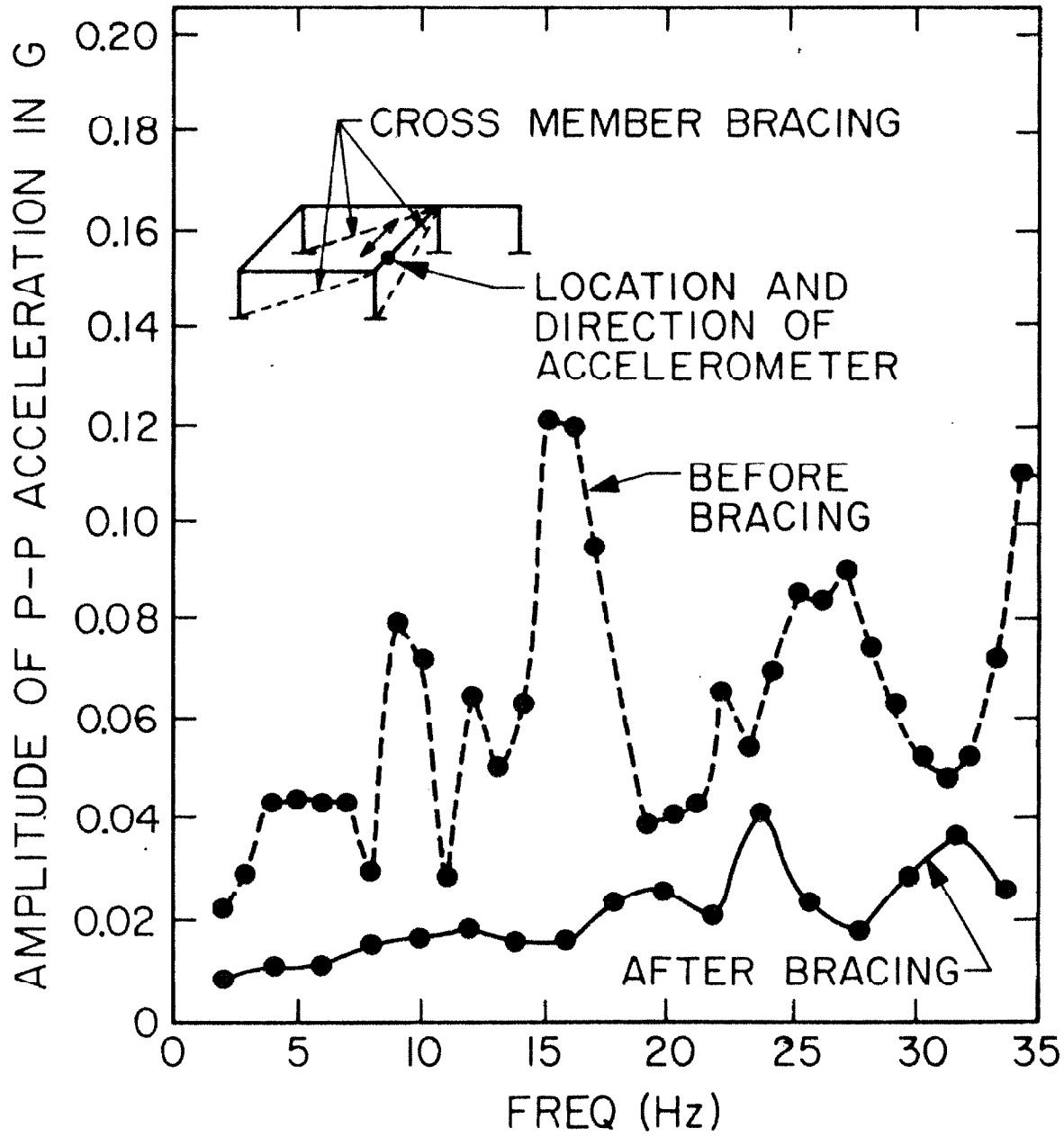

Fig. 2.23 Vibration level of the foundation in direction perpendicular to the pump axis.

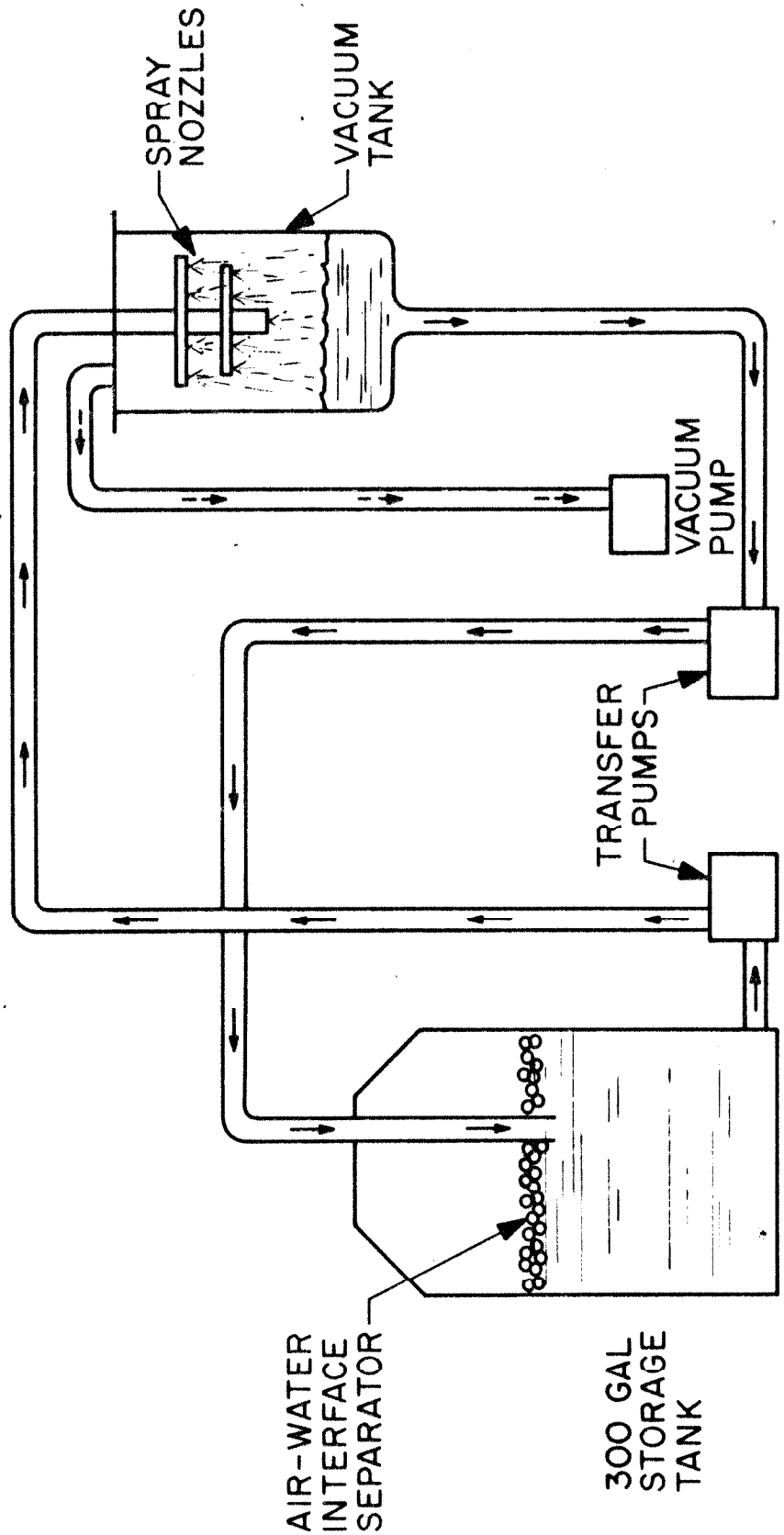

Fig. 2.24 Schematic drawing of the deaeration system.

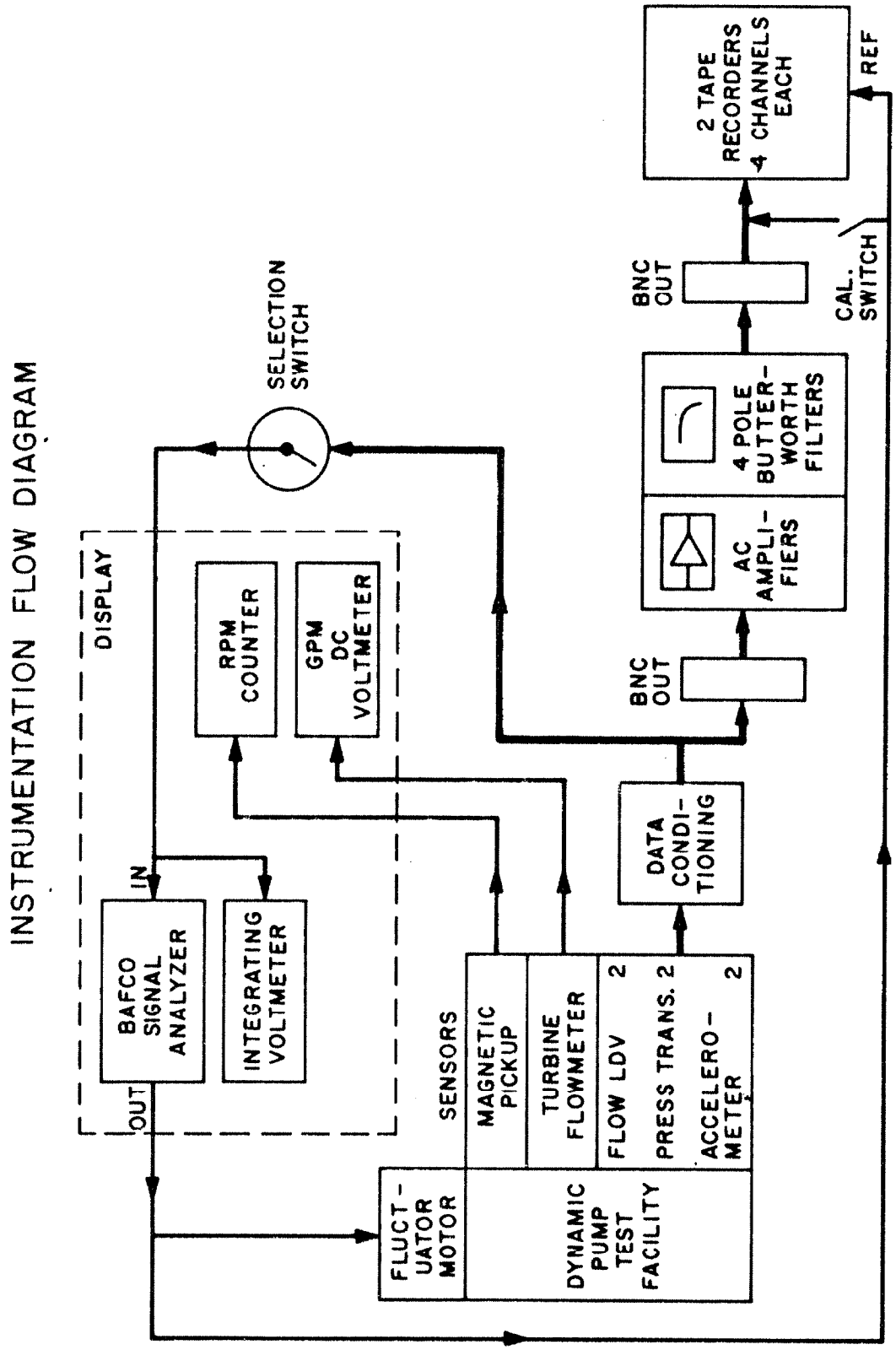

Fig. 2.25 Flow diagram of the instrumentation.

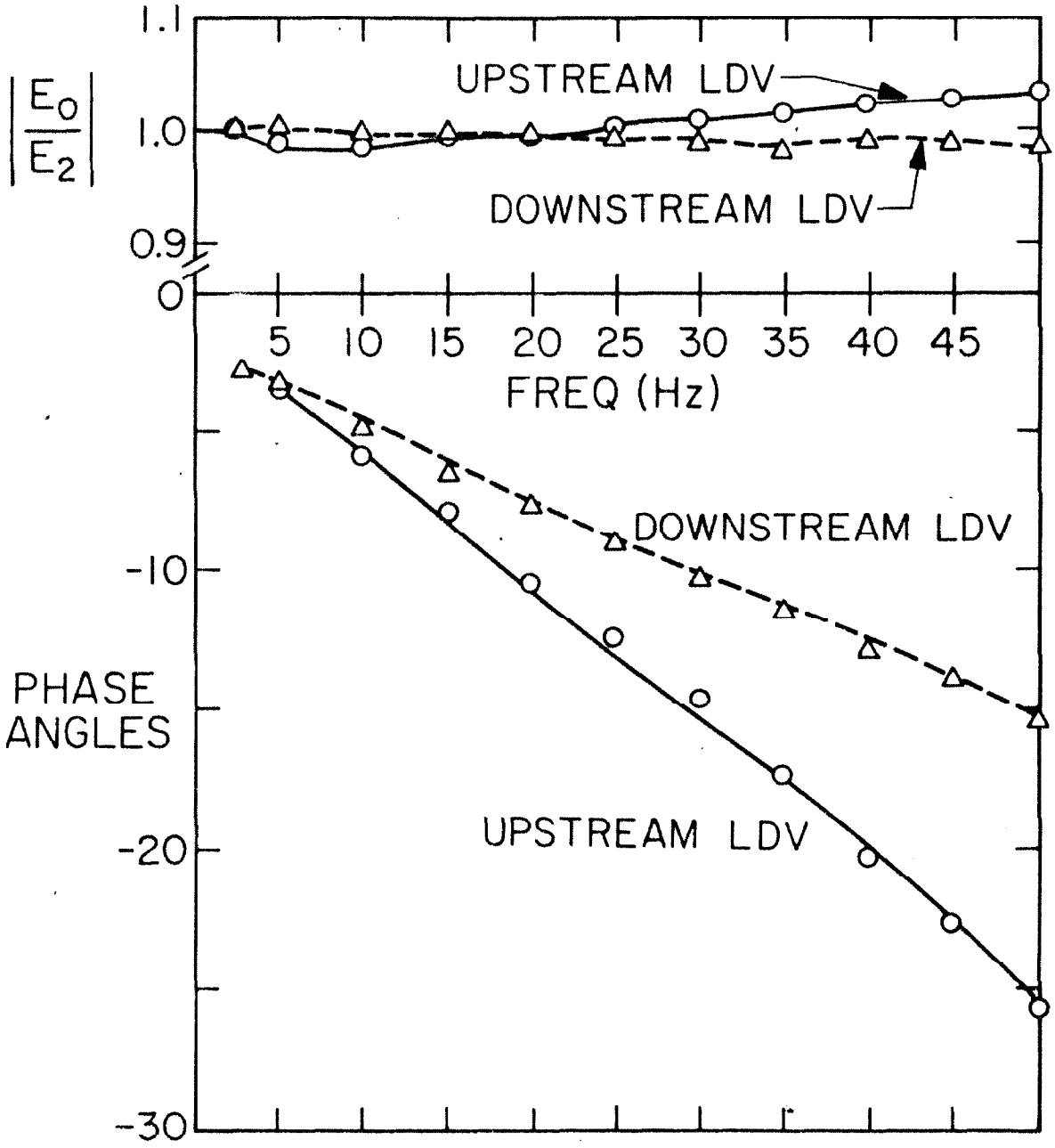

Fig. 2.26 Frequency response transfer functions of the two LDV systems.

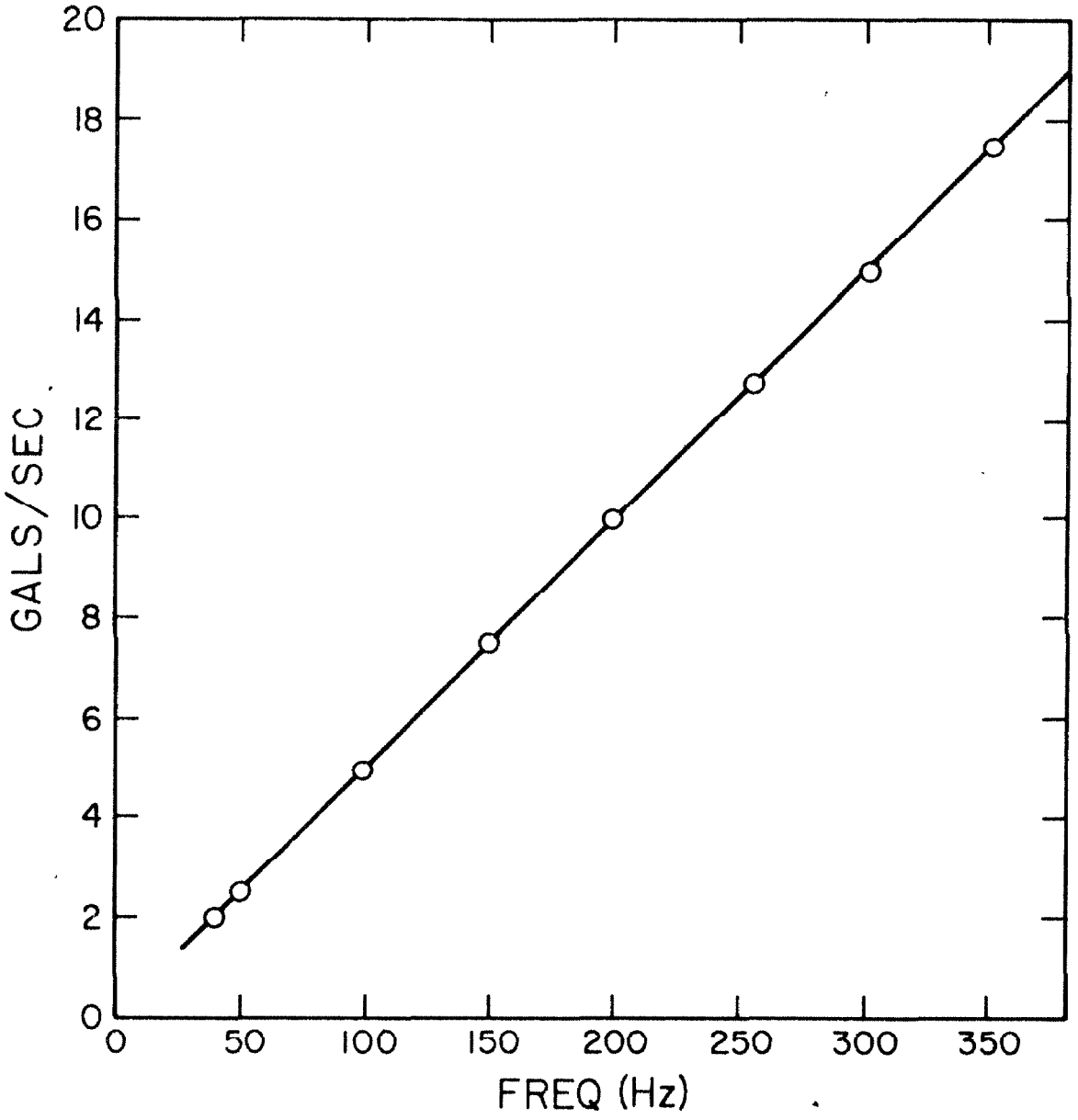

Fig. 2.27 Calibration curve of the Potter turbine flowmeter in water.

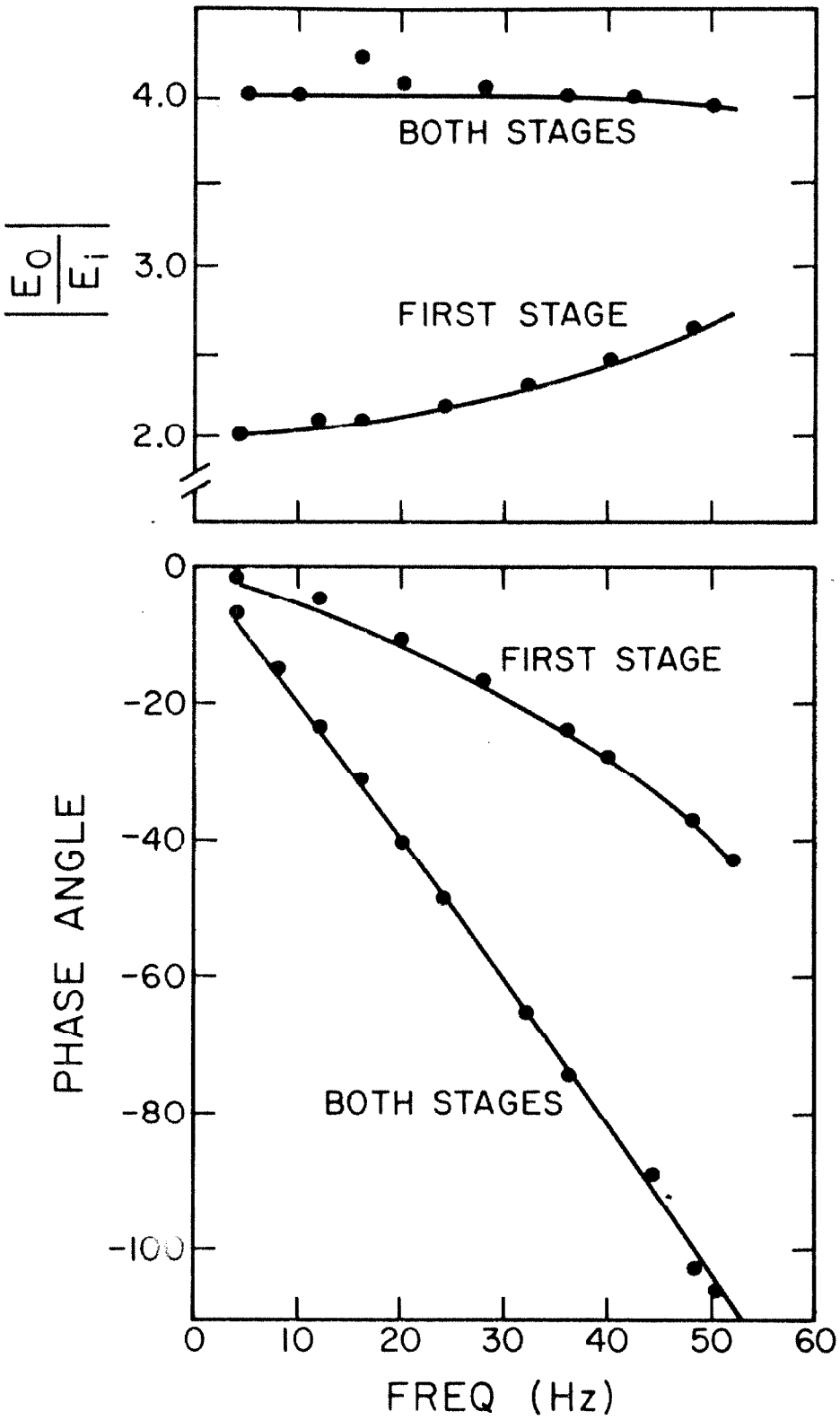

Fig. 2.28 Combined filter and ac amplifier frequency response transfer function.

III. EXPERIMENTAL PROCEDURE

Two types of experiments were performed, the steady and the unsteady experiments. The steady state experiment established the steady fully wetted and cavitating performance which in turn could shed some light on the unsteady performance of the pump. The unsteady experiment measured the transfer matrix for the inducer pump. As will be described in this and the following chapters, this matrix was measured both for fully wetted and cavitating flow.

3.1 Steady State Tests

3.1.1 Fully Wetted Performance

This experiment measured the performance of the inducer pump under fully wetted flow. The result will be expressed as the dimensionless head coefficient against flow coefficient. To avoid cavitation, the system was subjected to a high static pressure by pressuring the air bladder. The usual pressure used was about 40 psig as constrained by the design strength of the system. However, to achieve completely the fully wetted condition, the pump speed had to be kept under 6000 rpm.

During the experiment, a certain pump speed was selected. The flow rate as measured by the turbine flowmeter was varied by activating the silent throttling valve. The pressure rise across the impeller was read from a mercury water manometer connected across the system. From the pump speed, flow rate, and pressure rise across the pump, the head coefficient and flow coefficient could be obtained.

3.1.2 Cavitating Performance

The pump speed was kept at a constant value. The flow rate was also kept constant by activating the silent valve servo feedback system. The cavitating state was varied by adjusting the static pressure of the air bladder. In addition to the measurement of the pressure rise across the pump, the absolute pressure upstream of the pump was measured by a mercury manometer relative to atmosphere. A standard barometer provided the absolute reference. The head coefficient was plotted as a function of cavitation number for a constant flow coefficient.

3.2 Fluctuating Experiments

Before each fluctuating experiment, the following quantities had to be decided in advance. These were:

(a) Flow coefficient

(b) Cavitation number

(c) The values of fluctuating frequency. In this study, frequencies used were 4, 7, 14, 21, 28, 35, 42 Hertz.

(d) Pump rotative speed in rpm.

3.2.1 Preliminary Preparation

To begin the experiment in cavitating flow, the water was deaerated for a period of two to three days. This reduced the air content to a molar concentration of about three to four parts per million as measured by a dissolved oxygen meter.[1] After the water was brought up into

[1] Delta Scientific, Model 1010, Dissolved Oxygen and Temperature Meter

the test facility from the storage and deaeration system, it was circulated slowly around the loop for a few hours with the impeller running at a slow speed. These few hours of slow turning allowed enough time for the rotating seal to be wetted and for any air bubbles to float to the top and to be bled away. The heat exchanger cooling system was turned on during this period and cooled the water to a steady state temperature of about 68°F. The low temperature of water increased the solubility of air in water thereby reducing the release of dissolved air from water in the system. Such elaborate air content treatment was needed because it was suspected that the amount of air content played an important role in the inception of cavitation and in the development of cavitation in general. This procedure was not necessary for fully wetted experiments. The oil pump for the silent valve servo feedback control was switched on ready to control the flow rate. The last preparation was to check that the weak laser beam entered the photomultiplier pin hole.

3.2.2 Calibration

The calibration of the LDV is shown in Appendix B. To calibrate the pressure transducer, connections to the mercury manometers were bled to be free of air bubbles. These manometers were used for pressure transducer calibration as well as a supplementary system for steady pressure measurement. The pressure transducers were statically calibrated in place for each test by applying a pressure or vacuum to the air bladder. The vacuum readings were taken from the manometer and the high pressure readings were taken from a

precision Bourdon gauge. Typical calibration curves are shown in Fig. 3.1. The accelerometers were calibrated by orienting them relative to gravity in order to register signals corresponding to ± one g. The tape recorders were calibrated internally, then a reference sine wave with a given amplitude from the Bafco was recorded on all channels for calibration during playback. The recording speed was 15 in. per second. A slower recording speed would save the amount of tape used but would give a very unpleasant noise during playback in the voice channel which was used for identification. The reference sine wave signal used to drive the fluctuators was fed into the first channels of both recorders. The six fluctuating signals from the electronic low pass filter bank were connected to the second, third and fourth channels of the two recorders. Finally, the monitor outputs of the tape recorders were connected to the oscilloscope.

3.2.3 Test Operations

(i) The required steady mass flow rate which controlled the flow condition and the upstream pressure which controlled the cavitation number were calculated for a given inducer rotating speed. The main motor control was switched on and then adjusted to the desired speed. The flow rate was dialed from the variable resistance of the silent valve hydraulic control feedback system. The pressure of the air bladder was varied until the required upstream pressure was attained. The phase lock frequency was adjusted on both the LDV's processors until the doppler signal was properly locked by the phase lock loop. This concluded the steady state adjustments of the system.

(ii) For the fluctuating adjustments, the following items had to be decided in advance: the fluctuator combinations and the frequency of fluctuation. The necessity of several fluctuator combination sets was discussed in the introduction and system design. These fluctuator combinations usually consisted of three or four sets. They were: upstream fluctuator only; downstream fluctuator only; both fluctuators operating simultaneously with each one contributing about half of the required amplitude and lastly both fluctuators operating simultaneously with a phase shift from the last setting of 120 degrees.

(iii) To suit the amplitude requirement the Bafco output signal was dialed to a mid-range frequency of, say 20 Hertz; and the fluctuator motor was then switched on. About two minutes was needed for the fluctuator to reach its final speed. This was indicated on the phase error meter when it reached a null condition. For the particular fluctuator combination desired, the sleeve on the appropriate siren valves was adjusted until the upstream mass flow fluctuation had reached two percent amplitude level. This was determined by the percentage ratio of the vector sum of the in phase and quadrature component to the dc value of the mass flow. All these readings were taken from the upstream LDV. The setting which gave this condition would be used for all other frequencies with the same fluctuator combination. Although the other frequencies produced different amplitudes, they were of the same order of magnitude, proved to be within the linearity requirements and acceptable for data analysis.

(iv) The shut off valve from the oil pump to the silent valve was closed so that the oil pressure in the silent valve would be maintained

at the desired level and the pump speed was reduced to about 2000 rpm from the previously adjusted higher speed. This valve would then be reopened when the pump speed was raised again. This procedure was adopted for a faster silent valve response time because the oil pump did not have to pump from zero to full pressure when the valve was reopened. The whole maneuver attempted to minimize cavitation damage to the impeller as well as wear and tear to the system.

(v) The fluctuating frequency was then adjusted to the first required frequency. The pump speed was raised to the test speed after the fluctuators had reached the selected frequency. The silent valve shut off valve was reopened. The bladder pressure was readjusted to the desired value if needed. Air bleed valves were temporarily opened to let any trapped air to be bled away.

(vi) The two instrumentation recorders were turned on to record for two minutes at frequencies below 14 Hertz or one minute for frequencies above 14 Hertz as these were the times needed for the tracking unit to work properly during subsequent playback. During the recording time, all the dc levels of the velocities and pressures, which were indicated on an integrating voltmeter with a one second integrating time, were taken together along with the rotational speed and turbine flowmeter readings. Photographs of the impeller and oscilloscope traces were taken at this time if needed. After the recording was finished, the pump speed was slowed down to about 2000 rpm and the next frequency of fluctuation was dialed on the Bafco ouptut. After the fluctuator had achieved the set frequency, the same procedure as described

in this paragraph was repeated. This procedure was again repeated for all other frequencies.

(vii) Next, new fluctuator combination sets were chosen and implemented as mentioned earlier and followed by frequency adjustments, recordings, etc. After all the fluctuator combinations were completed and recorded, the experiment itself was finished.

3.2.3 Data Analysis Procedure

To begin the data playback from the recorders, the reference signal, which was recorded on channel one of the recorders, was connected through a low-pass filter to the tracking unit as described in Section 2.5.10. The recorded ac calibration signal was played and the output calibration knob of the recorder was adjusted. This was repeated for all channels.

The recorded signals which were the amplified, filtered ac signal of the velocity, pressure and acceleration were played back one channel at a time and their in-phase and quadrature voltage values relative to the reference on the tape were taken and written on tabulated data tables. Four random voltage readings of each recording were taken and their average value was computed and used. These ac values together with the dc values taken during the experiment were punched into computer cards to be processed by the computer.

3.3 Impeller V Experiments

The procedures mentioned in Section 3.2 were the final procedures developed and used for Impeller IV. Prior to these experiments

and during the development of the experimental methods, date were obtained on another impeller, the Impeller V. During that phase of the research, the data acquisition and reduction procedure were somewhat less refined. Thus, for example, there were no electronic filters to reduce the high frequency noise. Consequently a lower signal-to-noise ratio had to be analyzed by the Bafco signal analyzer. Tape recorders were not available at that time and all data processing had accomplished and logged in real time. This was done in the shortest time possible in order that the steady state conditions such as pump speed and flow rate did not drift away from the set value. Clearly the later data were better when the fluctuating quantities were recorded simultaneously and therefore analyzed at the same instant in time. An equally serious problem during the cavitating test is the possibility of small air bubbles accumulating in the downstream smoothing section despite frequent bleeding during an experiment. Although it is believed no such bubbles were actually collected, lengthy test times make this chance more likely. The experiments for Impeller V were carried out during the development of the entire system. Nevertheless the results for this impeller are of interest in their own right and will be presented in Chapter VI for a qualitative comparison with results from Impeller IV. However, for all the reasons mentioned, the reliability and accuracy of these data are lower than for the Impeller IV experiments.

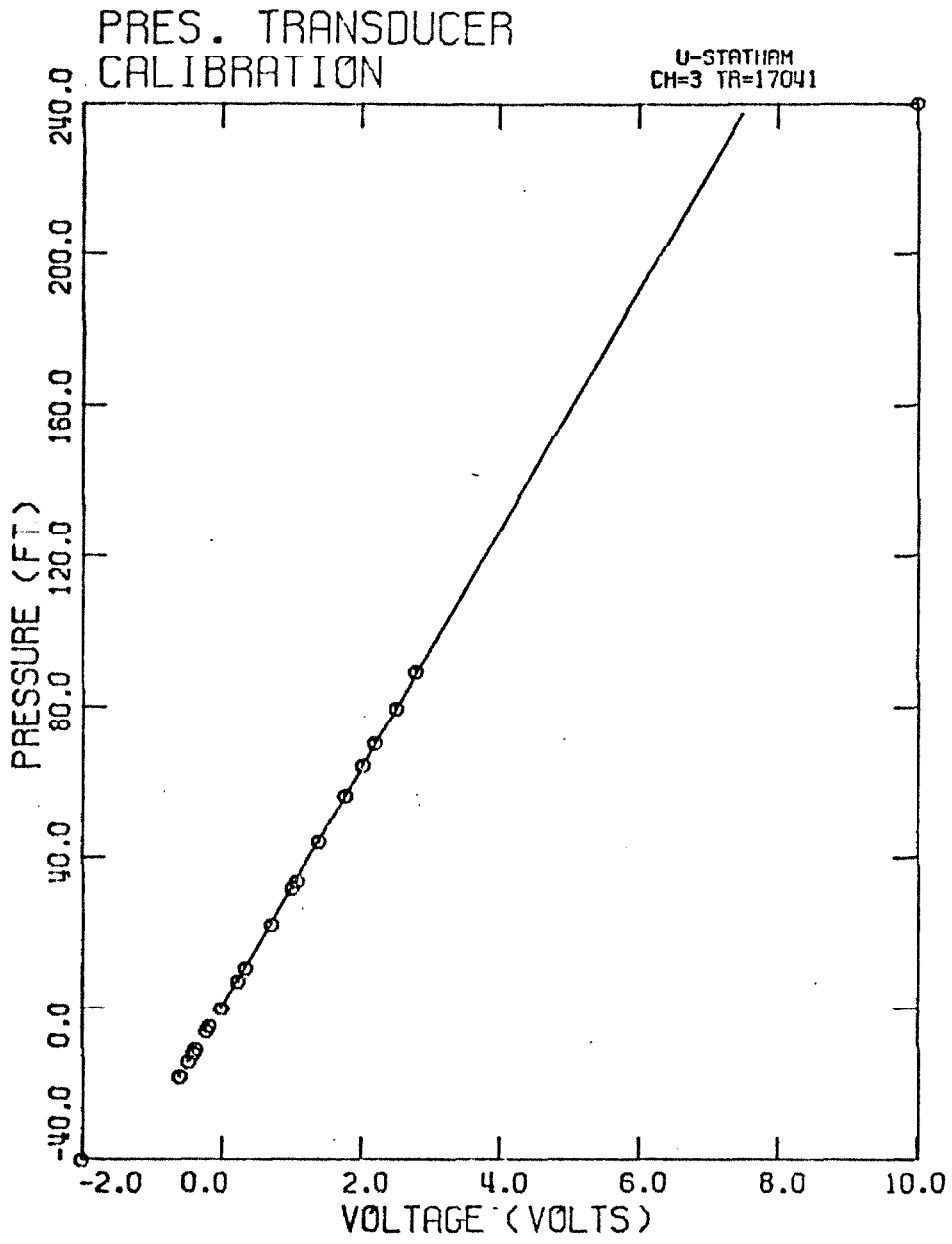

Fig. 3.1 Typical calibration curve of a pressure transducer.

IV. DATA REDUCTION

This chapter describes how the transfer matrix across the pump was calculated from the fluctuating pressure, velocity and acceleration measurements. The data reduction was done in three steps and these were accomplished by three computer programs. The necessity of three separate programs will be evident in the following description. Flow charts are provided in Appendix C. The first program, RAWDATA, calculated the required dimensionless groups using the voltage readings taken from experiment. The second program, TRANSCO, calculated a total transfer matrix between measuring stations and the last program, PUMA, reduced the total transfer matrix to the transfer matrix across the pump alone.

After playing back the recorded signals from the tape recorder, the following quantities were punched onto computer cards:

(a) calibration data for pressure transducers.

(b) acceleration calibrations.

(c) mean values of (i) rpm (pump speed in revolutions per min.).
(ii) gpm (flow rate in gallons per minute).

(d) the in-phase and quadrature voltage readings of upstream and downstream accelerometers.

(e) the dc, in-phase and quadrature voltage readings of the upstream and downstream laser doppler velocimeters.

(f) the dc, in-phase and quadrature voltage readings of the upstream and downstream pressure transducers.

The analysis was set up to process a batch of data at the same mean rotational speed, flow rate and upstream static pressure. This implied that the head coefficient, flow coefficient and cavitating number were identical. The cards were arranged in groups of the same fluctuator combinations following the experimental procedure and each of these groups contained data for a complete set of fluctuating frequencies.

4.1 RAWDATA Program

This program established the conversion factors of the instruments from voltages to the appropriate units. The pressure transducer and accelerometer calibration curves were calculated in the subroutine CALIB. The LDV velocimeter to volumetric flow rate conversion factors were obtained from comparing the dc voltage readings of each laser doppler velocimeter to the turbine flowmeter reading. All the above calculations were done in the MAIN program.

During the recording of the signals, all six of the ac signals passed through a bank of amplifiers and electronic filters. The effect of the amplifiers and the filters was corrected in the CORR subroutine. This subroutine also corrected for the transfer function of the LDV processor.

Based on the corrected in-phase and quadrature voltage readings and the conversion factors obtained, the following quantities were calculated:

(a) The upstream and downstream fluctuating pressures. They were expressed in feet of water for amplitude and degree for phase angle with respect to the sinusoidal reference signal.

(b) The upstream and downstream fluctuating mass flow rates. The in-phase and quadrature voltages were converted to velocities in feet per second in the four in. viewing sections. Since the LDV measured velocities in an inertial reference frame, the accelerometer readings were converted into velocities and subtracted from the LDV measurements. The calculated results were velocities relative to the structure. The amplitudes of the fluctuations in velocity, expressed as percentages of mean flow rate, were also calculated.

These eight quantities, upstream and downstream fluctuating mass flow rates and fluctuating pressures expressed in amplitude and phase angles were plotted against the frequency of fluctuation. These graphs were checked for smoothness of the data. Any data point which did not appear to fit into a smooth curve would be rechecked for errors in recorder playback, averaging process and/or key punching. Head coefficients, flow coefficients and cavitation numbers were also calculated based on the mean values of pressure, flow rate, and rotational speed.

The RAWDATA program finally calculated the fluctuating pressure, fluctuating flow rate and frequency in dimensionless form (see nomenclature). These computations were done in DIMGP subroutine. The calculated values were punched on computer cards; these cards had to be rearranged in groups of the same frequencies to be processed by the next program. However, within each group there was a complete set of different fluctuator combinations.

A subroutine COMP existed in the program to calculate the compliance and pump resistance as defined by Rubin. These were useful in

the beginning of the project to understand the measurements, especially in the fully-wetted experiment. However, these calculated quantities were not analyzed in the final stages of the project.

4.2 TRANSCO Program

The computer cards with the dimensionless pressure and mass flow rate values were reorganized in groups of the same frequency of fluctuation as mentioned in the last paragraph. The program treated the in-phase component as the real and the quadrature component as the imaginary part of a complex quantity. Then the TRANSCO program calculated a Z-matrix for each individual frequency using a special least-square fit process. The details of the least-square fit procedure are outlined in Appendix D. The real and imaginary parts of the elements of this Z-matrix were plotted as a function of frequency. Their values were also punched on computer cards to be processed by the next program. The TRANSCO program also had the capacity to calculate the Z-matrix using only a partial number of fluctuator combinations as long as the total number of combinations was greater than two. This was used in the fluctuator combination linear independency analysis as described in Section 5.7.

The Z-matrix so obtained was not the transfer matrix across the pump as will be discussed in Chapter VI; it actually represented the transfer matrix between the measuring stations. The differences between this Z-matrix and the matrix across the pump ZP consisted of the inertia of the water and compressibilities of water and structure situated between the measuring stations and the pump. A third program

PUMA was thus written to subtract the side effects and obtain the transfer matrix for the pump alone, defined as the ZP-matrix.

4.3 PUMA Program

This program reduced the Z-matrix obtained in the previous program to the transfer matrix of the pump alone. The transfer matrix between the measuring stations was assumed to be composed of three parts; the first part was the effect of the hydraulic system between the upstream measuring station and the beginning of the pump and this was expressed as an upstream matrix ZU; the second part was the effect of the pump itself and was expressed as the required pump matrix ZP and lastly the downstream matrix ZD was the transfer matrix connecting the end of the pump and the downstream measuring station. The contents of the ZU and ZD matrix were derived from dynamic fully wetted experiment and will be given in Chapter VI. The above mentioned ZU, ZD and Z-matrices which were calculated from TRANSCO program were used to calculate the required ZP pump matrix with the following scheme.

The three matrices ZU, ZD and Z were first transformed into YU, YD and Y matrices defined as

$$Y = Z + I \tag{4.1}$$

where I is the identity matrix. These Y-matrices had the normal transfer property that they satisfied the chain rule. Thus,

$$Y = YD \cdot YP \cdot YU \quad . \tag{4.2}$$

The YP-matrix was simply obtained from

$$YP = YD^{-1} \cdot Y \cdot YU^{-1} \quad . \tag{4.3}$$

The required pump matrix ZP was then obtained from

$$ZP = YP - I \quad . \tag{4.4}$$

All these processes were carried out in the PUMA program using specially written routines for complex value matrix manipulation. The real and imaginary parts of the elements of the ZP matrix were finally plotted as a function of frequency.

V. PERFORMANCE

5.1 Steady State Performance of the Inducers

5.1.1 Fully Wetted Performance

(I) Impeller III and V - The graphs of head coefficient against flow coefficient (for definition of these see nomenclature) for these two impellers are shown in Fig. 5.1. There is only a slight performance difference between the two impellers within experimental error although the Impeller V has swept back leading edges. The agreement with Acosta's (1958) two inch impeller upon which the design of the present impeller was based is excellent. The theoretical calculation by Acosta (1958) based on a nine degree straight cascade is also presented for comparison.

(II) Impeller IV - The graph of head coefficient against flow coefficient for Impeller IV, the quarter scale model of the low pressure oxidizer pump of the Shuttle main engine is shown in Fig. 5.2 with similar results for a 0.6 scale test impeller carried out by Rocketdyne (1974). It may be seen that the two curves are not the same. This is very surprising because these impellers are made from the same master tooling and the Reynolds number difference is insufficient to account for the discrepancy. The differences in the designs of the volutes may be responsible for this discrepancy.

5.1.2 Cavitating Performance

(I) Impeller V - The head coefficient against cavitation number curves for constant flow coefficient are shown in Figs. 5.3 and 5.4 for different pump speed. All the curves show that the head coefficient decreases as the cavitation number is reduced. This cavitation breakdown is more severe when the flow coefficient is lower. It can be seen from the curve that the slope at breakdown increases more rapidly for a lower flow coefficient.

(II) Impeller IV - A cavitating performance curve similar to Fig. 5.3 etc. for Impeller IV was not obtained because after the fatigue failure of Impeller III, we tried to reduce the operating time of Impeller IV to avoid material failure. Indeed the blade thickness of this impeller is particularly thin. However, a cavitating performance of the 0.6 scale test impeller as performed by Rocketdyne (1974) is given in Fig. 5.5 and the quarter scale model of Impeller IV is expected to perform similarly under cavitating conditions.

5.2 Fluctuating Quantities

Typical fluctuating quantities measured during fluctuating experiments are discussed here.

5.2.1 Fluctuating Velocity

Three typical curves of zero to peak amplitude velocity fluctuation expressed as a percentage of the mean flow are given in Figs. 5.6, 5.7 and 5.8. All these figures come from an experimental run with

Impeller V for a cavitation number of about 0.1. Each figure corresponds to operation under one fluctuator combination setting at various frequencies. Figure 5.6 corresponds to exercising the upstream fluctuator only; Fig. 5.7 corresponds to activating the downstream fluctuator only; and lastly Fig. 5.8 shows the velocity amplitude when both the fluctuators are operating. It can be seen that the amplitudes are all under four percent and mostly under three percent of the mean flow. The phase angles are all measured relative to the reference signal which drives the fluctuator motor.

5.2.2 Fluctuating Pressure

The fluctuating pressure amplitudes and phase angles for the same experiment described above are given in Figs. 5.9, 5.10 and 5.11. It can be seen that the zero to peak amplitude of pressure fluctuation is normally below 10 ft. of water. All the figures from 5.6 to 5.11 were actually used to calculate a ZP-matrix for experiment (3) in Section 6.1.

It is convenient at this point to clarify one very important point concerning the difference between oscillating static pressure rise and oscillating total pressure rise across the pump. Since the pressure transducer connections to the smoothing chambers were through a side port on the structure wall, the static fluctuating pressure rise is actually measured. However, from the unsteady Bernoulli equation this could be shown to differ from the total fluctuating pressure rise by a very small amount. The difference is represented by the term $U\,u'e^{j\omega t}$ and this is found to be small compared with $p'e^{j\omega t}$ in this

kind of flow where U is the mean flow and $u'e^{j\omega t}$ and $p'e^{j\omega t}$ are the fluctuating flow and fluctuating pressure respectively. Therefore, no distinction will be made between them in the present experiment.

5.3 Auto Oscillation

During the cavitating operation of the Impeller V, a self-sustaining oscillation of velocity and pressure sometimes occurred. This is not unlike the pogo oscillation encounters in liquid propellant rockets. The auto-oscillation may be an intermittent phenomenon of about two to three seconds duration or it may be a continuous phenomena. A typical photographic picture of the cavitation and the corresponding fluctuating velocity and pressure is given in Fig. 5.12 and the steady state condition when this occurs is shown in Fig. 5.3. In this particular case, the upstream fluctuating velocity reached an amplitude of 22 percent of the mean and the corresponding downstream amplitude was 27 percent. The fluctuating pressure rise was 47 ft. of water which was almost equal to the steady pump head rise of about 50 ft. and all these occurred at a frequency of 21 Hertz.

The boundaries of operating conditions when this occurs are not known precisely, but it usually occurred when there existed intensive backflow cavitation (as shown in photographs taken during the test) and the cavitation number dropped below 0.1. However, the auto-oscillation usually died down when the cavitation number was sufficiently low so that the impeller suffered a complete cavitation breakdown.

5.4 Pump Speed Variation

The variation of the pump speed to the fluctuating flow on the inducer is important because a change in the pump speed means a change in the angle of attack and this introduces one more variable to the problem. The mean speed of the electric motor varied less than 0.8 percent about the preset speed. This drift was usually less than 0.5 percent as measured by the frequency counter.

The magnetic pickup output was connected to a frequency to voltage converter with an output proportional to the pump speed. The voltage proportional to pump speed was displayed on the oscilloscope and shown to have a definite fluctuation at low fluctuating frequency. A typical value was 0.1 percent rpm fluctuation at 5 Hertz when the upstream mass flow fluctuation was about 2 percent. At frequencies higher than 10 Hertz, the pump speed variation was too small to be measured and is thought to be less than 0.05 percent.

From the analysis by Brennen and Acosta (1975), this pump speed variation effect is negligible. This is because the percentage pump speed variation is to be compared to the dimensionless group $\frac{p_u}{\rho U_{tip}^2 \sigma}$ as defined in their paper. This numerical group when evaluated for this experiment had a typical value of 30 percent which is much higher than the measured 0.1 percent.

5.5 Pressure Drop Across the Smoothing Chamber

The pressure transducers were attached on the walls of the smoothing chambers. In the parametric evaluation of the system as

will be discussed in Chapter VI, it is assumed that there was uniform pressure within the smoothing chamber. Only a small pressure drop was expected due to the effects of the perforated metals, honeycomb and screens.

The steady pressure drop across the chamber was measured by a carbon tetrachloride water manometer for flow rates within the experimental range (Fig. 5.13). It can be seen that this steady pressure drop was very small. To verify that the fluctuating pressure drop was also small, two pressure transducers were attached on the first half and the second half of the smoothing chamber to measure the pressure drop across the perforated metals, etc. During a typical flow of 180 gpm and an axial velocity of about 0.5 ft/sec inside the chamber and a 2 percent mean speed fluctuation, there was no measurable steady pressure difference above 0.2 psi and no fluctuating pressure difference above 0.2 psi amplitude. These values are the accuracy limit of the dc voltmeter and Bafco signal analyzer. This demonstrated that the fluctuating pressure drop across the smoothing chamber was negligible and that the pressure within the chamber could be assumed uniform.

5.6 Accuracy of the Result

To assess the accuracy of the measured elements of the transfer matrix, three essential points will be discussed here. These are: the accuracies of the instruments themselves; the capability of the signal analyzer to analyze signals with a high noise content; and the stability of the data reduction procedure which is needed to know how sensitive the calculated transfer matrix was when subjected to a small change in one of the input quantities.

The laser doppler velocimeter and pressure transducer systems, (including the transducer itself and the associated balancing unit and amplifier) had a typical linearity of 0.01 percent. This linearity, which came from the frequency-to-voltage converter for the LDV and came from the amplifier for the pressure system, is needed to determine the accuracies of the measured fluctuating quantities. The noise level of the pressure transducer systems was 0.1 percent whereas the LDV had an electronic noise of 0.2 to 0.5 percent as determined by measuring the noise at a no-flow condition. The tape recorders had a typical accuracy of 1 percent. The total accuracy thus far is about 1.5 percent.

Typical oscilloscope pictures of the signal traces during a fluctuating flow condition are shown in Fig. 5.14. It can be seen that the fundamental frequency was marred by higher harmonics and flow noise. This is more apparent at the lower frequency of fluctuation where the excitable higher frequencies are still within the response range of the hydraulic system and the measuring instruments. The nearly square wave traces at the low frequency are due to the design of the fluctuators as mentioned in Section 2.4.7. However, these signals introduced random fluctuation on the readings from the Bafco analyzer and this represented the noise rejection capability of the analyzer. Typically this scatter was less than 6 percent of the readings and the reading itself had an accuracy of 1 percent. Thus, the values of the measurements to be processed by the data reduction procedure had a maximum error range of 9 percent of the value.

As mentioned in Chapter IV, the data reduction procedure first corrects the data for the effect of filters and amplifiers from their combined dynamic calibration curves. These curves were measured to an accuracy of 1 percent. To investigate the stability of the least square fit procedure in calculating the transfer matrix, a test data sample was supplied to the program. The stability of the procedure was determined by perturbing the elements of the data sample and the procedure was considered stable if the corresponding perturbed transfer matrix only changed by a proportionately small amount. It was found that the procedure was stable. Thus, it was concluded that the overall accuracy of the calculated transfer matrix was about 10 percent.

5.7 Linearly Independent Data Sets

The TRANSCO program used data from a number of different fluctuation settings to calculate the required Z-matrix. Since the program required only a minimum of two sets, we could use a partial number of total combination sets to calculate the Z-matrix for experiments which involved more than two fluctuator settings.

To demonstrate this, let us take an experiment where three fluctuator combinations were used; these were:

(A) Upstream fluctuation only

(B) Downstream fluctuation only

(C) Upstream and downstream fluctuation together.

We can produce four different Z-matrices by using the following combinations:

(α) A + B + C	(γ) A + C
(β) B + C	(δ) A + B

A sample of this is given in Fig. 5.15. The data showed a wide scatter for different choices of combinations. The first combination (α) is considered the most meaningful one since it comprises all the sets and thus is the total average. It was observed that although the scatter is wide, the Z calculated from the combination (δ), A+B, is always closest to the total average. That is, the best partial combination comes from using the purely upstream fluctuator and purely downstream fluctuator actions. This result is because purely upstream and purely downstream fluctuations produce the two most linearly independent sets of data. The result which is farthest apart from the total average result is the combination γ. This γ combination consisted of set A, upstream fluctuator alone and set C, both fluctuator functioning. This is because the pressures and mass flow rate response of the two fluctuators functioning is dominated by the upstream fluctuator action. This means that the two fluctuators' combined action is a very close resemblance to the set A. This will be clear when comparing the pressure and mass flow rate between Fig. 5.6 and Fig. 5.8 also between Fig. 5.9 and Fig. 5.11. Consequently results from the A and C sets are not as linearly independent as the other combination thus the data show a wide scatter.

This linear dependency is also demonstrated in the denominators in the equations calculating the Z elements in the least square fit procedure (see Appendix D). The denominator is a measure of the degree of dependence of data sets. It will be zero for linearly dependent sets. In the examples given in Fig. 5.15, it was found that the combinations involving single fluctuators had the maximum denominator.

A simple analogy to the above discussion is in the fitting of points to a straight line. In most of the cases, the two farthest points usually define the best straight line.

5.8 Linear Transfer Matrix Assumption Test

One of the basic assumptions in the present study of the dynamics of cavitating pumps was that all the velocities and pressure fluctuations were small. They should be small enough that they are small departures from the mean state and a linear transfer matrix may be defined. This was investigated by carrying out two types of tests at medium cavitation number.

The first test was an "amplitude" test in which we tried to verify that if the amplitude of one fluctuating quantity was increased by a certain amount, all of the other associated fluctuating quantities would increase proportionally. For the conditions chosen this appears to be the case for a sample graph shown in Fig. 5.16. Transfer matrices calculated from different amplitudes of fluctuation but with the same steady flow and cavitating condition showed that the values of the elements were the same for all amplitudes within experimental error.

The second test invoked directly the property of a linear system that the transfer function of a linear system at a certain frequency has the same value whether it is measured with a pure sine wave signal or whether this frequency is imbedded in noise with other frequencies present. The signals in the present experiment approximate a square wave and therefore there was a high third harmonic content in addition to the fundamental. It was possible in the present system to measure the

transfer matrix of the third harmonic of the command signal using the special frequency multiplier capability of the Bafco signal analyzer. The third harmonics of the four Hertz and seven Hertz fundamental were chosen for measurement (frequencies of 12 and 21 Hertz respectively). The elements of the transfer matrix for these values were calculated and are compared with the transfer matrix measured from the fundamental in Fig. 5. 17. The occasional wide departure probably occurs because of the low signal to noise ratio due to the low level of the third harmonic signal. The low third harmonic content is shown in Fig. 5. 14 (these traces with a fundamental frequency of 7 Hertz were used to analyze the 21 Hertz behavior shown in Fig. 5. 17). These two tests confirmed that the linear assumption was justified in this experiment.

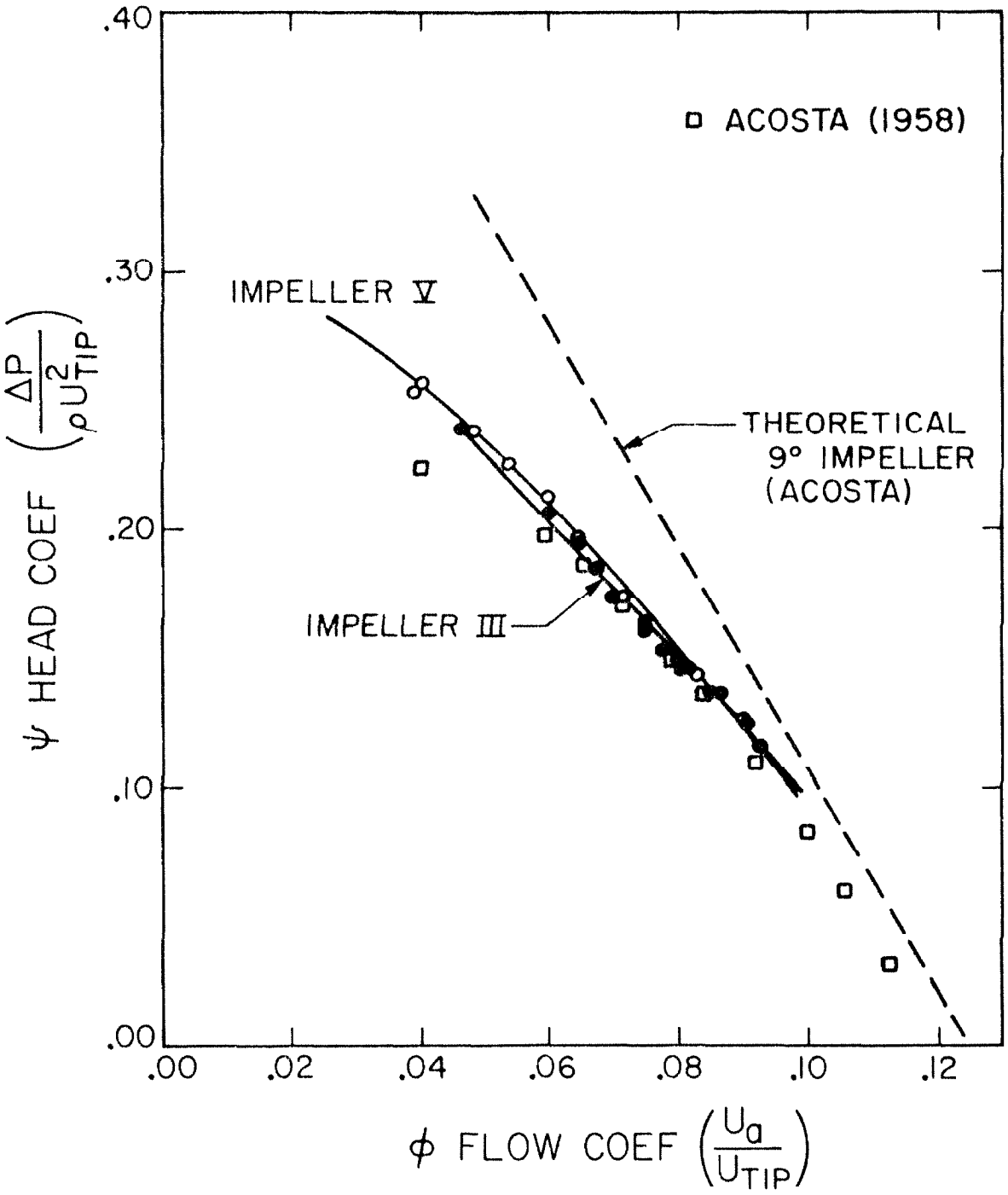

Fig. 5.1 Fully wetted performance of Impeller III and V.

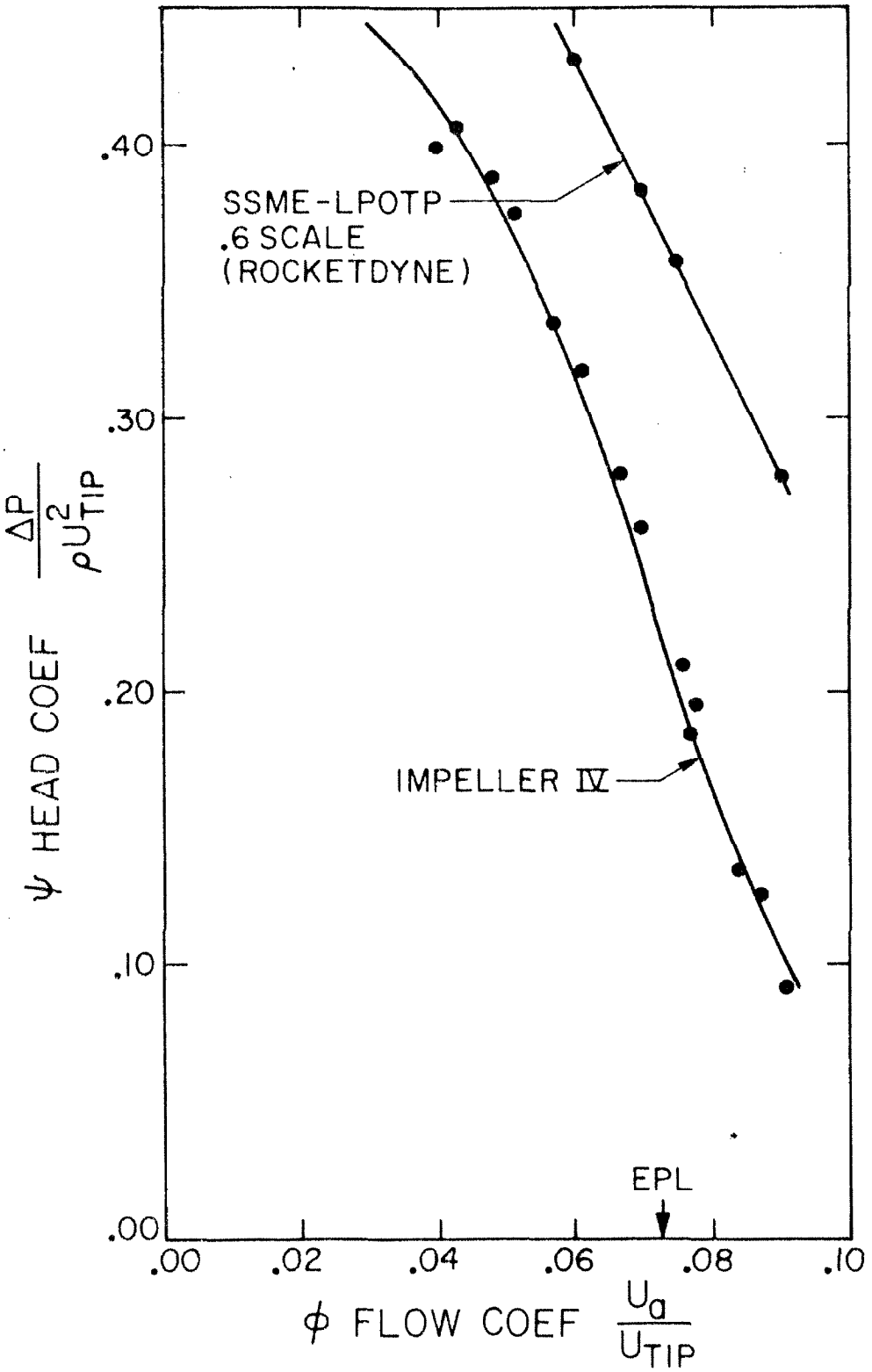

Fig. 5.2 Fully wetted performance of Impeller IV and 0.6 scale model by Rocketdyne.

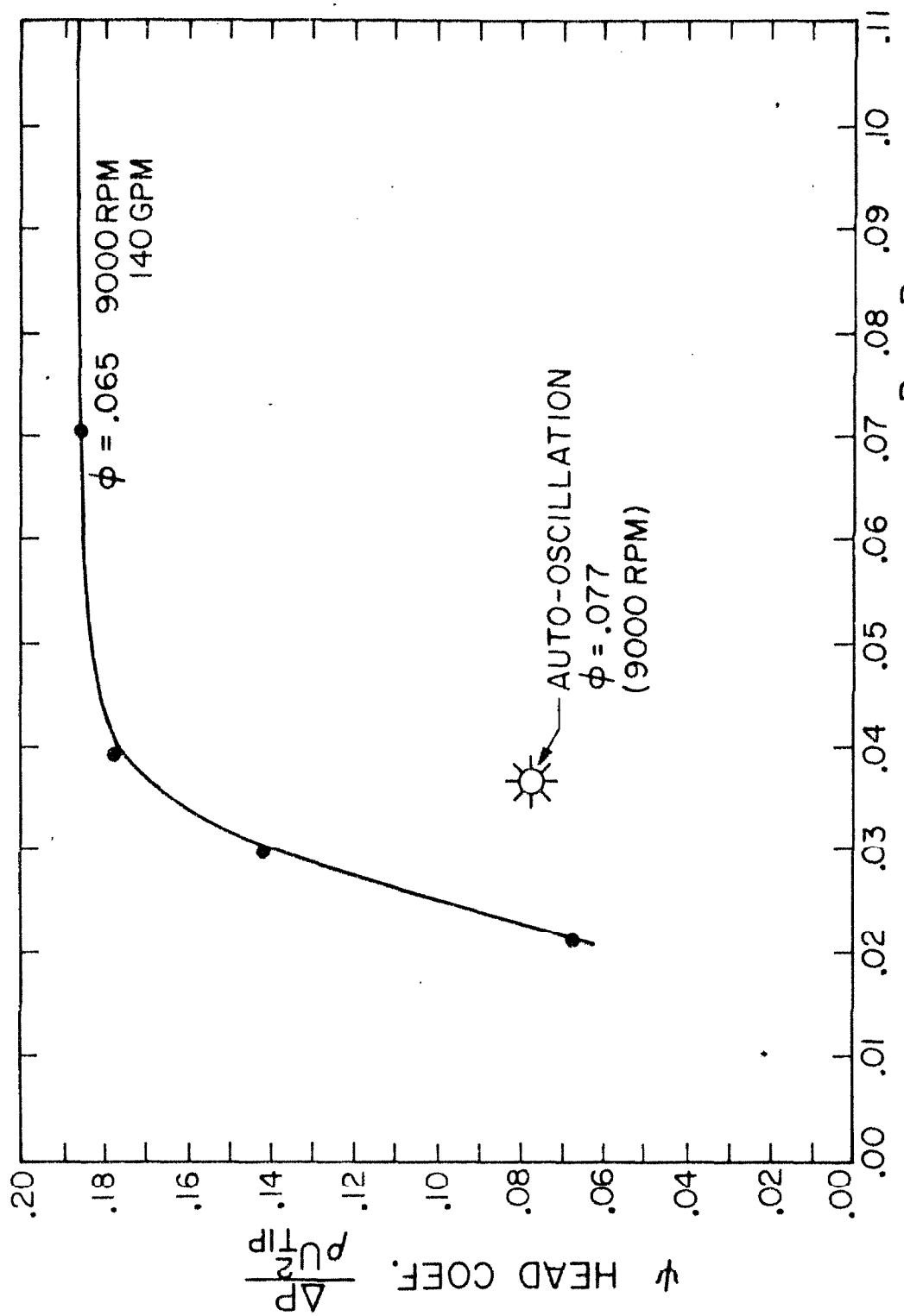

Fig. 5.3 Cavitating performance of Impeller V at 9000 rpm where $\varphi = 0.065$.

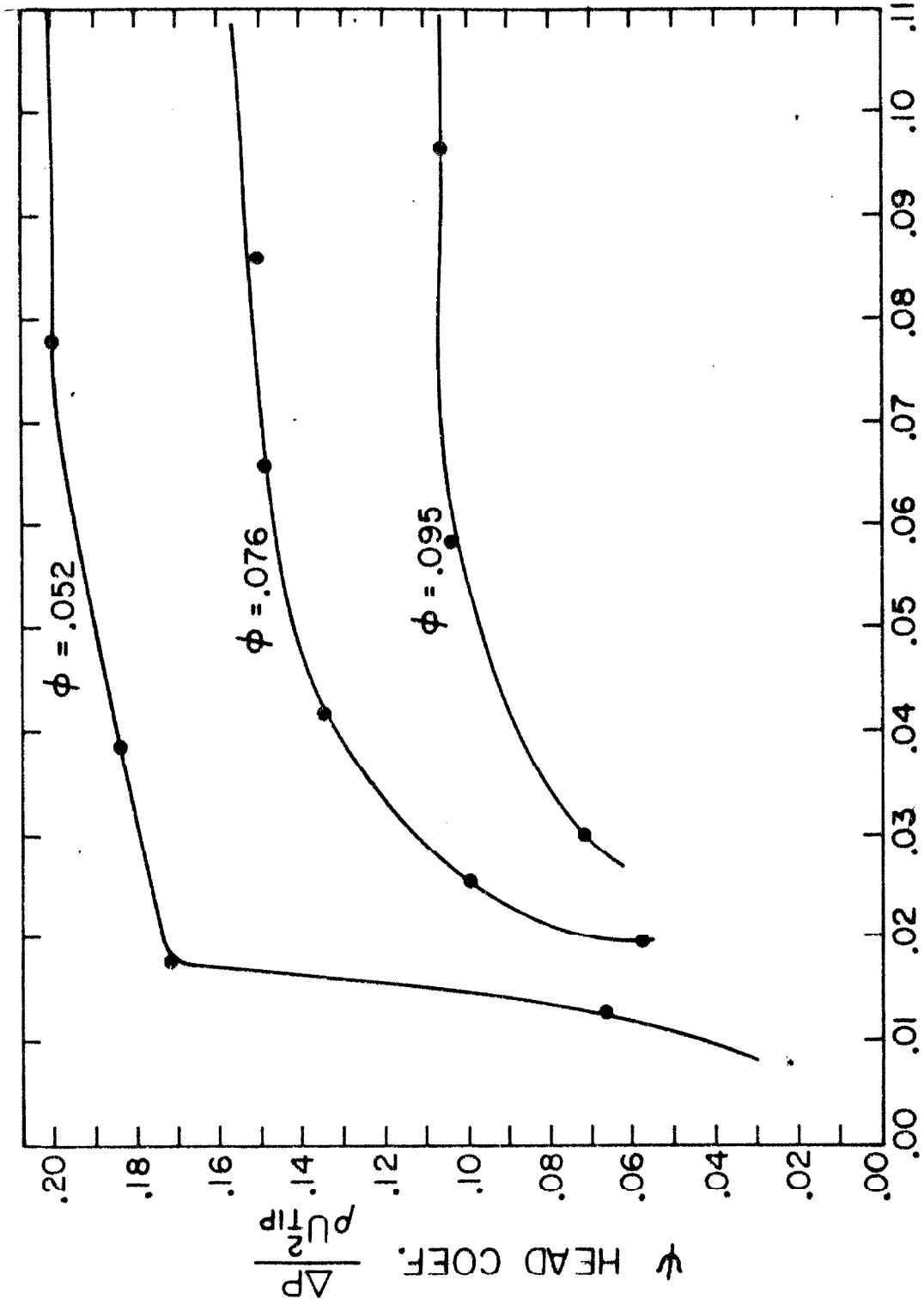

Fig. 5.4 Cavitating performance of Impeller V at 11500 rpm where $\phi = 0.052$, 0.076 and 0.095.

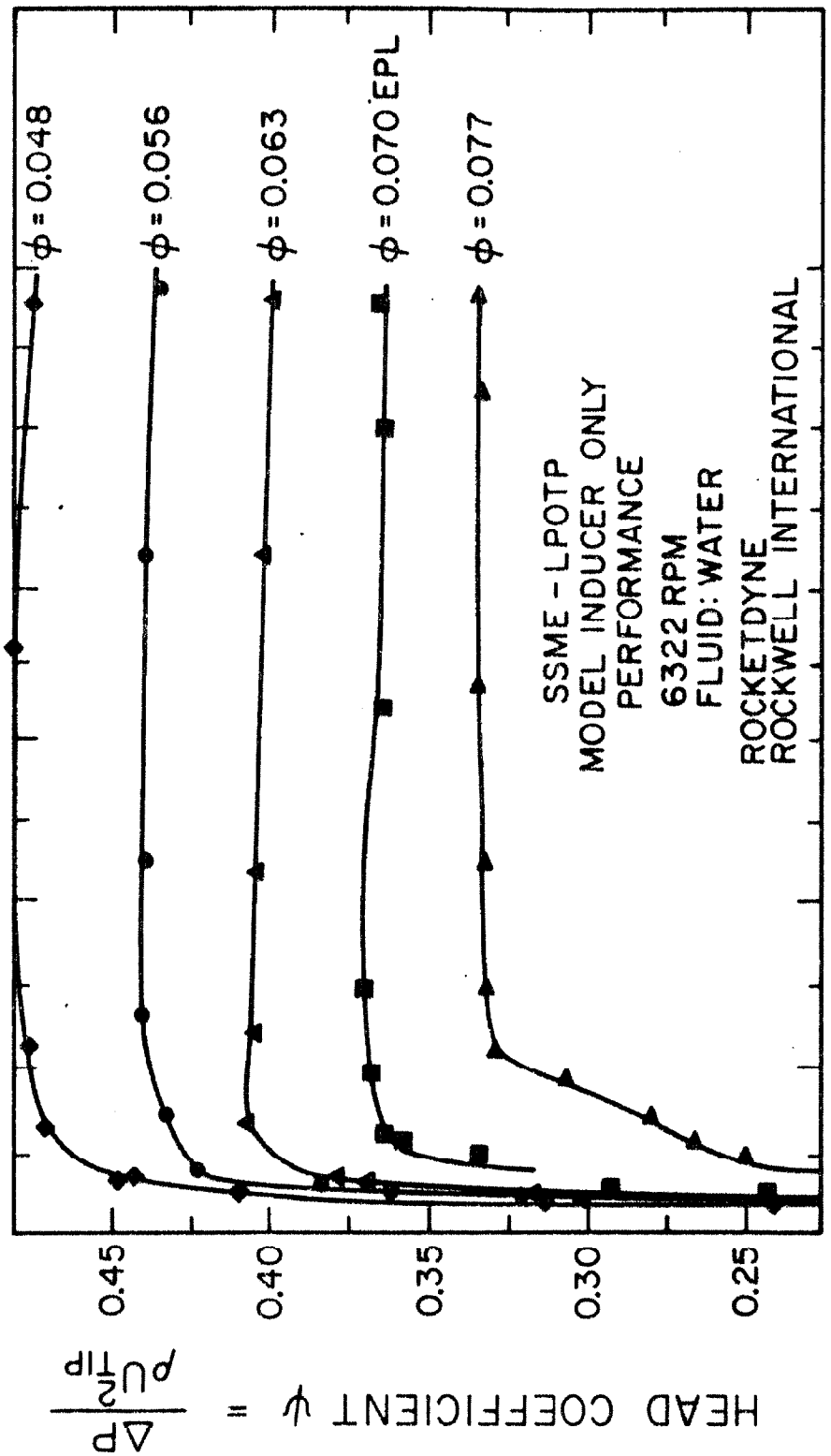

Fig. 5.5 Cavitation performance of a 0.6 scale test model provided by Rocketdyne.

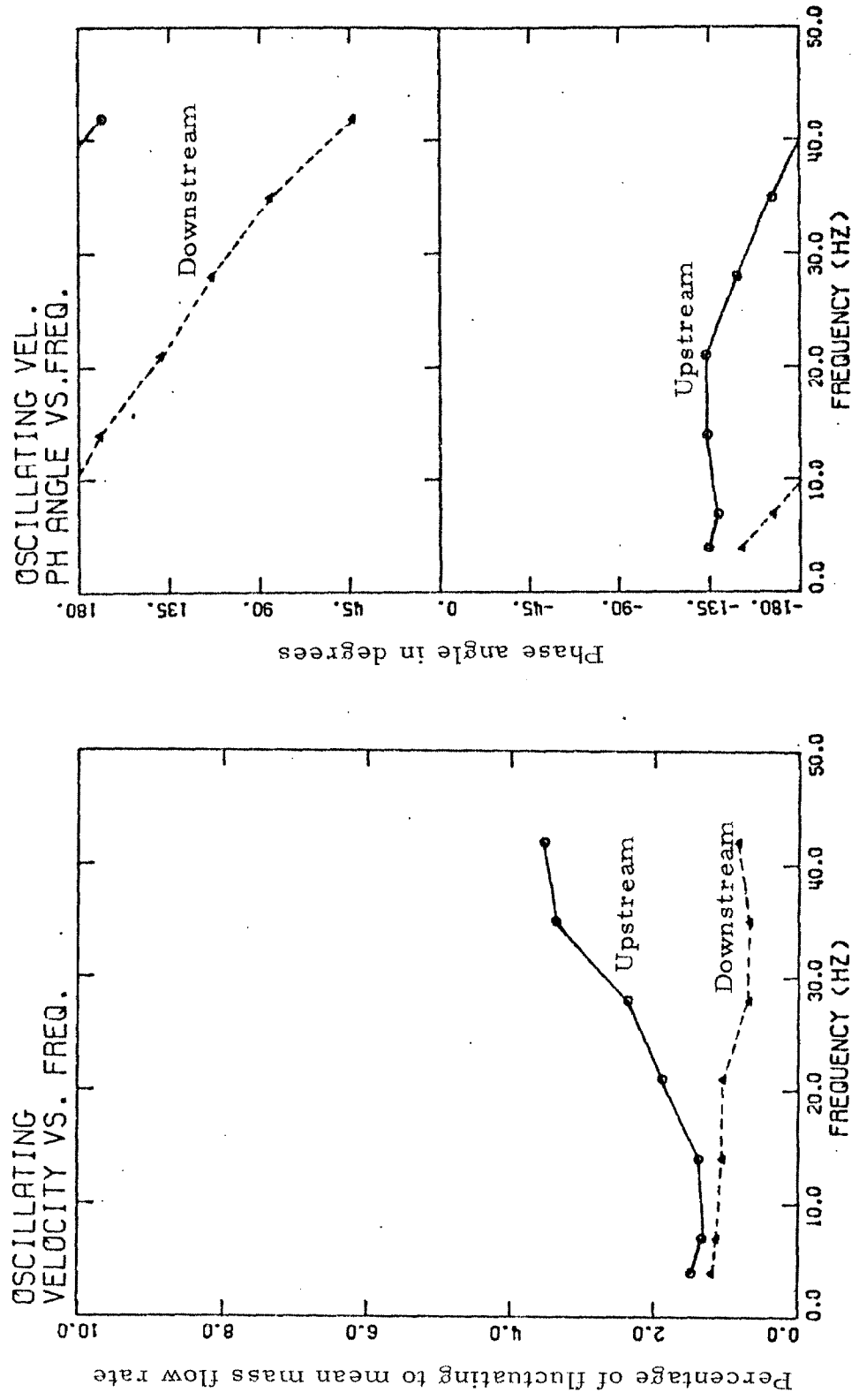

Fig. 5.6 Fluctuating velocities produced by operating the upstream fluctuator only.

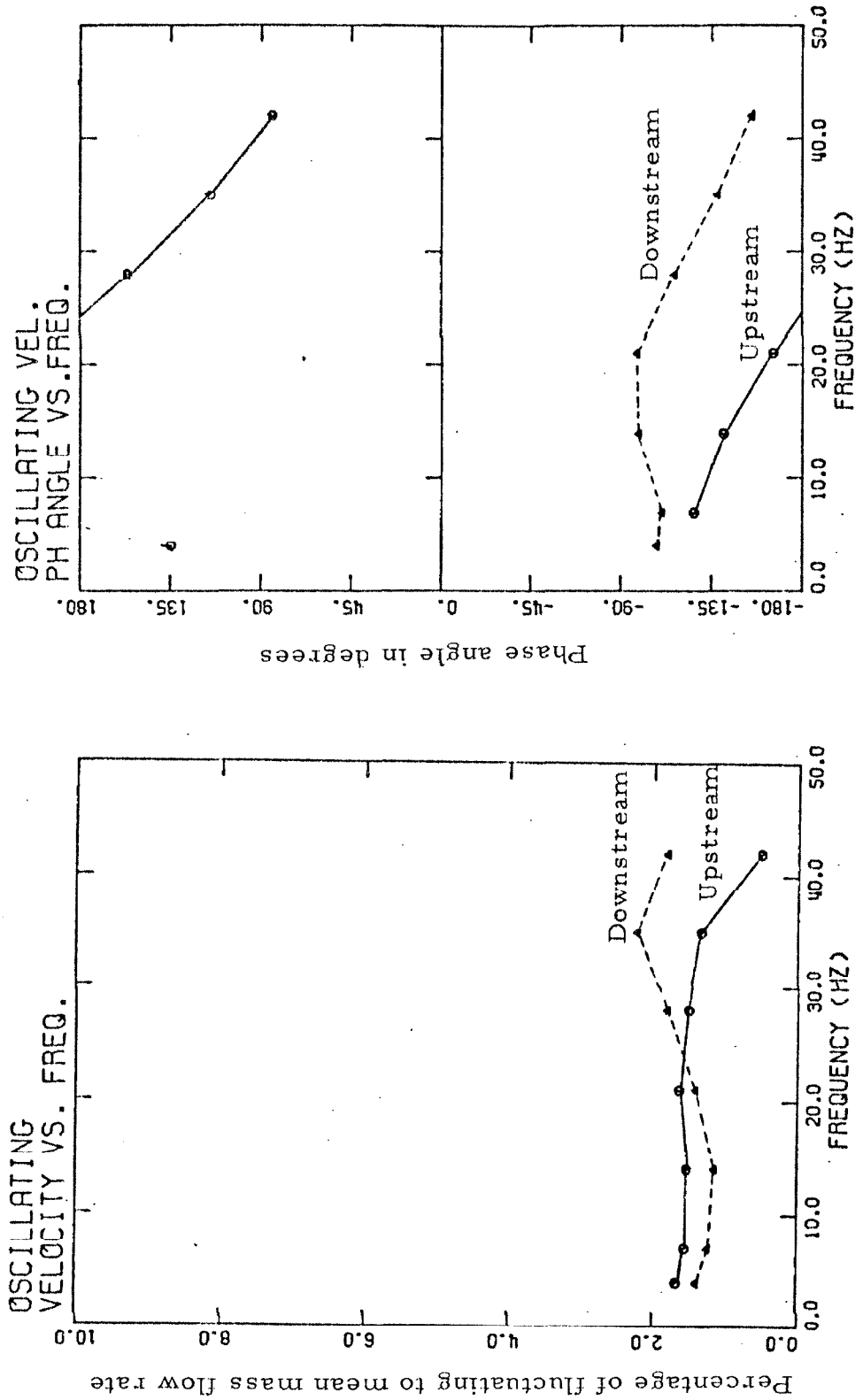

Fig. 5.7 Fluctuating velocities produced by operating the downstream fluctuator only.

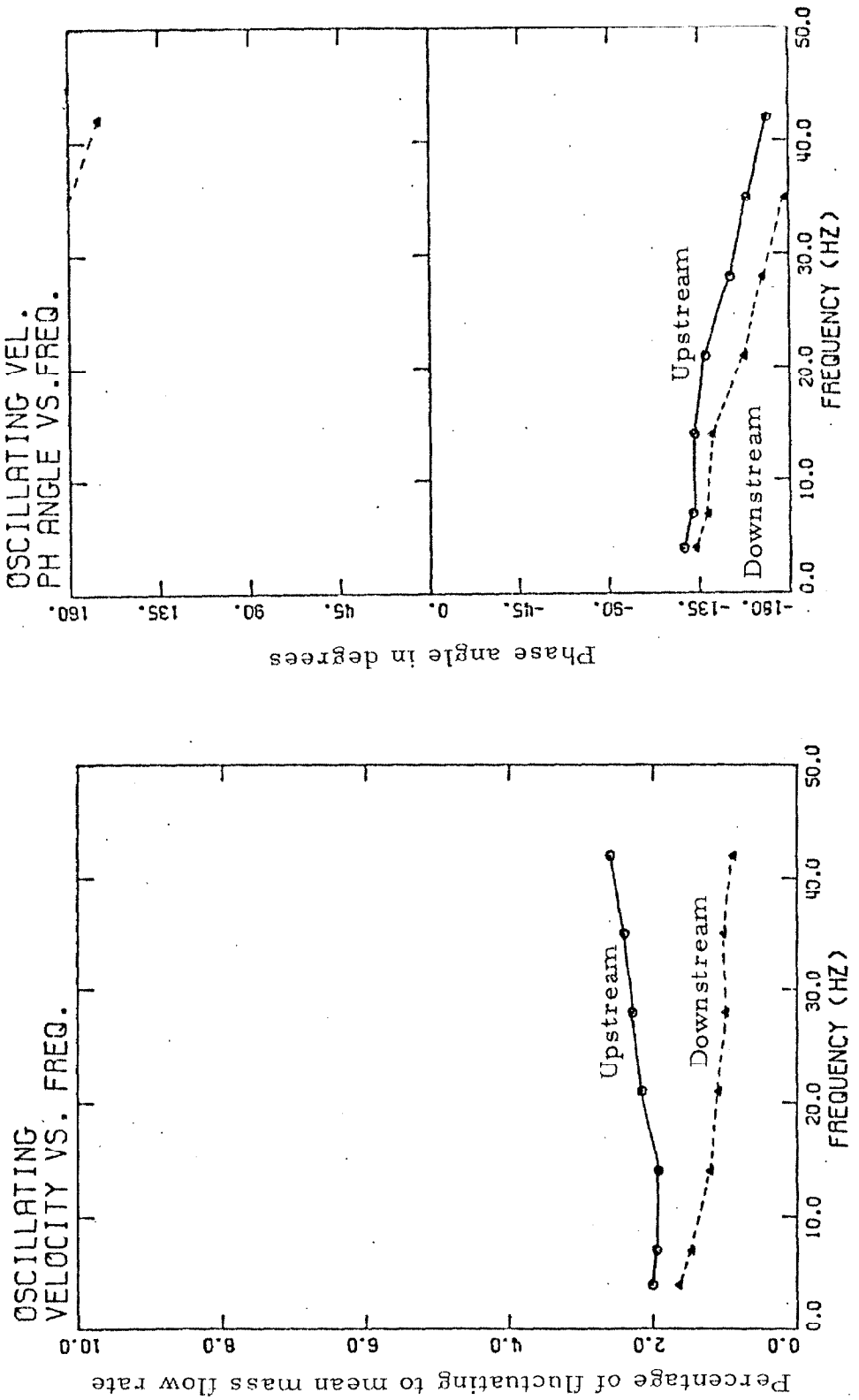

Fig. 5.8 Fluctuating velocities produced by operating both the fluctuators together.

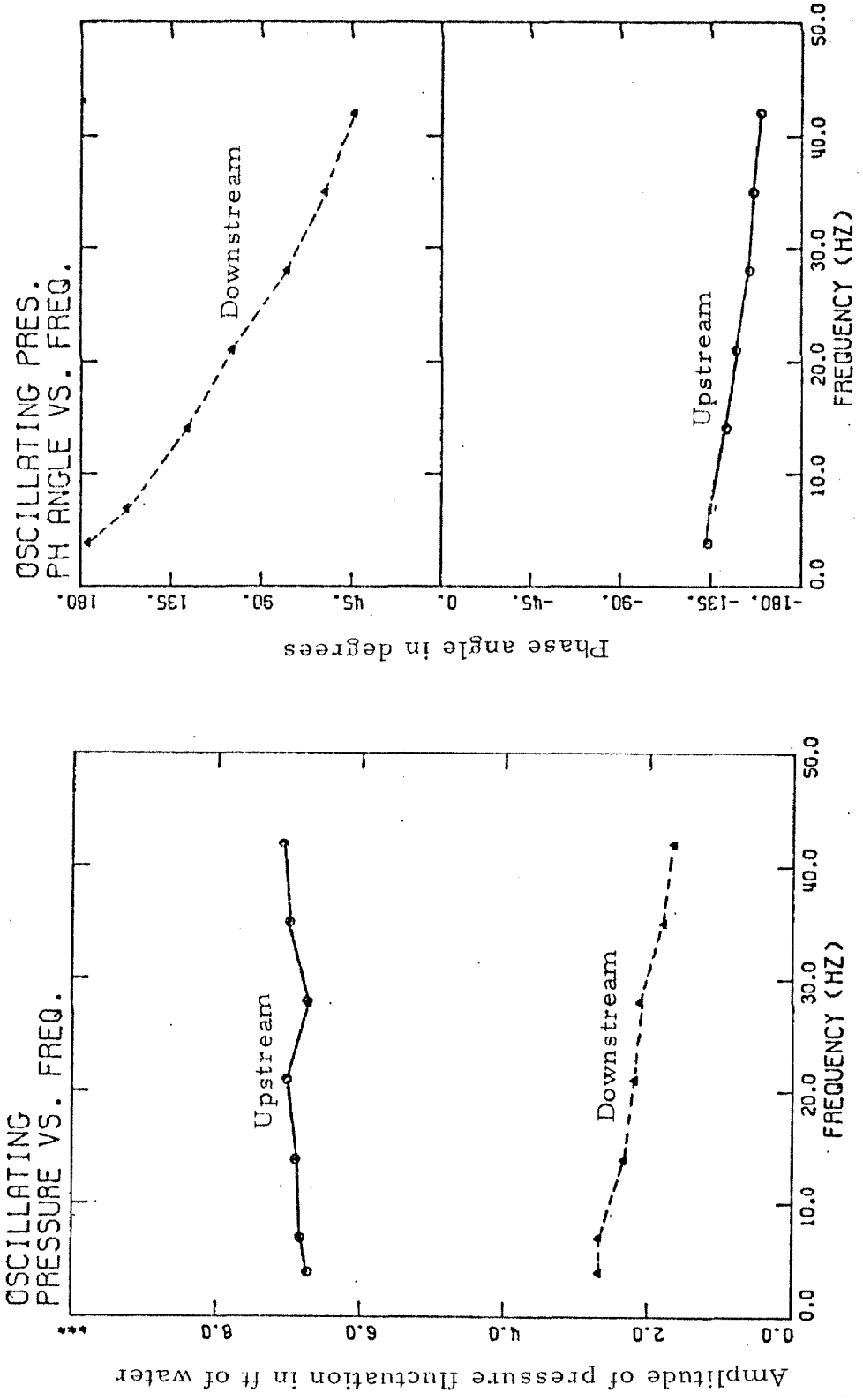

Fig. 5.9 Fluctuating pressures procuced by operating the upstream fluctuator only.

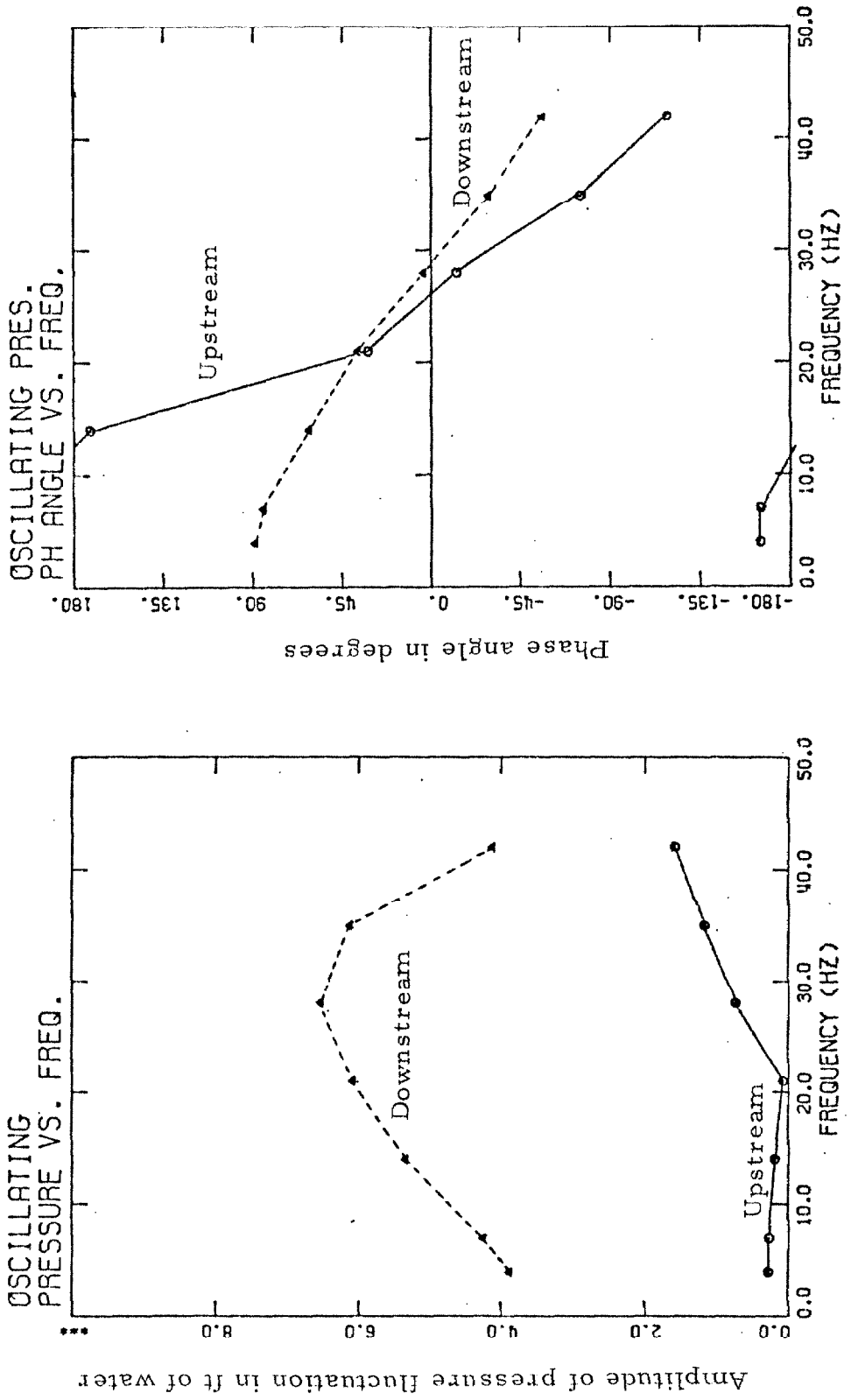

Fig. 5.10 Fluctuating pressures produced by operating the downstream fluctuator only.

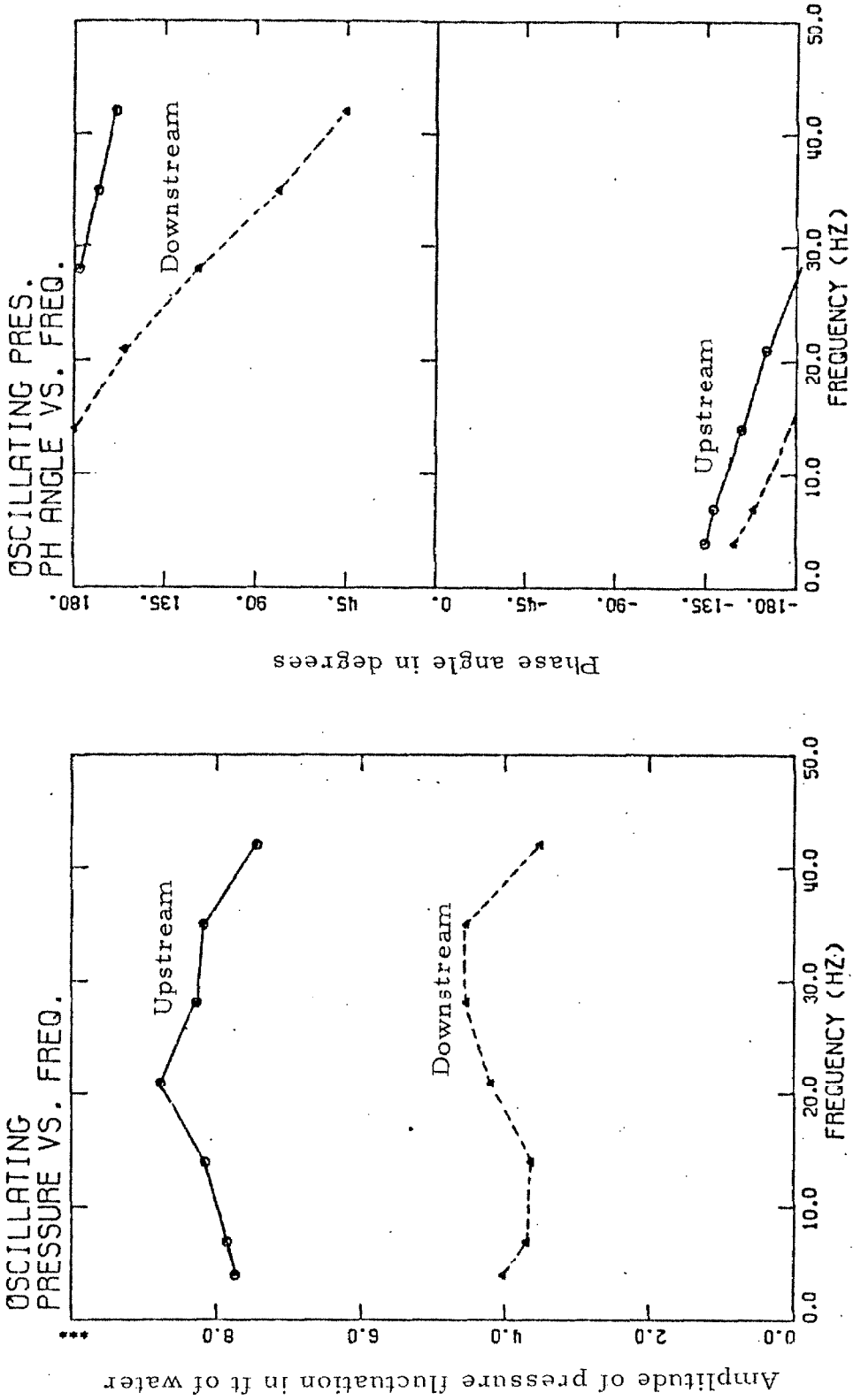

Fig. 5.11 Fluctuating pressure produced by operating both the fluctuators together.

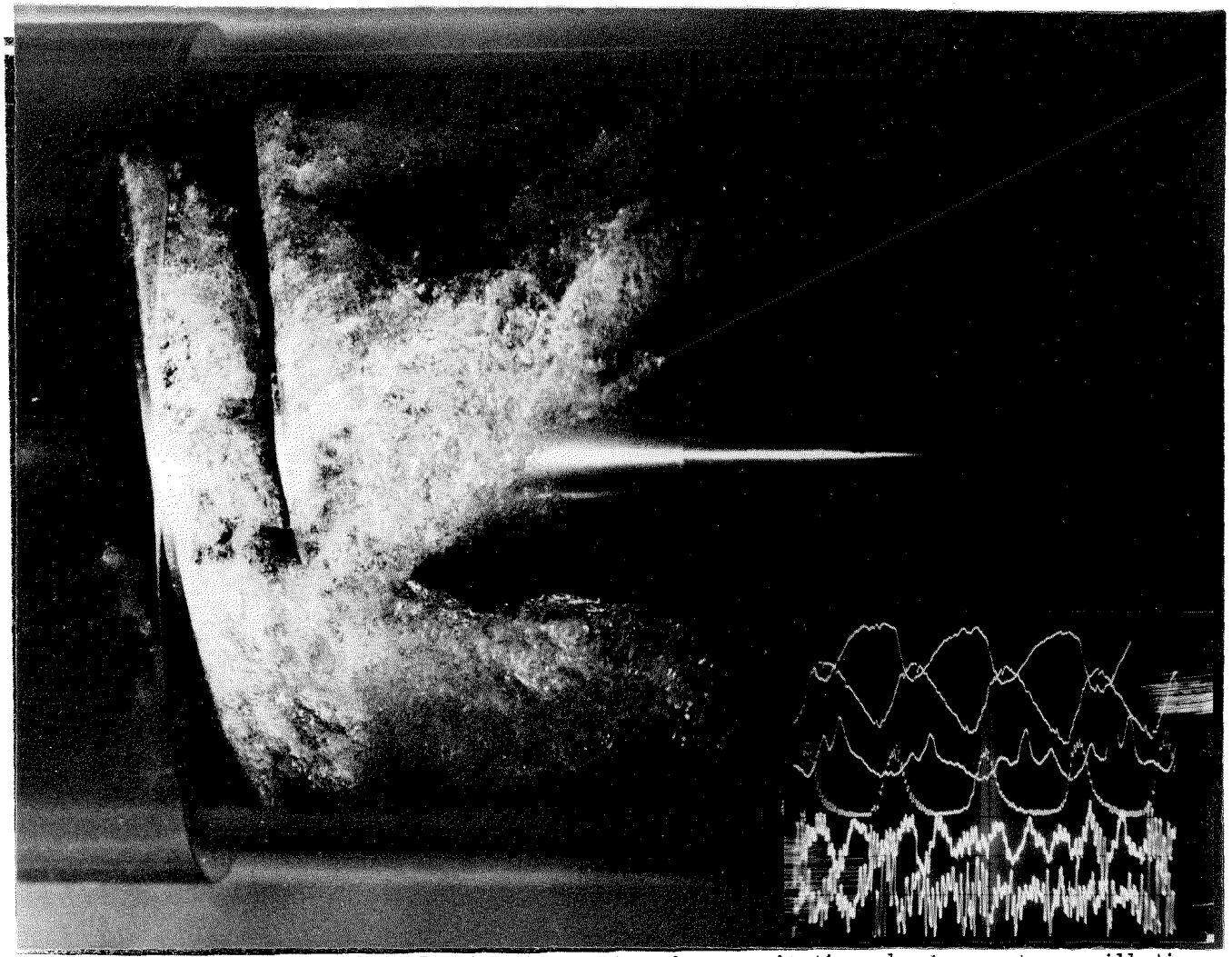

Fig. 5.12 Photograph of Impeller V showing extensive cavitation during auto-oscillation at 21 Hertz. The mean flow coefficient is 0.077 and the cavitation number is 0.036. The insert block shows traces (from top to bottom) of upstream mass flow rate, downstream mass flow rates upstream pressure, downstream pressure and up and downstream accelerations.

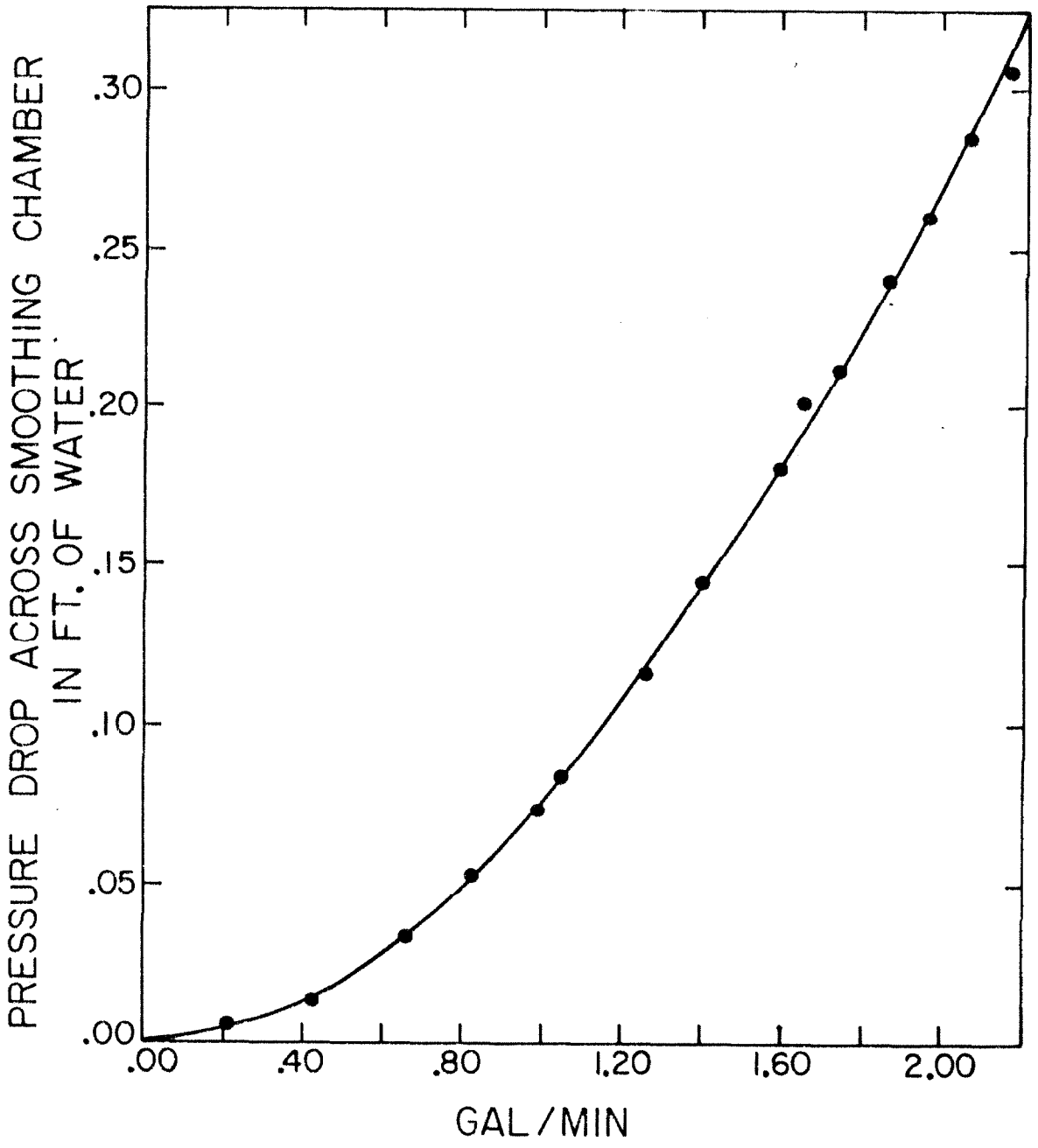

Fig. 5.13 Steady pressure drop across the smoothing chamber.

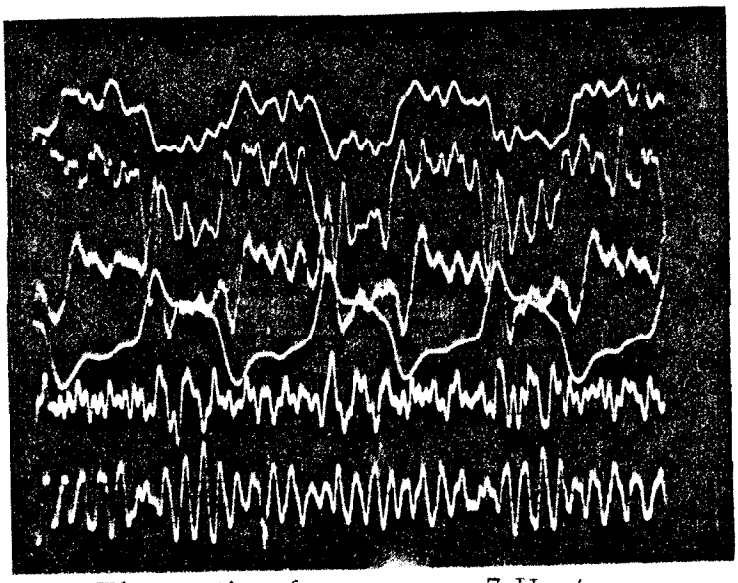

Fluctuating frequency = 7 Hertz

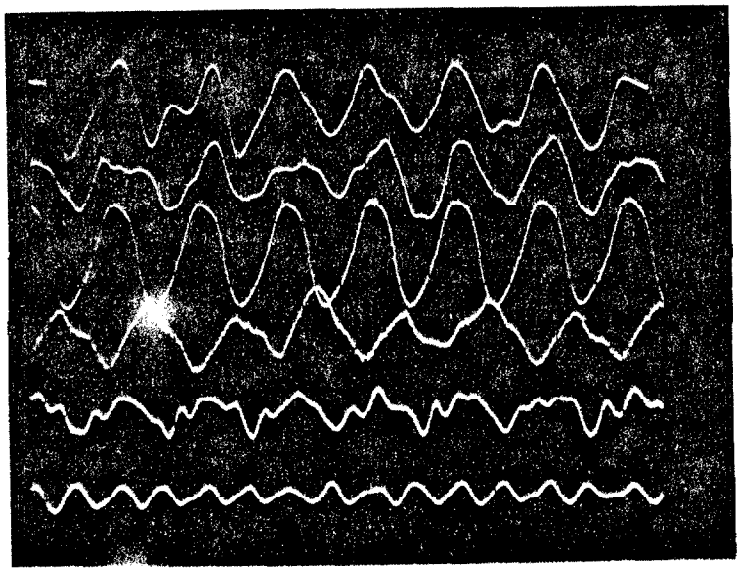

Fluctuating frequency = 35 Hertz

Fig. 5.14 Oscilloscope pictures of the fluctuating frequencies. The order of the traces from top to bottom are: upstream LDV, downstream LDV, upstream pressure, downstream pressure, upstream acceleration and downstream acceleration.

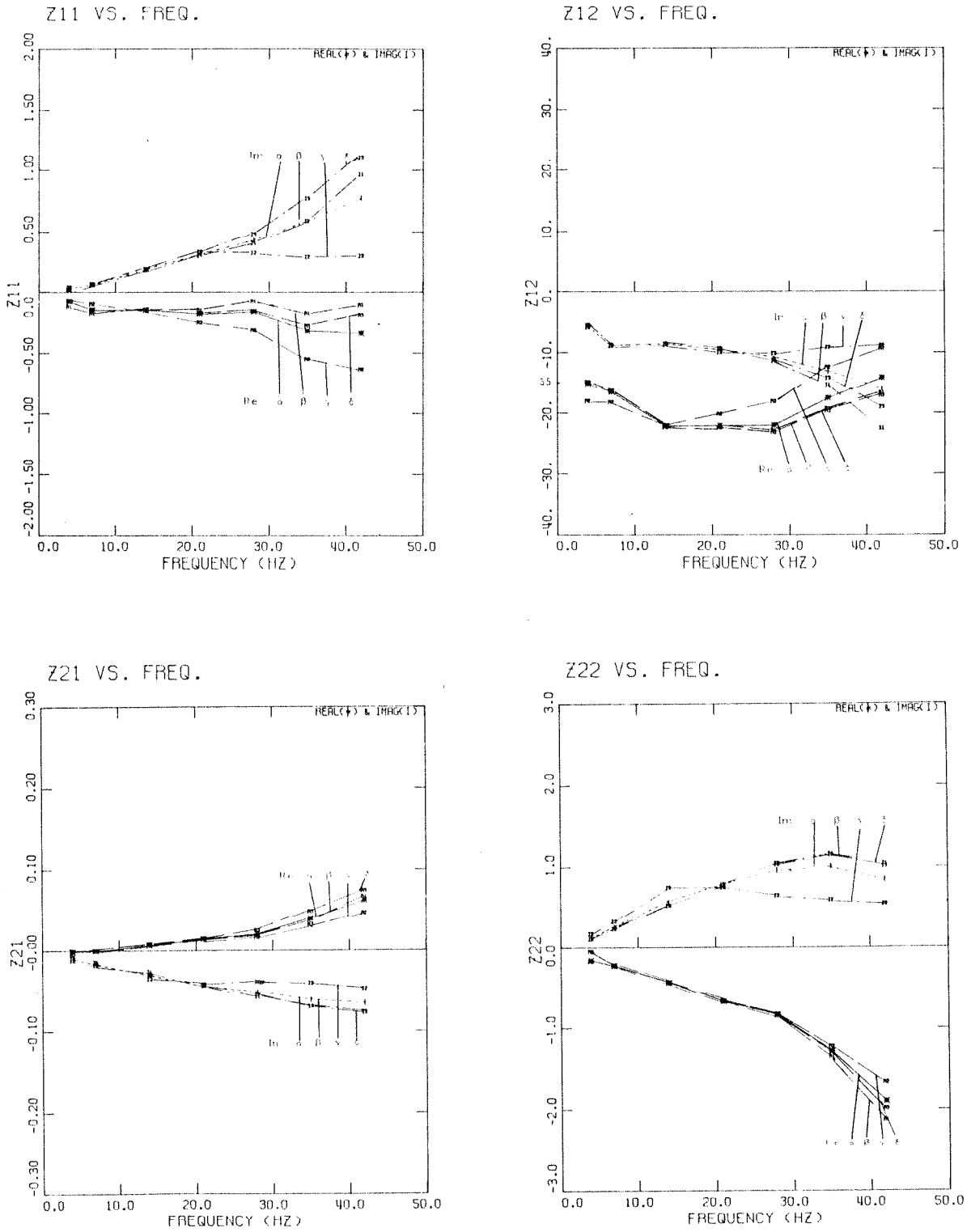

Fig. 5.15 Z-matrix produced by different combinations of fluctuator settings.

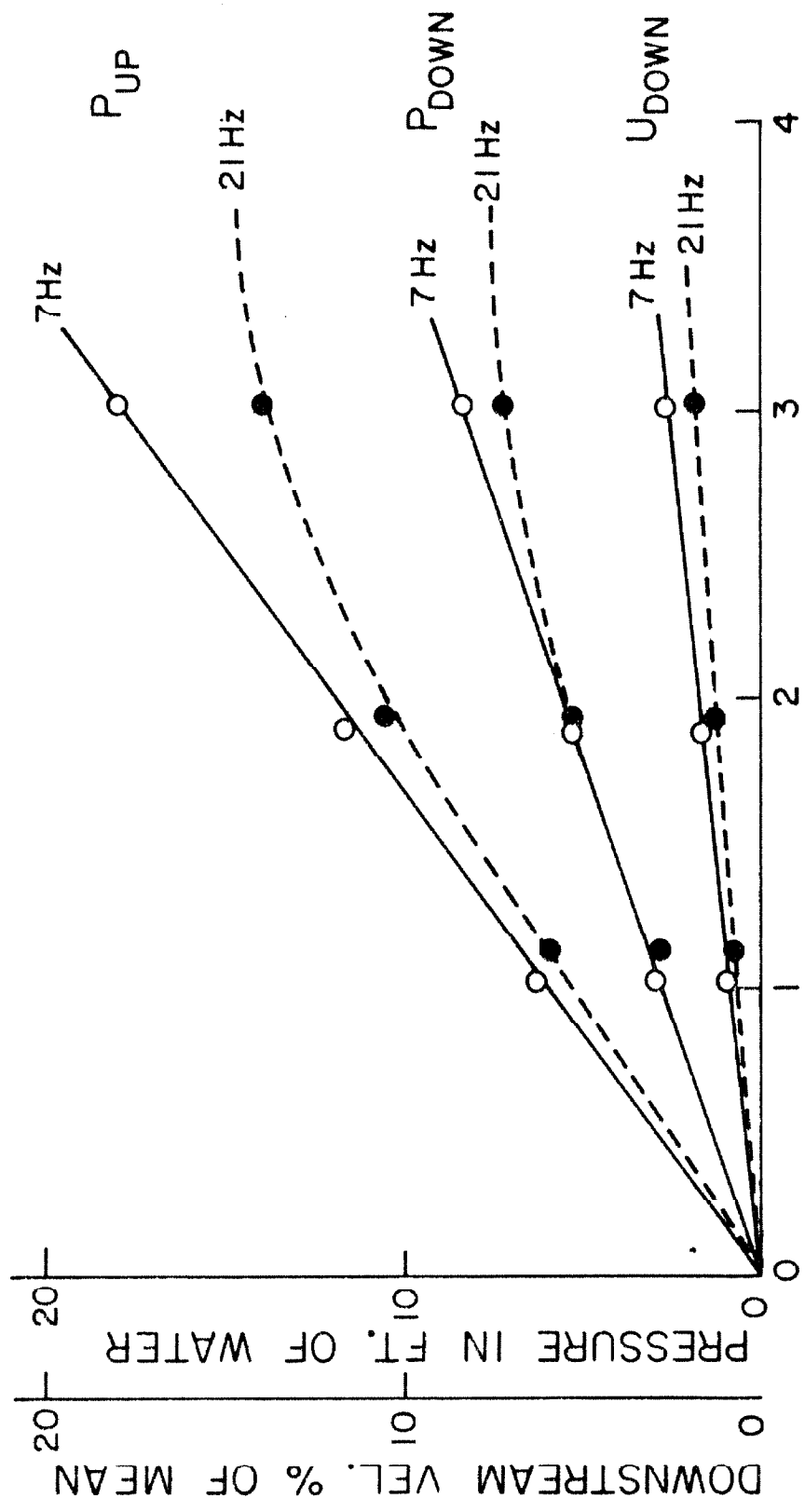

Fig. 5.16 Linearity assumption tests showing the fluctuating upstream pressure, fluctuating downstream pressure and downstream fluctuating velocity against increasing amplitude of upstream fluctuating velocity at 7 and 21 Hertz.

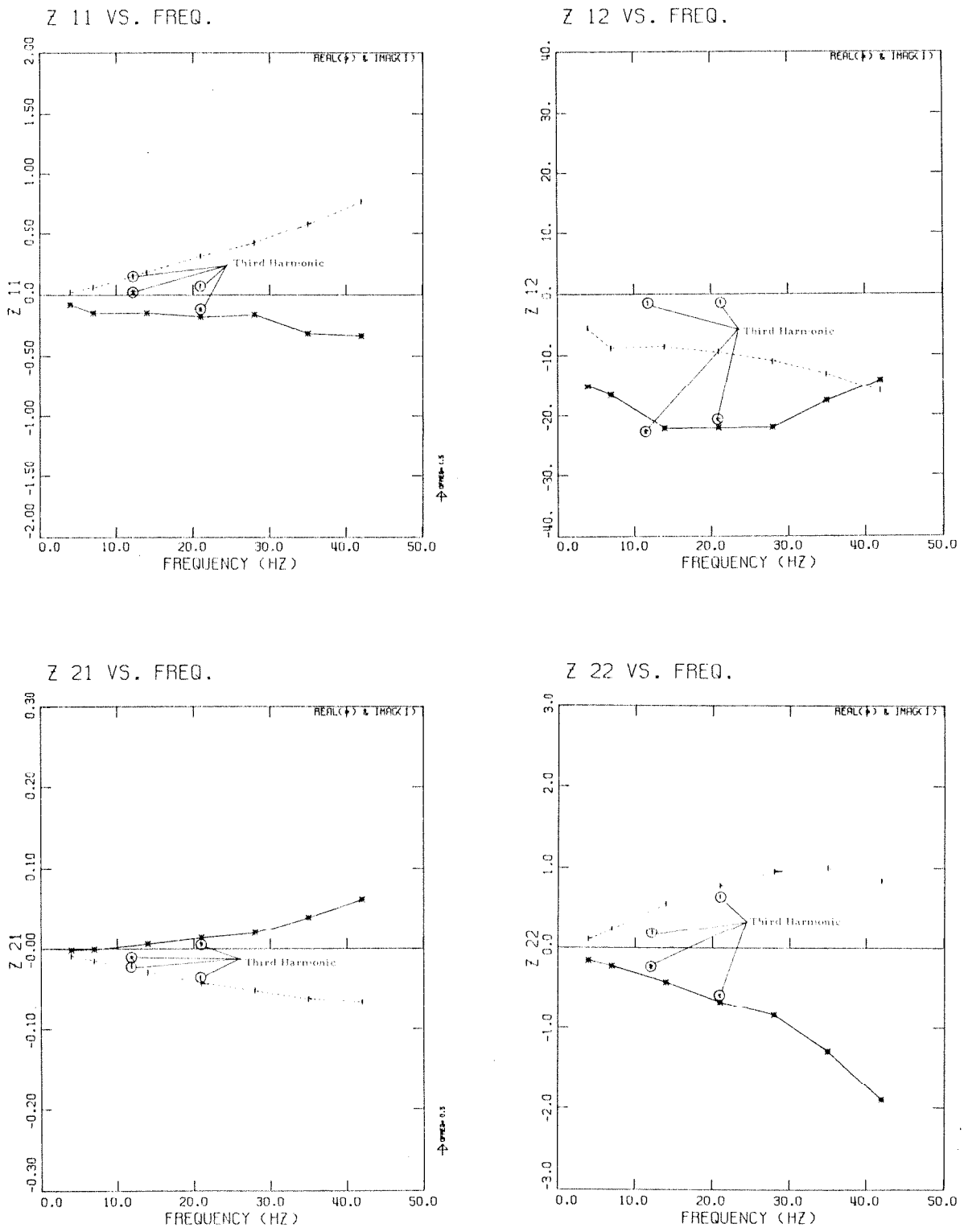

Fig. 5.17 Z matrix from measuring the third harmonics from the fluctuating signals.

VI. RESULTS AND DISCUSSIONS

This chapter will start with a discussion of the effects on the measurements of the hydraulic components between the two measuring stations. Effects of the hydraulic components between the measuring stations and pump have to be subtracted out in order to obtain the required pump matrix ZP. Following this the components of the ZP pump matrices will be plotted as functions of frequency. The behavior of the matrix components will be compared with values predicted using quasi-static analysis based on the steady state pump characteristics.

A total of five experiments using two impellers, Impeller IV and Impeller V, are presented. The five experiments were conducted in the following ways: one in a fully-wetted condition, two under cavitating conditions with Impeller IV, one under fully wetted conditions with Impeller V and one under cavitating conditions for the same impeller. As discussed in Section 3.3, the results for Impeller V are less reliable than results from Impeller IV.

6.1 System Effects

First, it is essential to define what hydraulic components comprise the pump and to identify the location of the measuring stations. For the definition of the pump, it is convenient to choose the plane connecting the leading edges of the inducer blades as the beginning of the pump and to choose the flange at the exit of the volute as the end of the pump. In general practice, a volute is usually considered as part of a pump. Further, the dynamics of the volute would be very hard to analyze and to express in simple analytic form. Thus the volute is

included as a part of the pump.

The identification difficulties of the measuring stations arise because the pressure measurements were taken from the smoothing chambers whereas the mass flow measurements were taken from the LDV viewing sections. The pressure and mass flow measuring stations were physically separated by a converging nozzle (see Fig. 2.5). It is convenient to refer the measuring stations to a single upstream and downstream point. The main concern here is the compliance effect of the converging nozzles. The converging nozzles had thick metallic walls and contained a relatively small amount of water. Their estimated combined compliance effect was calculated to be too small to cause any measurable fluctuating mass flow rate difference across it. This meant that the fluctuating mass flow rate at the end of the converging nozzle must be very close to that at the end of the smoothing chamber. Therefore the flanges joining the smoothing chambers and the convergent nozzles are considered as the upstream and downstream reference stations.

Having defined the measuring stations and the pump, we divide the hydraulic system between the measuring stations into three sections. These are: the upstream section between the upstream measuring station and the beginning of the pump; the pump itself and a downstream section between the end of the pump and the downstream measuring station. The next step is to identify the dynamics of the upstream and downstream sections using lumped parameter models.

To estimate the effects of the upstream and downstream section, we have to look closely at the construction and contents of each section.

The upstream section consists of a convergent nozzle and a straight pipe section leading to the pump. The nozzle and the straight pipe have thick aluminum walls and thus negligible compliance. The volume of water contained was also too small to contribute to any appreciable compliance effect. Thus no compliance value was assigned to this section. However, the inertance was calculated to be appreciable and the individual contributions were 0.156 sec^2/ft^2 for the convergent nozzle and 0.411 sec^2/ft^2 for the straight section leading to the pump.

The downstream section consisted of the divergent nozzle immediately following the volute and the downstream smoothing chamber. The smoothing chamber contained a large volume of water and had a thin wall relative to its radius. From the known compressibility of water and the known volume of water inside the smoothing chamber, this compliance was estimated to be 0.01 in^3/psi. Assuming small oscillating expansion and using linear theory for the radial expansion of a thin wall cylinder, the compliance of the downstream smoothing chamber structure also was shown to be 0.01 in^3/psi. Thus the total compliance was about 0.02 in^3/psi. As for the inertial effect, there is no accurate way to calculate the inertance for the complex separated flow in the divergent nozzle. The inertance of the convergent nozzle (0.156 sec^2/ft^2) was assumed for this. Finally the water inside the smoothing chamber contributed 0.12 sec^2/ft^2 to the inertance. During the preceding discussion, we did not mention the viscous resistance across any section. The viscous stress on the walls of all the sections was calculated, appeared not to have any appreciable effect on the measurements, and thus was neglected. The pressure drop due to the

screens etc. in the smoothing chamber was measured in Section 5.5 and was also found to be negligible compared with the measured resistance. Therefore, no resistance terms were included in the upstream or downstream section dynamics. To summarize all the foregoing factors we expect an upstream inertance of 0.57 sec^2/ft^2, a downstream inertance of 0.28 sec^2/ft^2 and a downstream compliance of 0.02 in^3/psi. The sum of the inertance terms, 0.85 sec^2/ft^2, is relatively small compared with the inertance of the pump as will be discussed in Section 6.2. (The calculated compliance of the downstream smoothing chamber was found to be smaller than values determined from experiment and this value will be modified in Section 6.2.) All these inertance and compliance values were used to extract the ZP pump matrix from the total transfer matrix Z as measured between the stations (implemented in the PUMA program) see Fig. 6.6 for an electrical circuit representation of these components.

6.2 Fully Wetted Experiments

Two sets of experimental results for fully wetted flow (one for each impeller) will be presented here. The Z total matrices will be discussed first, followed by discussion of the ZP pump matrices.

6.2.1 The Experiments

Experiment (1)—In this experiment Impeller IV was operated in the fully wetted condition. Although this experiment was designed to avoid any cavitation, a small thread of cavitation was present at the leading edge as seem from the photographs taken during the experiment (see Fig. 6.1). The actual static pressure used was 40 psig. The mean speed and discharge were 9000 rpm and 165 gpm

respectively which correspond to a head coefficient of 0.25 and a flow coefficient of 0.07. At this pump speed, a fluctuating frequency of 50 Hertz leads to a dimensionless frequency of about 0.52. The calculated cavitation number for this experiment was 0.51. Three sets of experiments with different fluctuator combinations were performed. The total transfer matrix Z for this experiment is given in Fig. 6.2.

Experiment (2)-This is another fully wetted experiment similar to experiment (1) except here Impeller V was used. Again, there was the unavoidable thread of cavitation as seen in the photographs of Fig. 6.3. This experiment was operated at mean conditions of 6000 rpm and 128 gpm corresponding to a flow coefficient of 0.088 and a head coefficient of 0.12. Four sets of fluctuator combinations were used and the calculated total Z matrix is given in Fig. 6.4.

6.2.2 Discussion of the Z-matrices

The most important feature observed from these Z-matrices is the non-zero values of Z_{21} (see Fig. 6.2 and 6.4). This confirmed that there was a hydraulic system compliance between the measuring stations which was addressed in Section 6.1. Although the photographs of the inducers (see Figs. 61. and 6.2) indicated that there were small traces of cavitation at the leading edge of the vanes, a simple estimation of the compliance effect of these small vaporous bubbles from its observed volume showed that the effect was much too small to account for the values of Z_{21} observed. This compliance value must come from the downstream smoothing chamber. We could further assume that the pump was in a truly fully wetted state and that its pump gain factors compliance and mass flow gain factors discussed in the

Introduction were all zero. Therefore when the system effects of the upstream and downstream sections were subtracted from the fully wetted total transfer matrix, the resultant pump matrix should only contain a pump resistance and a pump inertance term (Z_{12} only). Together with the inertance of the upstream section and the inertance and compliance of the downstream section, an electrical analogy was deduced from the above discussion and its circuit diagram is shown in Fig. 6.5. The total transfer matrix Z for this analysis is determined to be

$$Z = \begin{pmatrix} 0 & R - j\omega(L_u + L_p + L_d) \\ -j\omega C & -\omega^2 C(L_u + L_p + L_d) + j\omega CR \end{pmatrix} \qquad (6.1)$$

where R is the pump resistance, C is the compliance of the downstream smoothing chamber and its water content, ω is the fluctuating frequency and L_u, L_p and L_d are the upstream inertance, pump inertance and downstream inertance respectively.

It can be seen that the forms of the curves in Figs. 6.2 and 6.4 follow the form of Eq. (6.1) very closely. Thus this equation will be used to investigate the experimental results. The compliance and total inertance values were measured from the gradient of the graphs from the imaginary Z_{21} and imaginary Z_{12} by drawing a best fitted straight line through the origin. Their measured values are tabulated in Table 6.1 with the estimated value as calculated from Section 6.1. The pump resistance will be discussed in the next section (6.2.3) after the system effects have been subtracted out.

TABLE 6.1

	Compliance		Inertance $L_u + L_p + L_d$	
	Dimensionless	Dimensioned	Dimensionless	Dimensioned
	K	C	DL	
		in^3/psi		sec^2/ft^2
Exp. (1) Imp. IV	0.2	0.032	44	3.0
Exp. (2) Imp. V	0.066	0.030	27	2.7
			$L_u + L_d$	
Estimation from Sec. 6.1		0.02		0.85

The system compliance values 0.032 and 0.030 in^3/psi between the two experiments agree very well. However, these values are much higher than the calculated value of 0.02 in^3/psi from the compressibility of water and expansion of structure. This is because the estimate just mentioned was very rough. Further, the experimental value is actually the total compliance between the two, measuring stations instead of just the smoothing chamber. Compliance contributions from other structural components and the volume of water between the stations but outside the smoothing chamber were hard to estimate due to the complex geometry of each part. In the data reduction procedure, all these effects were attributed to the smoothing chamber and the value of 0.032 in^3/psi was assigned to be the compliance of the chamber.

The experimental measured inertances of 3.0 and 2.7 sec^2/ft^2 are much higher than the sum of upstream and downstream inertance. The difference is obviously the inertance value of the pump. One possible explanation for the higher inertance value of Impeller IV as compared to Impeller V is that the Impeller IV has a thick hub section after the blades thus causing a restricted area. This restricted area should increase the inertance.

6.2.3 Discussions of ZP pump matrix

From the Sections 6.1 and 6.2.2, inertances and compliance values were assigned to account for the upstream and downstream system effect such that pump transfer matrices ZP can be extracted from the total matrix Z. Figure 6.6 shows the assigned system values and circuit diagram and Section 4.3 shows how the PUMA program accomplishes this. The reduced ZP matrices for experiments (1) and (2) are illustrated in Figs. 6.7 and 6.8.

The expected zero values of ZP_{11}, ZP_{21} and ZP_{22} (see introduction for their significance) for fully wetted flows are clearly demonstrated in the figures. The occasional slight drifts from zero at higher frequencies in Fig. 6.7 may be caused by an overly simplistic model for the system effects. This might be improved by a more sophisticated model like the addition of an extra inertance after the compliance in Fig. 6.6. However, the wide departure from zero for ZP_{21} and ZP_{22} of Fig. 6.8 is considered to be purely experimental error.

We now focus our attention to ZP_{12} the pump impedence term. The imaginary part of ZP_{12} represents the inertance of the pump. If a

simple inertance were assumed for the pump, then the imaginary part of ZP_{12} would be a straight line passing through zero and decreasing with frequency. Both experimental results show that this is very nearly true except that a two points linear extrapolation at low frequency in Fig. 6.7 does not go through zero. However, the non-zero value is small and probably due to experimental error.

The first feature of the pump resistance (negative real part of ZP_{12}) to be investigated is the linear low frequency extrapolation. We expected this extrapolated value to agree with the pump resistance value from the steady state performance curve (see Introduction). The linear extrapolated values were 10 and 5 for Impeller IV and Impeller V. The pump resistance value as obtained from their steady state performance value for the corresponding flow coefficients were 15 and 5.3. There is good agreement between the two values for Impeller V. The discrepancy between 10 and 15 for Impeller IV may be due to a more complicated function of pump resistance at low frequency. This is not surprising since Impeller IV is of a more complicated design than Impeller V and also it has the addition of a stator stage.

As seen from Figs. 6.7 and 6.8 when the frequency increases, the pump resistance of Impeller IV increases until at a dimensionless frequency of 0.3 it starts to decrease. The pump resistance of Impeller V, also begins to decrease at a dimensionless frequency of 0.3. This could be interpreted as the slope of the pump performance curve first decreasing slightly (or remaining relatively constant) and then increasing towards a horizontal slope as indicated in Fig. 6.9. This feature is

more pronounced during the cavitating tests as will be seen in Section 6.3. It is interesting to speculate upon the effect when the pump resistance crosses zero and becomes negative. The corresponding behavior of the slope in Fig. 6.9 would be to reach a positive value. This means an increase in the flow rate will increase the head rise across the pump. This, in turn, would tend to increase the flow through the hydraulic circuit and hence the pump. Such an unstable situation may be responsible for the auto-oscillation phenomena described in Section 5.3. Up to the present time, no negative pump resistance has been measured either under fully wetted or cavitating conditions (see also Section 6.3). However, we anticipate that negative pump resistance values could appear for experiments with very low cavitation numbers. It is not possible to measure the pump transfer matrix during auto-oscillation (as described in Section 5.3) under the present experimental setup.

In general, cascade theory is used to analyze the performance of axial flow turbomachines. In the present study, it would be desirable to compare the experimental result with the analysis of the dynamic response of a cascade subjected to a time varying inlet velocity. No suitable analysis could be found, however. Although calculation on the unsteady response of axial flow turbomachines to an upstream disturbance exists in the literature (see Henderson 1972), the calculation is for the case of spatial variation in the incoming velocity field and not of time variation as in the present case. This calculation is therefore not directly applicable here.

In an effort to get a qualitative understanding of this phenomenon,

the results of the oscillating single airfoil analysis will be recalled here (see e. g. Fung 1968). Furthermore, the single airfoil result is a limiting case of the cascade calculation when the cascade blades are very far apart.

The single airfoil analysis we shall examine is the special case of a planar airfoil subjected to a sinusoidal time varying vertical gust with constant horizontal velocity. One of the results of this calculation is the complex lift coefficient which is the fluctuating lift force normalized by the product of the amplitude of sinusoidal vertical velocity and free stream velocity. This is called the Sears' function and is reproduced in Fig. 6.10. This can be considered analogous to the pump impedance $-Z_{12}$. Here we shall examine the Sears' function at low dimensionless frequencies. This low frequency range implies that the wavelength of the sinusoidal gust is much longer than the chord length which is the case in the present experiment. We may liken the real part of the Sear's function to the pump resistance. We see from Fig. 6.10 that the real and imaginary part of the Sears' function decreases with increasing frequency when the frequency is low and assumes a more complex behavior at a higher frequency. In the present experiment, the pump resistance in general decreases with increasing frequency. However, the imaginary part of pump impedence $(-Z_{12})$ is positive and increases with frequency. This means that the phases between the real and imaginary part between the two cases are different. No explanation can be offered here for this surprising finding. Overall, this example shows that important unsteady effects can occur in the unsteady fully wetted flow of turbomachines.

6.3 Cavitating Experiments

The pump transfer matrices for three cavitating experiments will be presented and discussed here. Some of the results will be compared quantitatively with the quasi-steady blade cavitation calculation by Brennen and Acosta (1975).

6.3.1 The experiments

Experiment (3) — This experiment was performed with Impeller IV. The mean conditions were 9000 rpm and 165 gpm. These conditions correspond to a flow coefficient of 0.07 and a head coefficient of 0.25. The mean cavitation number was 0.11 which resulted in only a moderate amount of cavitation. It can be seen in the photographs of the impeller during the experiment (Fig. 6.11) that there were distinctive patches of tip clearance cavitation on the blades but little blade cavitation. At this cavitation number, the condition of cavitation is far from the region of performance breakdown as can be seen by referring to the cavitation performance curve of the 0.6 scale model obtained by Rocketdyne 1975 (see Fig. 5.5). Three sets of results with different fluctuator combinations were obtained and the calculated ZP pump matrix is shown in Fig. 6.12.

Experiment (4) — This experiment was also performed using Impeller IV and the mean conditions were the same as in experiment (3). The only difference was that the cavitation number had a lower value of 0.046 resulting in more extensive tip clearance cavitation as shown in Fig. 6.13. Unfortunately, the fully developed tip cavitation obscures somewhat the observation of cavitation elsewhere in the impeller. During the experiment, the flow upstream of the pump was observed to

have entrained a small number of minute bubbles. The amount was much too small to cause interference with the LDV measurement, however, a certain amount of bubble compliance as discussed by Brennen 1973 could be expected. The cavitation performance curve from Fig. 5.5 indicated that this condition should cause slight performance deterioration. Again, the ZP-matrix was calculated from the results of three different fluctuator settings and is shown in Fig. 6.14.

Experiment (5) — This cavitating experiment with Impeller V was run under similar mean conditions to those of experiment (2). The conditions were a rotation speed of 6000 rpm and a flow rate of 128 gpm giving a flow coefficient of 0.09 and a head coefficient of 0.12. The cavitation number was 0.12. The increased blade spacing of this impeller compared with Impeller IV allowed clearer observation of cavitation (see Fig. 6.15). It can be seen that there was a moderate amount of tip cavitation though not extensive enough to obscure the observation of any other forms of cavitation. The pump matrix from four fluctuator combination experiments is shown in Fig. 6.16. As mentioned in Section 3.3, these data are less reliable than those of Impeller IV and they are presented here for a qualitative comparison with that other impeller.

6.3.2 Discussions

All the elements of the pump matrices ZP (Figs. 6.12, 6.14 and 6.16) were plotted as functions of fluctuating frequency. The calculated dimensionless frequencies (see Eq. 1.9) are also shown and denoted by DFREQ. We will compare these experimental results with the quasi-linear calculations and discuss the significance of the matrix elements

for the dynamic performance of pumps.

(i) ZP_{11} — The measured ZP_{11}, the pump gain factor term, will first be compared with the steady state expectation. As mentioned in Section 6.3.1, the mean flow conditions of these experiments indicated no severe performance deterioration from which one might expect small values of the pump gain factor. Tangents to the steady state performance curve (Fig. 5.5) at the mean flow conditions suggest low frequency values of 0.02 for experiment (3) and 0.09 for experiment (4). It is readily seen from Figs. 6.12 and 6.14 that the experimental values of ZP_{11} are much greater than these values; indeed the values approach unity at the higher frequencies. This is of major importance because large values of ZP_{11} imply significant deterioration of pump cavitation performance under dynamic conditions. Another result of experiment (4) at low frequency is the negative value of the linear extrapolation to zero frequency from the two lowest frequency data points. This negative value indicates a negative gradient of the cavitating performance curve. However, this may be due to a more complex function at the lower frequencies and more data points at this region are needed to verify this.

One of the most surprising features of Figs. 6.12 and 6.14 is the existence of an imaginary part which is not predicted by the quasi-steady analysis. This means that

there is a phase shift between the upstream pressure and the pressure rise across the pump even in the absence of mass flow fluctuations. The real and imaginary parts of ZP_{11} for experiments (3) and (5) have the same general behavior but the curves of experiment (4) where the cavitation number was lower have quite a different shape. This may be due to differences in the way different degrees and forms of cavitating flow respond dynamically. Experiment (4) might have traces of blade cavitation at the leading edge besides the extensive amount of tip cavitation whereas experiments (3) and (5) had only tip cavitation. Unfortunately the extensive tip cavitation of experiment (4) prevented the observation of any blade cavitation.

However, one cannot rule out the possibility that the observed ZP_{11} for experiment (4) was a nonlinear effect due to the magnitude of the fluctuation of the cavitation number. This is an experimental limitation which is inherent in the present facility. Since the experiment requires a minimum velocity fluctuation so that it can be measured by the LDV, a minimum pressure fluctuation is required. The amplitude of this pressure fluctuation may bring the instantaneous operating point into the breakdown region where high pump gain factors could be expected. During experiment (4), the amplitude of the upstream pressure fluctuation was almost constant over the whole frequency range but differed for different fluctuator settings. At some fluctuator settings,

the resulting fluctuation of the cavitation number was quite large. For the three fluctuator settings used in experiment (4), the cavitation number fluctuated between 0.02 and 0.09, between 0.04 and 0.05 and between 0.02 and 0.08. The lowest value here is well into the breakdown region (Fig. 5.5). If straight lines are drawn in Fig. 5.5 between the cavitation number pairs given above, the resulting slopes of these lines would lead to pump gain factors of 0.78, 0.91 and 0.22 respectively. These values may partially explain the large values of ZP_{11} measured but do not explicitly account for the appearance of an imaginary part.

In an attempt to shed further light on these effects, photographs of the cavitation were taken at various points in a cycle during the dynamic experiments (Fig. 6.13) and these were compared with the photographs of cavitation breakdown taken by Rocketdyne (1974) during steady state experiments on the 0.6 scale model. It appeared that the cavitation during fluctuating flow was not as extensive as in the breakdown state. The Rocketdyne photographs showed that the cavitation extended all the way through the four blade inducer and into the twelve blade tandem stage. On the other hand the photographs taken at the point of maximum cavitation in the dynamic experiments showed that the cavitation only extended through the four blade section but not into the twelve blade stage. In comparing the two sets of photographs, the cavitation form of the dynamic

experiment would not be extensive enough to cause breakdown. This appears to suggest that the large ZP_{11} measured was due to dynamics of the flow. The contradiction between the photographic demonstration and cavitation number fluctuation cannot be resolved until further experiment can be carried out with much lower fluctuation of cavitation number. However, the above discussion does not apply to the ZP_{11} of experiments (3) and (5) where the cavitation number fluctuation was less than 25 percent of the mean cavitation number.

In conclusion it was observed that the measured values of ZP_{11} were much higher than the steady state pump gain at the mean cavitation number. This together with the unexpected existence of an imaginary part, demonstrated that the dynamic performance of turbomachines can be influenced significantly by cavitation in a manner which is not predicted by quasisteady analysis.

(ii) ZP_{12} – From Figs. 6.12 and 6.14, the linear extrapolations of the pump resistance (negative of the real part of ZP_{12}) from the two lowest frequency data points have values of 12 and 10 for experiments (3) and (4). However, the pump resistance as measured from the steady state performance curve would have a value of 15 for both experiments. At higher frequencies, the pump resistance decreases and the rate of decrease is higher when the cavitation number is lower. This is not surprising since cavitation reduces the

contact surface area between the fluid and the impeller surface. This reduces the viscous drag on the fluid and could lead to reduced resistance. The implications of further reduction of pump resistance and the possibility of negative values was discussed in 6.2.3 and will not be repeated here.

The low frequency values of the imaginary part of ZP_{12} behave like an "ordinary" inertance term in the sense that it has a definite negative gradient and is proportional to frequency and the linear extrapolation goes through zero. At higher frequencies, the slope of the imaginary part of ZP_{12} increases implying a decrease in the effective inertance. Furthermore the rate of increase is higher for experiment (4) where the cavitation number was lower. This may be due to the reduction in the mass of fluid inside the pump in the presence of cavitation. However, this cannot explain the positive gradient shown in experiment (4) which indicates a negative effective inertance. The possibility that the imaginary ZP_{12} may become positive at lower values of cavitation number than those investigated may have consequences for auto-oscillation similar to those of the real part of ZP_{12}.

(iii) ZP_{21} – Surprisingly, experiment (3) produced no measurable cavitation compliance as shown in Fig. 6.12 although photographs of the impeller (Fig. 6.11) showed distinct patches of cavitation. However, as seen in Fig. 6.14 experiment (4) did produce measurable cavitation compliance. The

appearance of a real part of ZP_{21} is unexpected from the quasi-steady blade cavitation calculations (see Brennen and Acosta 1975). In order to compare the experimental results with the quasi-steady calculation, an imaginary compliance is introduced into Eq. (1.11) and we define

$$ZP_{21} = -j\omega(K_B + jK_{BI}) \quad . \tag{6.1}$$

The values of K_B and K_{BI} were measured from the gradient of ZP_{21} of experiment (4) at low frequencies and are listed in Table 6.2 together with the quasi-steady estimates.

TABLE 6.2

	Compliance		Mass flow gain factor	
	K_{BI}	K_B	M_{BI}	M_B
Experiment (4)	0.06	0.32	2	0.6
Quasi-steady blade cavitation calculation		0.01		0.53

The experimentally measured compliance value K_B, is much higher than the quasi-steady blade cavitation compliance. This may be explained by the fact that the experimental cavitation form was mainly tip cavitation. Thus the compliance value measured was most probably due to tip cavitation and not blade cavitation.

One interesting qualitative comparison can be made between the compliance data for experiment (4) and the

bubble compliance calculations by Brennen (1973). The real compliance of experiment (4) (K_B as defined in Eq. (6.1), the negative gradient of the imaginary part of ZP_{21}) starts at a positive value at zero frequency. But as the frequency increases K_B begins to decrease and finally crosses zero into negative values. The imaginary compliance K_{BI} (gradient of real ZP_{21}) starts at a small negative value at zero frequency and as frequency increases, K_{BI} first decreases but then increases and crosses zero into positive values. These trends are qualitatively similar to the calculated results of Brennen. This seemed to further confirm that the compliance value measured was a kind of bubbly tip cavitation.

(iv) ZP_{22} – This term is certainly measured to be non-zero disproving the zero value assumption prior to the calculations by Brennen and Acosta (1975). Even more surprising is the existence of a real part with values higher than the imaginary part. In a manner similar to the compliance term, we modify Eq. (1.13) to include an imaginary mass flow gain factor M_{BI}:

$$ZP_{22} = -j\omega(M_B + jM_{BI}) \tag{6.2}$$

The low frequency approximation of the real and imaginary mass flow gain factors were measured from Fig. 6.14 for experiment (4) and are listed in Table 6.2. The measured

M_B value is very close to the quasi-steady calculated value. This may be merely a coincidence since as demonstrated earlier the main form of cavitation in this experiment was tip cavitation and not blade cavitation. However, this does mean that the tip cavitation can give rise to a mass flow gain factor term. Note that the slopes of both the real and imaginary parts of ZP_{22} do not change greatly at the higher frequencies.

The ZP_{22} of experiment (3) has very small values. When this was compared with the ZP_{22} of experiment (1), the fully wetted case, they were found to be comparable. Since the ZP_{22} of the fully wetted case was considered to be an experimental error, the measured ZP_{22} of experiment (3) was also considered to be within experimental error range.

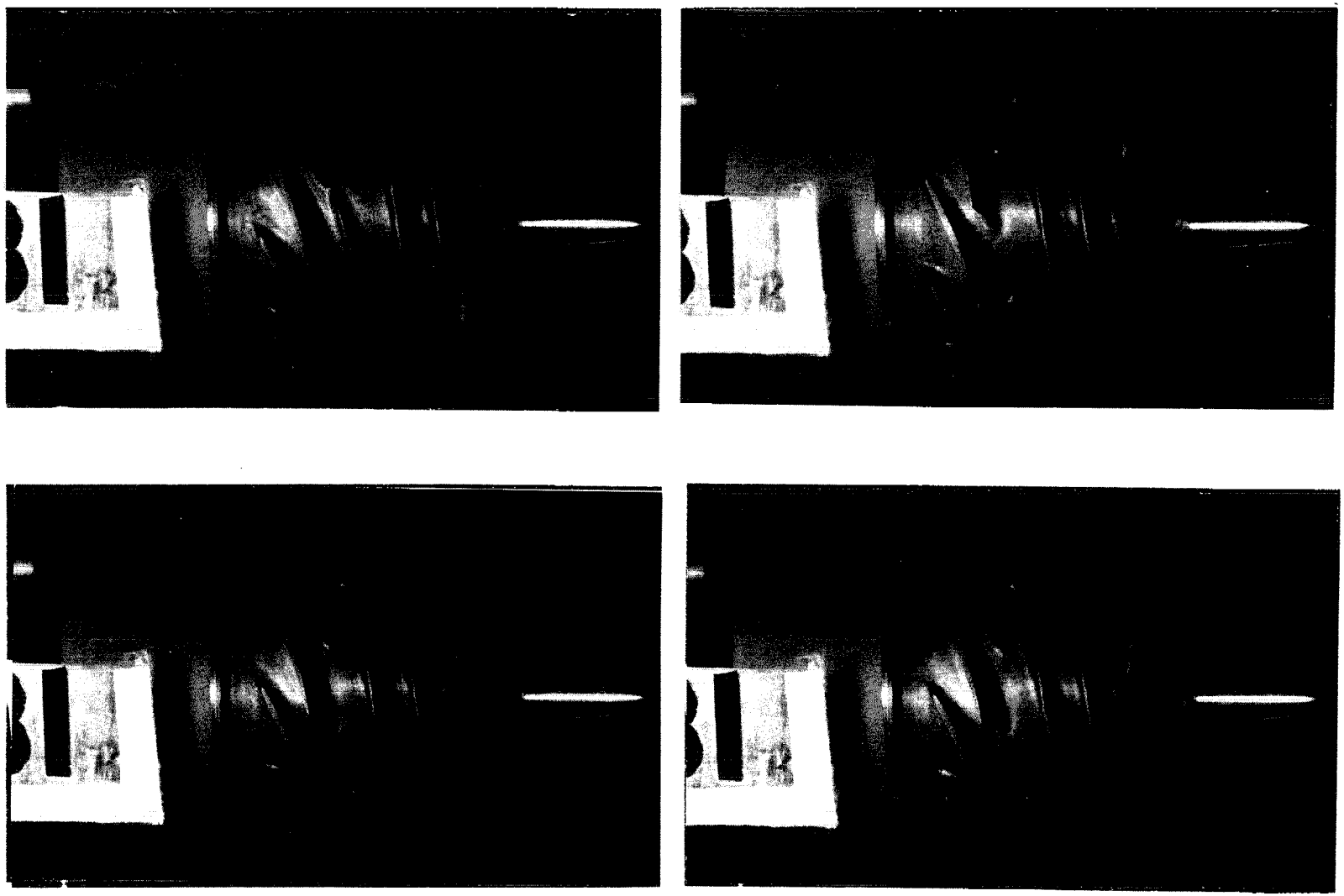

Fig. 6.1 Photographs of Inducer IV during experiment (1), a fully-wetted condition. These photographs were taken randomly when the fluctuating frequency was 14 Hertz.

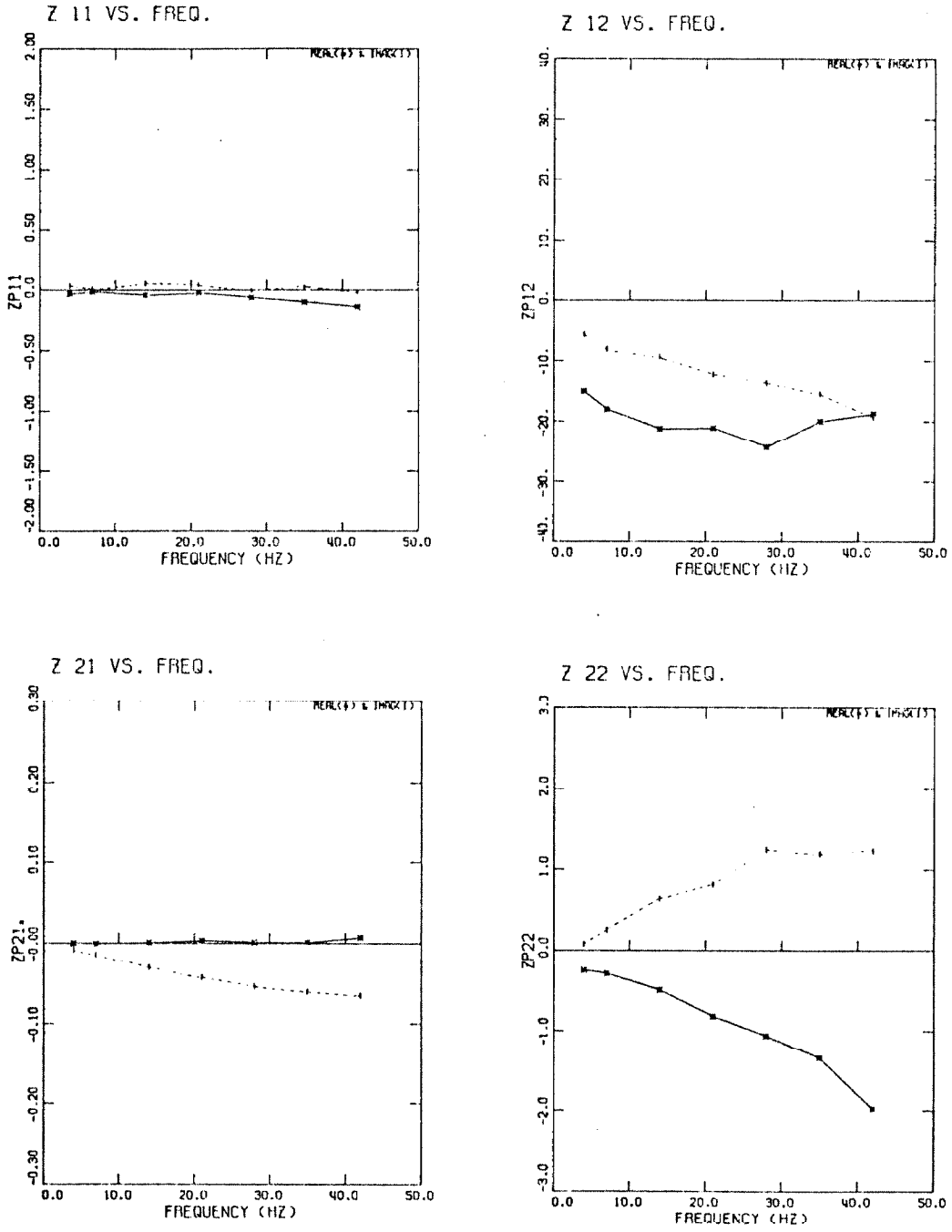

Fig. 6.2 Z-matrix of experiment (1), fully wetted conditions for Impeller IV where $\sigma = 0.51$ $\psi = 0.25$ and $\phi = 0.07$.

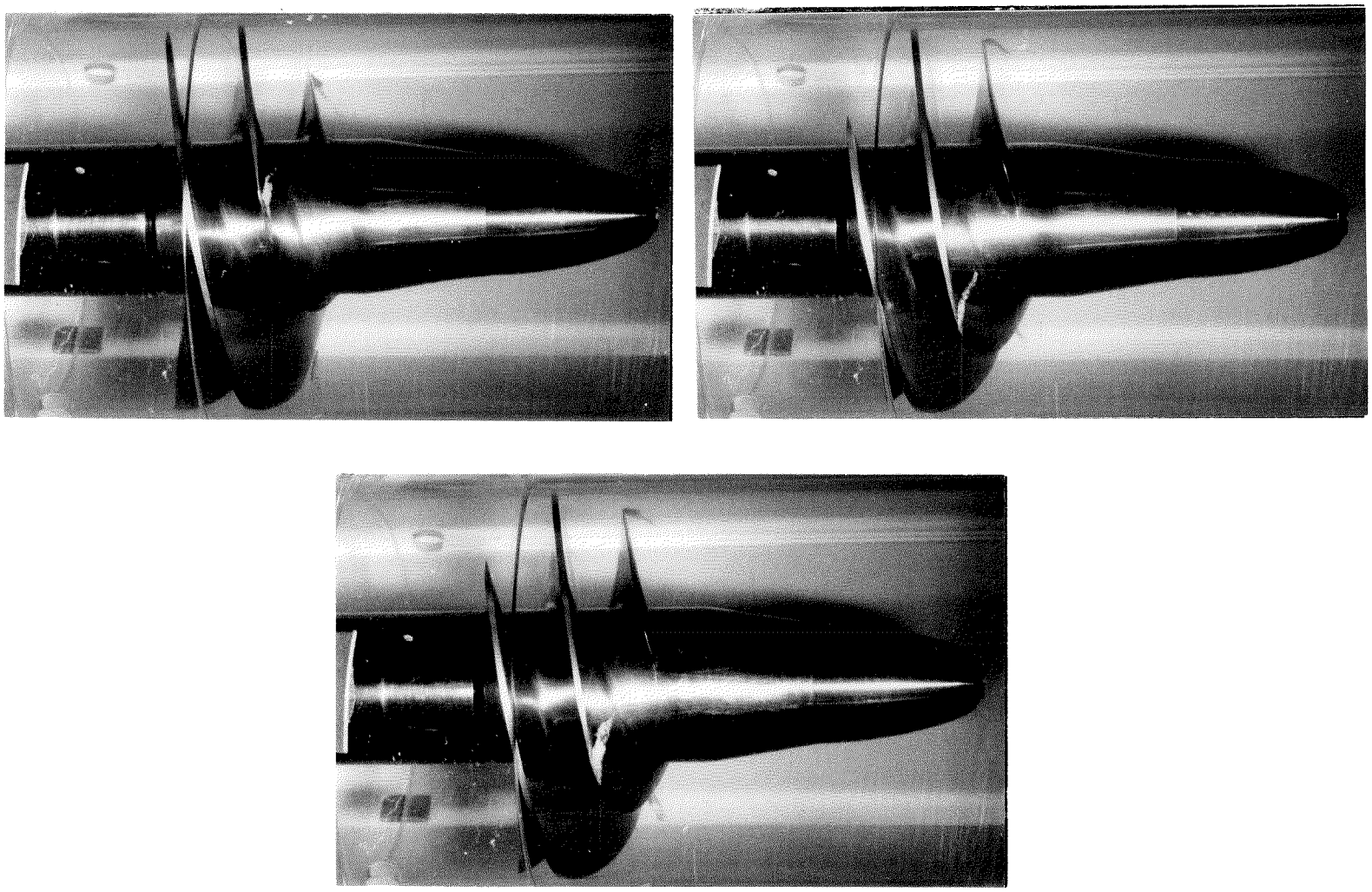

Fig. 6.3 Photographs of Inducer V during experiment (2), a fully-wetted condition. These photographs were taken randomly when the fluctuating frequency was 21 Hertz.

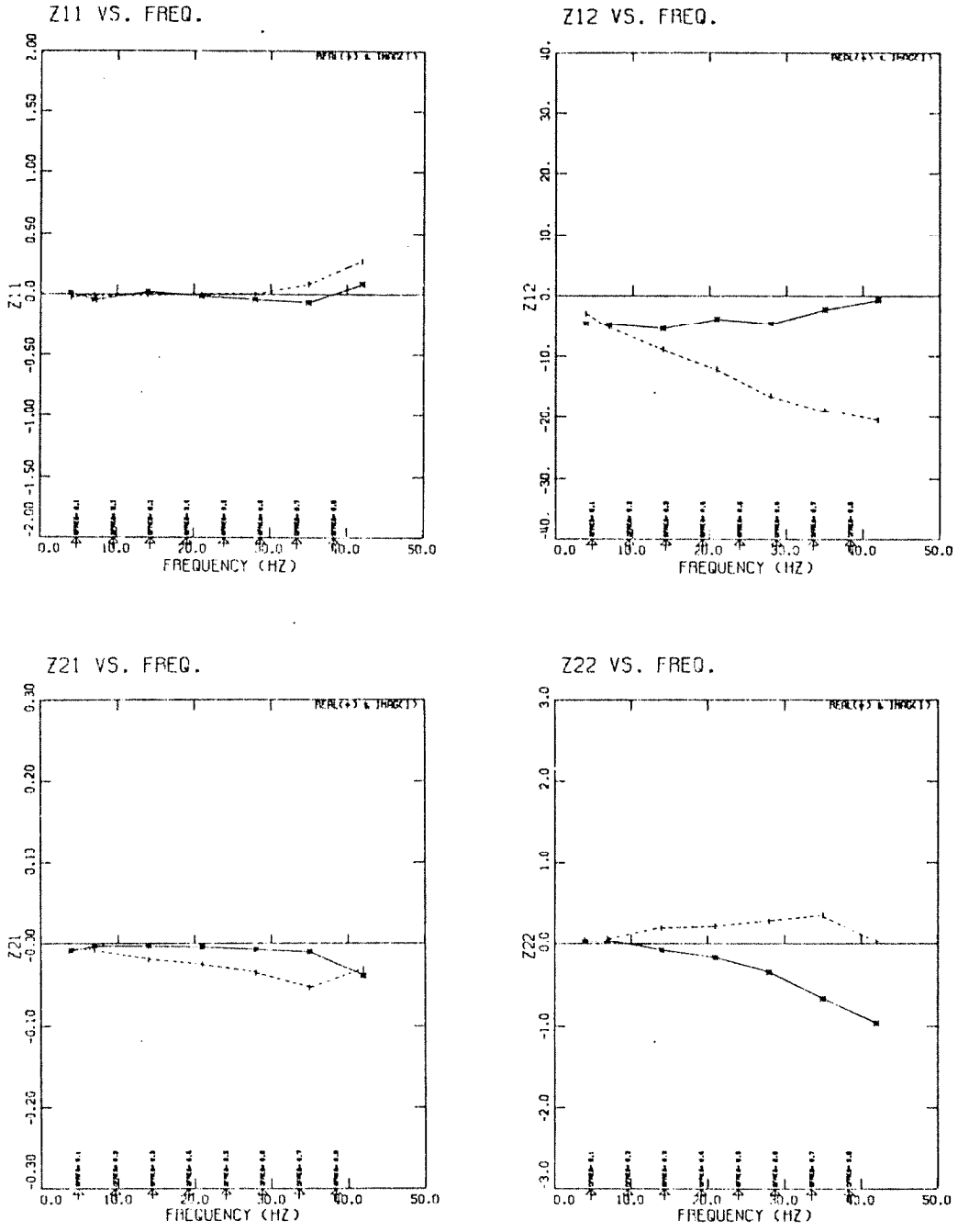

Fig. 6.4 Z-matrix of experiment (2), fully wetted conditions for Impeller V where $\sigma = 0.82$ $\psi = 0.12$ and $\phi = 0.088$.

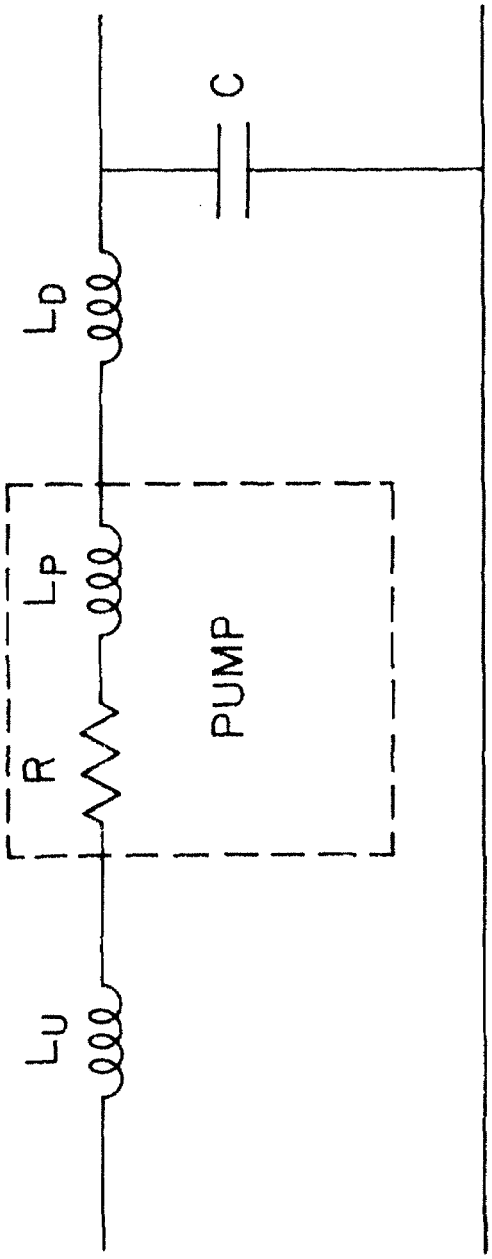

Fig. 6.5 Lumped parameter electrical analogy of the fully wetted experiment.

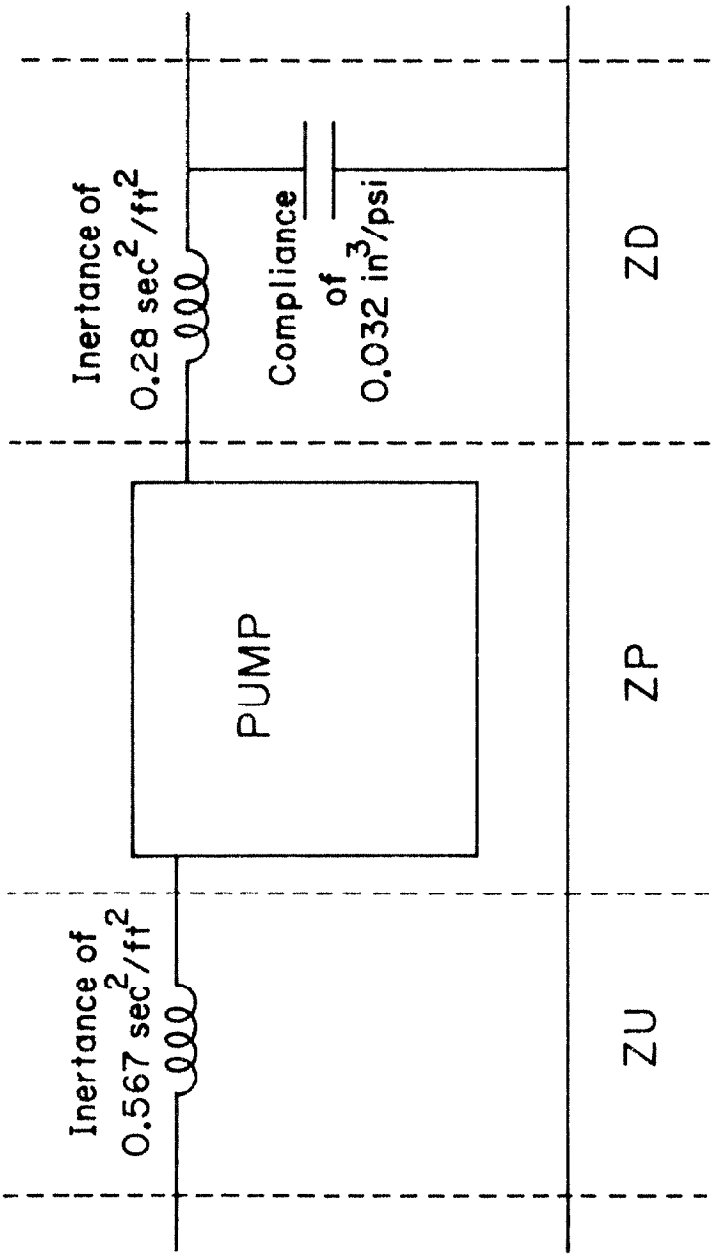

Fig. 6.6 Diagram showing the values of the system characteristics used for the ZP pump matrix reduction.

---Linear extrapolations

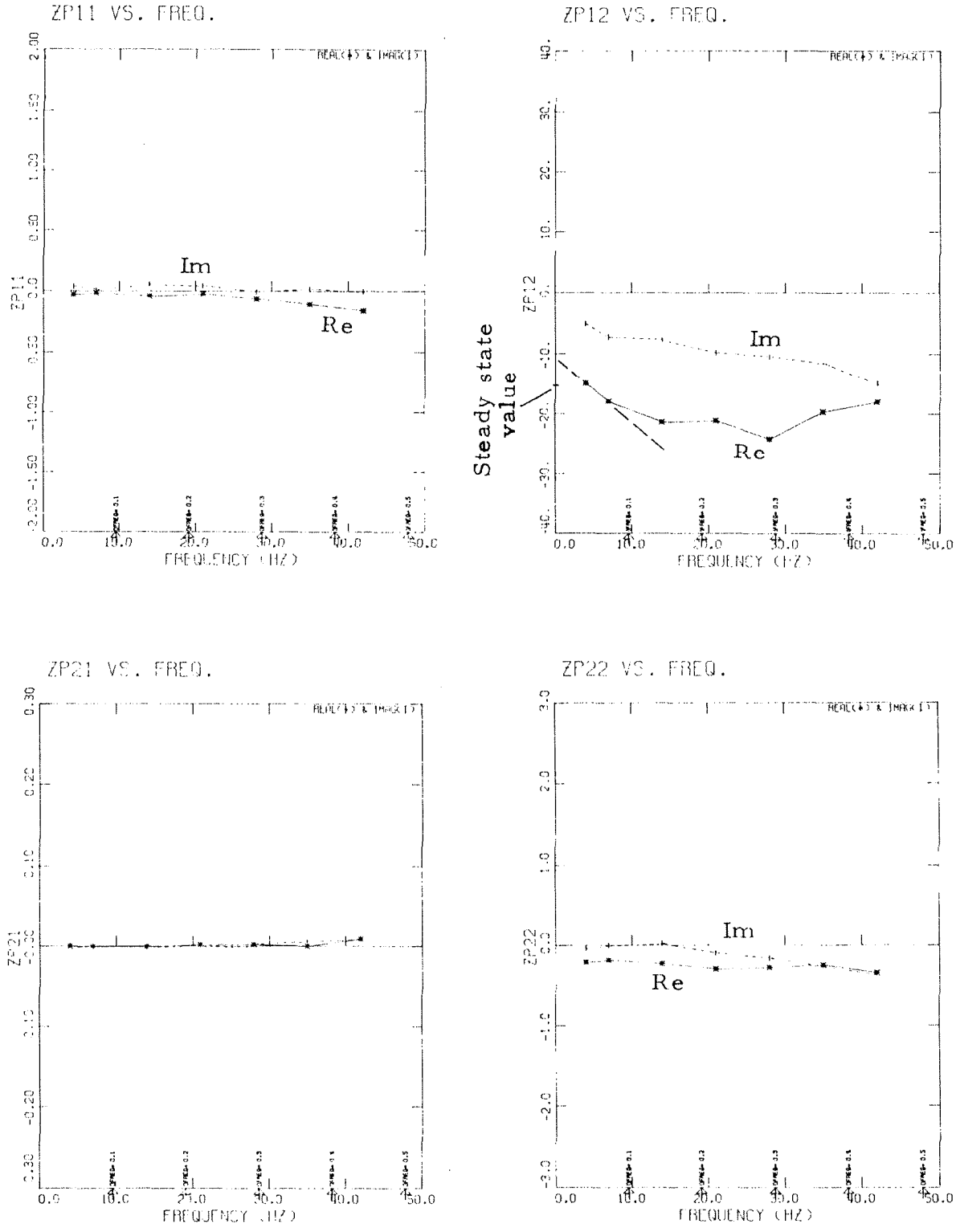

Fig. 6.7 ZP-matrix of experiment (1), the fully wetted condition for Impeller IV where $\sigma = 0.51$ $\psi = 0.25$ and $\phi = 0.07$.

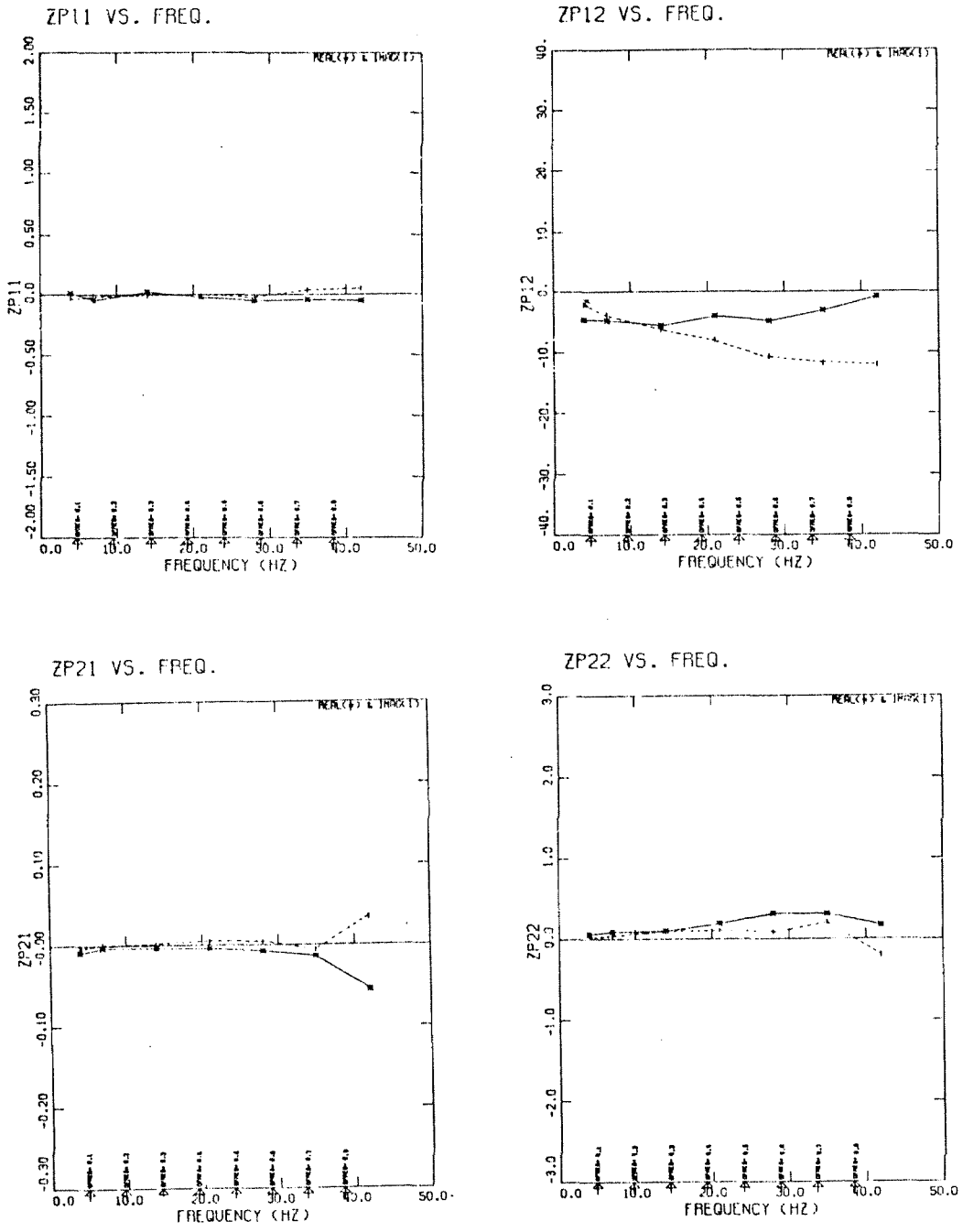

Fig. 6.8 ZP-matrix of experiment (2), the fully wetted condition for Impelier V where $\upsilon = 0.82$ $\psi = 0.12$ and $\phi = 0.087$.

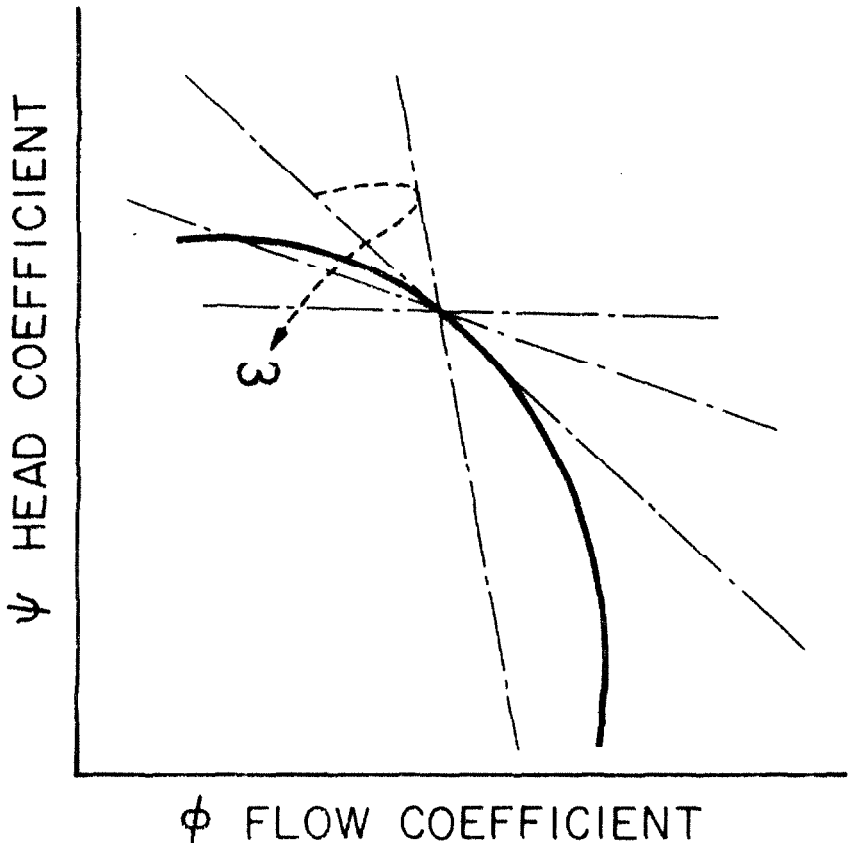

Fig. 6.9 Diagram showing the change of the pump resistance, slope of the curve, with increasing frequency.

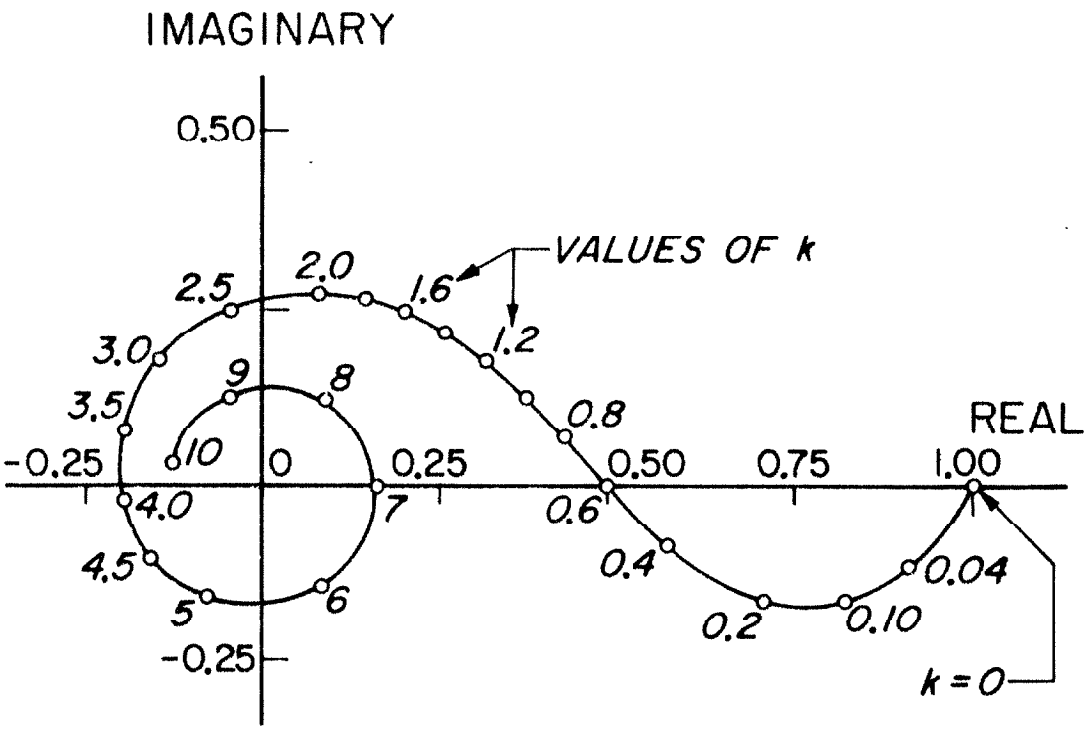

Fig. 6.10 Vector diagram showing the real and imaginary parts of Sears' function, $\varphi(k)$, as a function of the reduced frequency k when k is defined as $k = \frac{\omega b}{U}$. In this equation, ω is the oscillating frequency, b is the semichord length of the airfoil and U is the mean velocity.

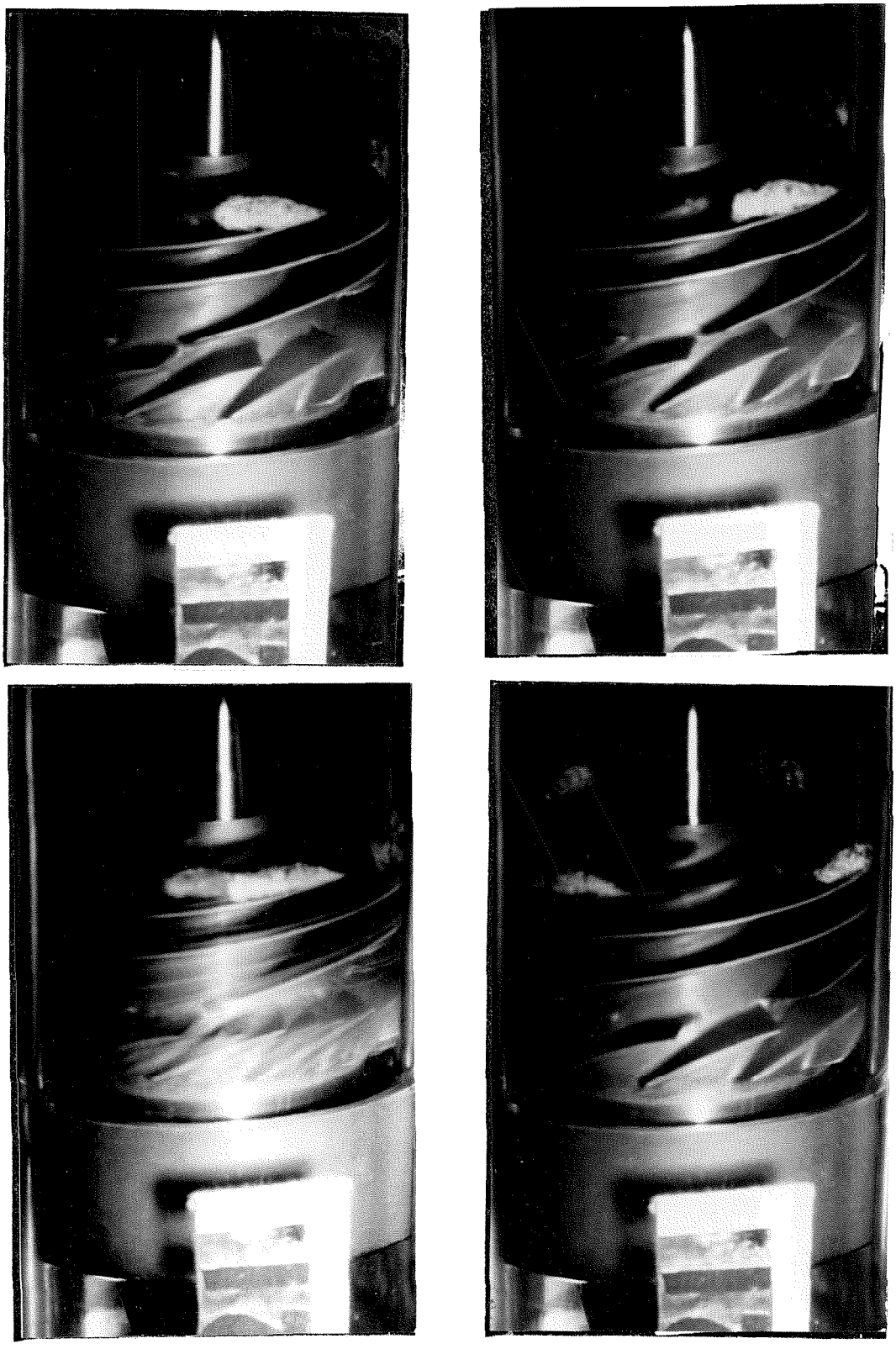

Fig. 6.11 Photographs of the cavitating Impeller IV during experiment (3) where $\sigma = 0.11$ $\psi = 0.26$ and $\varphi = 0.07$. These photographs were taken randomly when the fluctuating frequency was 7 Hertz.

---Linear extrapolations

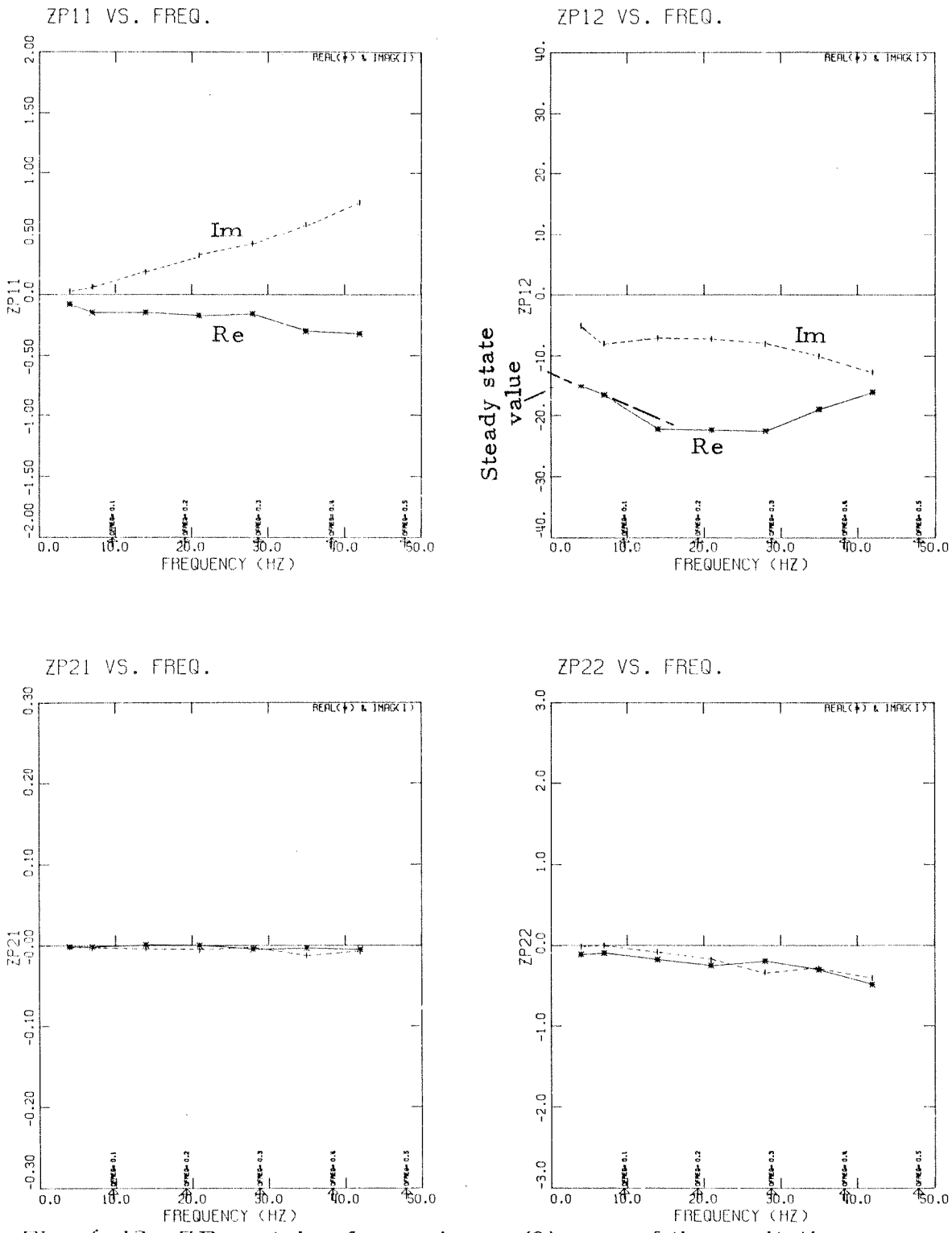

Fig. 6.12 ZP-matrix of experiment (3), one of the cavitating experiments for Impeller IV where $\sigma = 0.11$ $\psi = 0.26$ and $\phi = 0.07$.

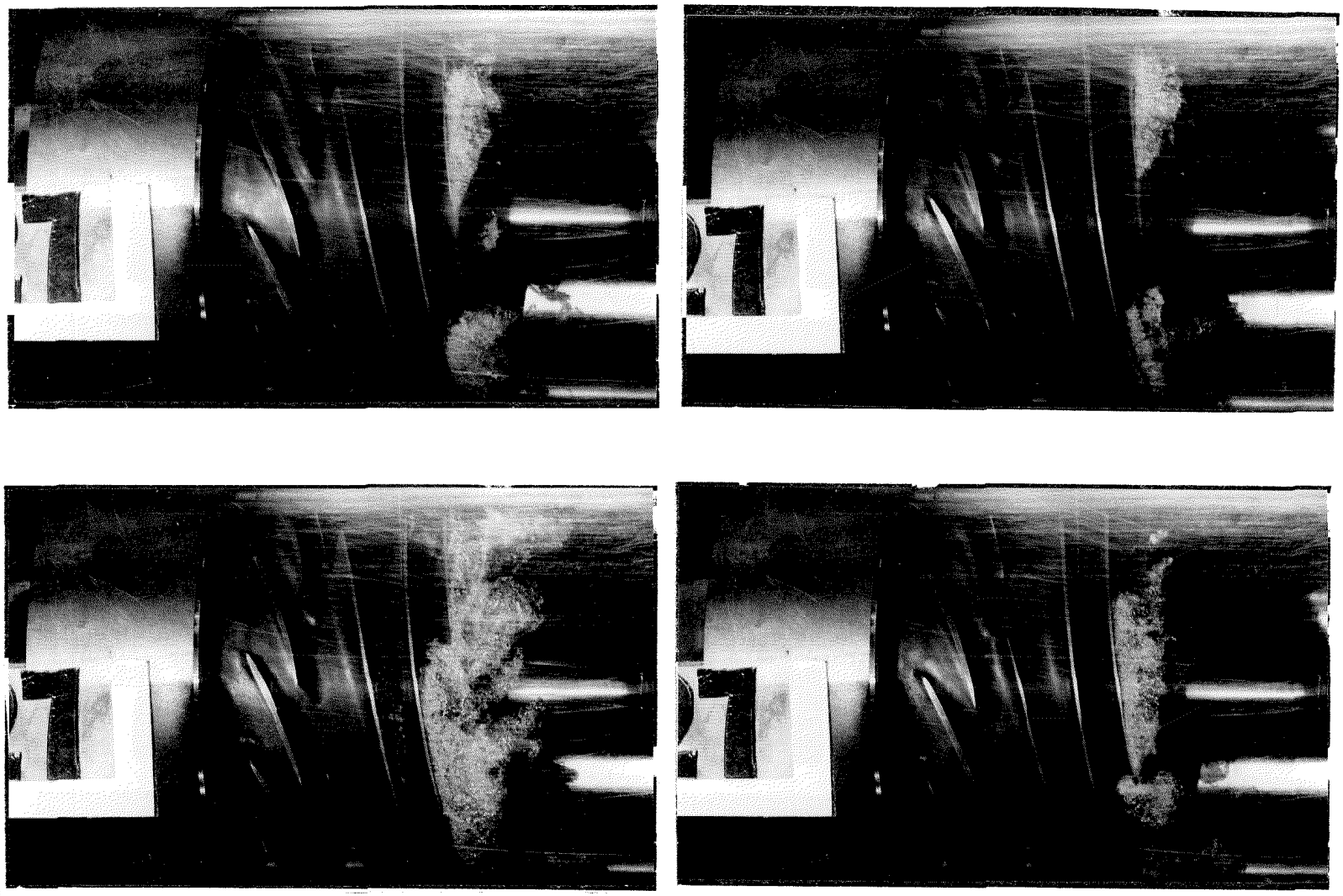

Fig. 6.13 Photographs of the cavitating Inducer IV during experiment (4) where $\sigma = 0.046$ $\psi = 0.25$ $\varphi = 0.07$. These photographs were taken randomly when the fluctuating frequency was 35 Hertz.

— — —Linear extrapolations

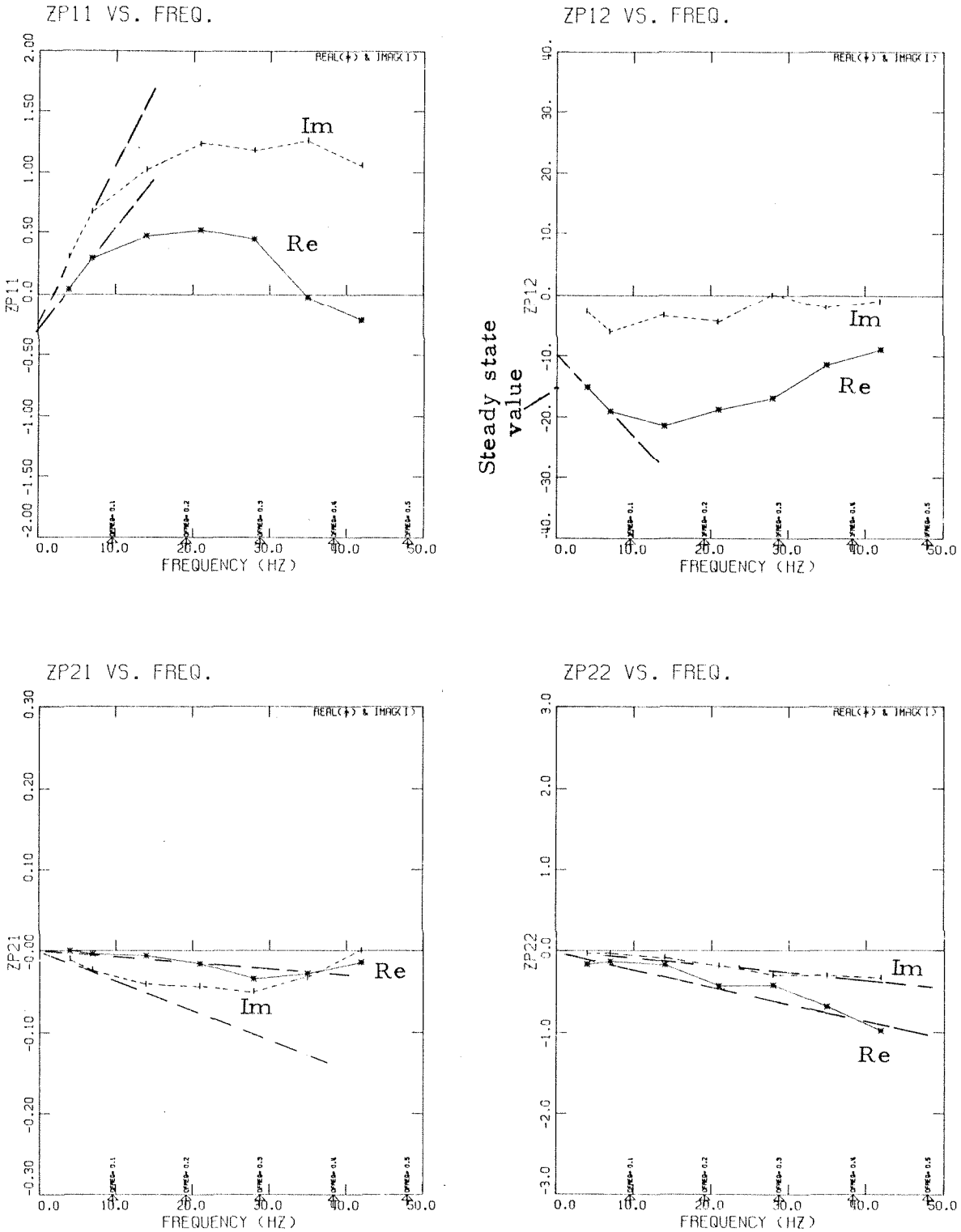

Fig. 6.14 ZP-matrix of experiment (4), the second cavitating experiment for Impeller IV where $\sigma = 0.046$ $\psi = 0.25$ and $\phi = 0.07$.

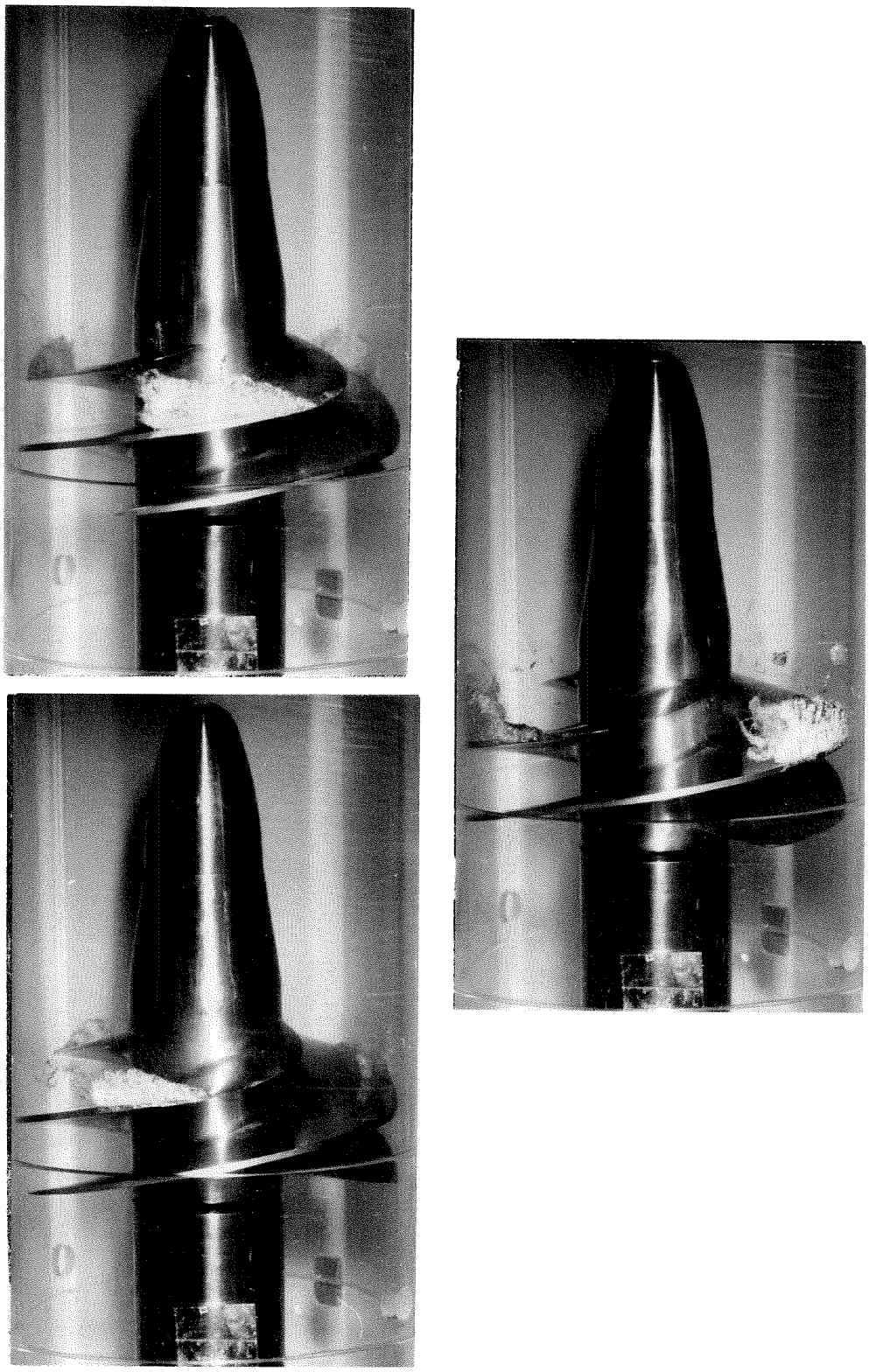

Fig. 6.15 Photographs of the cavitating Impeller V during experiment (5) where $\sigma = 0.12$ $\psi = 0.12$ and $\varphi = 0.087$. These photographs were taken randomly when the fluctuating frequency was 4 Hertz.

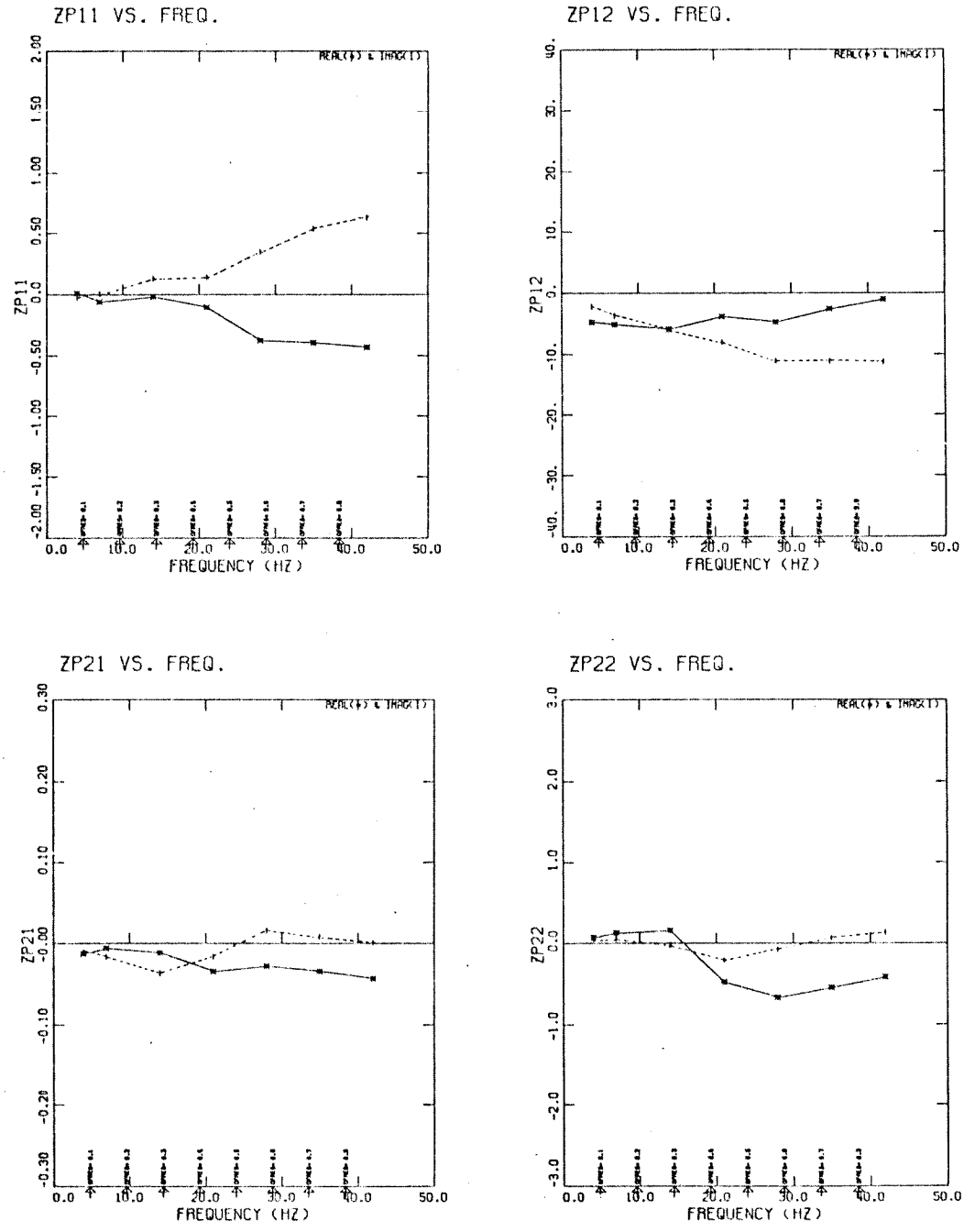

Fig. 6.16 ZP-matrix of experiment (5), the cavitating experiment for Impeller V where $\sigma = 0.12$ $\psi = 0.12$ and $\phi = 0.087$.

VII. SUMMARY AND CONCLUSION

The dynamic response of a cavitating inducer pump has been investigated experimentally in the present research. The repeatability and the agreement of experimental results when carefully controlled and when the system effect is removed demonstrate that it is possible to measure the transfer function of a pump operating at constant rotational speed. The present experiments show that the dynamic response of cavitating pumps has a very complex behavior in frequency which cannot be explained by extrapolations from steady-state performance nor quasi-steady analysis. These findings appear in all of the eight coefficients of the transfer function matrix. This is particularly so for the pump gain, ZP_{11}, the results for which were unexpected. There is rather a large phase lead for this term and the increase in magnitude with frequency of pump gain represents a deterioration of cavitation performance under dynamic conditions.

The remaining coefficients of the pump transfer function all show a behavior with frequency that cannot fully be accounted for by the quasi-steady assumption. Some particularly significant features in this respect are:

(1) The pump resistance appears to become smaller at the higher frequencies for both impellers.

(2) There are both real and imaginary parts for the pump "compliance" unlike the approximations that have been made to date in the field. In addition, there are important changes with frequency that cannot be accounted for with quasi-steady

cascade theory.

(3) The tests on Impeller IV reveal that the compliance is much larger than that deduced from quasi-steady cascade theory. Observations reveal that the predominant form of cavitation is bubbly tip clearance flow and not blade cavitation.

(4) The mass flow gain factor (associated with the term ZP_{22}) appears to be significant and should be taken into account in pump dynamic representations. It too, is seen to have real and imaginary parts. The quasi-steady blade cavitation calculation of this effect predicts only an imaginary part.

There are a few areas in which future experimental research should be directed to improve the experimental results:

(i) There is a need for a better fluctuator. As can be seen from the oscilloscope traces of the signals, they all appear to be in the form of square waves at the low frequency end. This produces a low signal-to-noise ratio for the basic frequency component and thus reduces the accuracy of the result. An ideal fluctuator will produce a precise sine wave which can be easily analyzed.

(ii) Tha laser doppler velocimeter measures the velocity at a point inside the flow channel. This is satisfactory but not ideal. A true mass flow rate measuring system will be needed to give a more true representation of the ZP-matrices. Hopefully, the new system will not need the

downstream smoothing chamber which introduces a large system compliance.

(iii) The present data acquisition system of recording and playback is very time consuming. The total time required for one ZP-matrix consisting of experiment, playback and signal analyzing, data averaging and computer processing needs a minimum of thirty man-hours. A considerable amount of time will be saved if the experiment can be recorded digitally. The digital records can be processed directly by the computer.

(iv) With the improvements above it would be possible to carry out the experiments at much lower levels of excitation, 0.5 percent mass flow fluctuation or less.

(v) Finally, there is a need for a tip cavitation compliance calculation similar to the bubble compliance calculated by Brennen (1973) such that a quantitative comparison can be made directly to the present experiments.

REFERENCES

Acosta, A. J., 1958, "An experimental study of cavitating inducers", Proc. of Second O. N. R. Symposium on Naval Hydrodynamics, August 25-29 (ACR-38).

Acosta, A. J., 1975, "Unsteady effects in flow rate measurement of the entrance of a pipe", Technical Brief, California Institute of Technology, Division of Engineering and Applied Science.

Anderson, D. A., Blade, R. J. and Stevens, W., 1971, "Response of a radial-bladed centrifugal pump to sinusoidal disturbances for non-cavitating flow", NASA, TN D-6536.

Brennen, C., 1973, "The dynamic behavior and compliance of a stream of cavitating bubbles", J. Fluids Eng., Vol. 95, Series 1, No. 4, 1973, pp. 533-542.

Brennen, C., and Acosta, A. J., 1973, "Theoretical, quasi-static analysis of cavitation compliance in turbopumps", Journal of Spacecraft and Rockets, Vol. 10, No. 3, pp. 175-180.

Brennen, C., and Acosta, A. J., 1975, "The dynamic transfer function for a cavitating inducer", ASME, 75-WA/FE-16.

Fanelli, M., 1972, "Further considerations on the dynamic behavior of hydraulic turbo-machinery", Water Power, pp, 208-222.

Farrel, E. C. and Fenwick, J. R., 1973, "Pogo instabilities suppression evaluation", NASA Report CR-134500.

Fung, Y. C., 1968, "Aeroelasticity", Dover Press.

Ghahremani, F. G., 1970, "Turbopump cavitation compliance", Report No. TOR-0059(6531-01)-2, Aerospace Corporation, El Segundo, California.

Gibbs, K. P. and Oliver, A. G., 1973, "Special requirements for pumps for sodium cooled fast reactors". Pumps for Nuclear Power Plant, Convention sponsored by the Fluid Machinery and Nuclear Power Plant Groups of the Institute of Mechanical Engineers, University of Bath, April 22-25, pp. 119-124.

Goldstein, R. J., and Adrian, R. J., 1971, "Measurement of fluid velocity gradients using Laser Doppler Techniques", Review of Scientific Instruments, Vol. 42, No. 9.

Henderson, R. E., 1972, "The unsteady response of an axial flow turbomachine to an upstream disturbance", Cambridge University, England.

Jaeger, C., 1963, "The theory of resonance in hydro-power systems, discussion of incidents and accidents occurring in pressure systems, J. Basic Eng., Vol. 85, pp. 631-640.

Jönsson, L., 1974, "Laser velocity meter for water flow with low particle concentration", Journal of Hydraulic Research, Vol. 12, No. 1.

Kamijyo, K. and Suzuki, A., 1973, "An experimental investigation of flat-plate helical inducers for rocket turbopumps", National and Aerospace Laboratory of Japan, NAL TR-345.

Kim, J. H. and Acosta, A. J., 1974, "Unsteady flow in cavitating turbopump", J. Fluids Eng., Vol. 96, pp. 25-28.

King, J. A., 1970, "Low speed inducers for a rocket engine feed system", NASA Report CR-72716, R-8272.

Knapp, R. T., Daily, J. W. and Hammitt, F. G., 1970, Cavitation, McGraw-Hill, Inc., New York, N. Y.

Liao, G. S., 1974, "Protection of boiler feed pump against transient suction decay", J. Eng. for Power, Vol. 96, pp. 247-255.

Liao, G. S. and Leung, P., 1972, "Analysis of feedwater pump suction pressure decay under instant turbine load rejection", J. Eng. for Power, Vol. 34, pp. 83-90.

Lock, M. and Rubin, S., 1974, "Passive suppression of POGO on the Space Shuttle", NASA Report CR-132452.

NASA, 1970, "Prevention of coupled structure-propulsion instability", NASA Report SP-8055.

NASA, 1971, "Liquid rocket engine turbopump inducers", NASA Report SP-8052.

Natanzon, M. S., Bl'tsev, N. I., Bazhanov, V. V. and Leydervarger, M. R., 1974, "Experimental investigation of cavitation-induced oscillations of helical inducers", Fluid Mechanics, Soviet Research, Vol. 3, No. 1, pp. 38-45.

Norquist, L. W. S., Marcus, J. P. and Ruscio, D. A., 1969, "Development of close-coupled accumulators for suppressing missile longitudinal oscillations (POGO):, AIAA 5th Propulsion Joint Specialist Conference, AIAA Paper No. 69-547.

Rocketdyne Report, 1969, "Investigation of 17-Hz, closed-loop instability on S-II stage of Saturn V", Rocketdyne Division, Rockwell International, Report No. R-7970.

Rocketdyne, 1974, "Test results of SSME low pressure oxidizer turbopump model inducer", Internal letter No. R/H 4194-3074.

Rothe, K., 1974, "Turbopump configuration selection for the Space Shuttle Main Engine", ASME 74-FE-23.

Rubin, S., 1966, "Longitudinal instability of liquid rockets due to propulsion feedback (POGO):, J. Spacecraft and Rockets, Vol. 3, No. 8, pp. 1188-1195.

Rubin, S., Wagner, R. G. and Payne, J. G., 1973, "POGO suppression on space shuttle – early studies", NASA Report CR-2210.

Sack, L. E. and Nottage, H. B., 1965, "System oscillations associated with cavitating inducers", J. Basic. Engr., Vol. 87, Series D, No. 4, pp. 917-925.

Stevans, W. and Blade, R. J., 1971, "Experimental evaluation of a pump test facility with controlled perturbations of inlet flow", NASA Report No. TN D-6543.

Streeter, V. L., and Wylie, E. B., 1974, "Waterhammers and surge control", Ann. Rev. Fluid Mech., Vol. 6, pp. 57-73.

Stripling, L. B. and Acosta, A. J., 1962, "Cavitation in turbopumps — Part I", J. Basic Engr., Vol. 84, No. 3, pp. 326-338.

Wagner, R. G., 1971, "Tital II engine transfer function test results", Report No. TOR-0059 (G471)-9, Aerospace Corporation, El Segundo, California.

Vaage, R. D., Fidler, L. E. and Zehnle, R. A., 1972, "Investigation of characteristics of feed system instabilities", Final Report MCR-72-107, Martin Marietta Corporation, Denver, Colorado.

APPENDIX A

LASER DOPPLER VELOCIMETER

The laser doppler velocimeter requires a transparent working fluid with some light scattering particles moving with the fluid. The principle is based on the doppler frequency shift due to the movement of a reflecting surface. In this particular case, a laser beam is split into two beams, a weak one and a strong beam. Particles in the fluid scatter the light in the strong beam. This scattered light is mixed with the weak beam in a photomultiplier. The two beams, being of different frequency, produce a voltage output from the photomultiplier with frequency equal to the doppler beat frequency as given by

$$\nu_d = \left(\frac{n}{\lambda}\right) \underline{u} \cdot (\underline{k}_{ss} - \underline{k}_i)$$

where ν_d is the beat frequency, n is the refractive index of the fluid, λ is the vacuum wavelength of the incident radiation, $\underline{u}$ is the particle velocity, and $\underline{k}_i$ and $\underline{k}_{ss}$ are the unit vectors in the direction of the incident and scattered light. Thus the doppler frequency is directly proportional to the velocity of the flow. For a more detailed description see Jönsson 1974, Goldstein and Adrian 1971.

In the present system which was conceived and designed by Dr. S. Barker formerly at this Institute, the beam of a 5mw He-Ne continuous laser[1] is split into two parallel beams by a precision glass block tilted at a slight angle to the beam direction. One of the beams

---

[1] Spectra Physics No. 120

which will eventually shine directly into the photomultiplier[2] is weakened by a neutral density filter and is referred to as the weak beam whereas the other one is referred to as the strong beam. The direction of the measured velocity is in the plane of the two beams and perpendicular to their bisector. The velocity of the fluid in the direction defined above, V, is given by

$$V = \frac{\lambda_o \nu_D}{2n \sin(\theta/2)}$$

where ν_s is the beat frequency, λ_o is the laser wavelength, n is the refractive index of the fluid and θ is the angle between the two beams. The two beams are focused to cross at the center of the flow channel by a 50 cm (19.3 in.) converging lens. The two beams intercept with a scattering volume of about 0.79 in. in length and 0.006 in. width. The output of the photomultiplier is an ac voltage having a frequency equal to the doppler frequency as given above.

The rest of the system consists of electronic processing of the doppler signal to give a voltage directly proportional to the velocity. The signal out of the photomultiplier is amplified first by a pre-amp stage and finally by two more stages. The last amplifier stage has a voltage limiter and shapes the signal to approximate a square wave. This output is connected to a phase-lock loop[3] where the output is a more precise square wave. The improved wave form leads to a better signal-to-noise ratio. The square wave is fed into a frequency divider and hence into a frequency to voltage converter.[4]

---

2 RCA No. 8645 photomultiplier
3 Signetics NE 565A
4 Anadex No. P1-408R

The frequency divider divides the frequency into a more convenient frequency for the frequency to voltage converter which can only accept up to 50k Hertz. The normal operating range of the doppler frequency is of the order of 80K-200k Hertz. Finally, the output of the frequency to voltage converter is a voltage proportional directly to the measured velocity. These details are sketched in the flow diagram of Fig. A1.

Two such systems[5] were constructed to be used in this study. They are essentially identical except for slight differences in the frequency to voltage converters. The two converters were purchased at different times and have different model numbers.[6] The calibration of these systems is given in Appendix B.

[5] CIT Aeronautics electronics shop, Mr. V. Sodha

[6] The latter Anadax model PI-608R

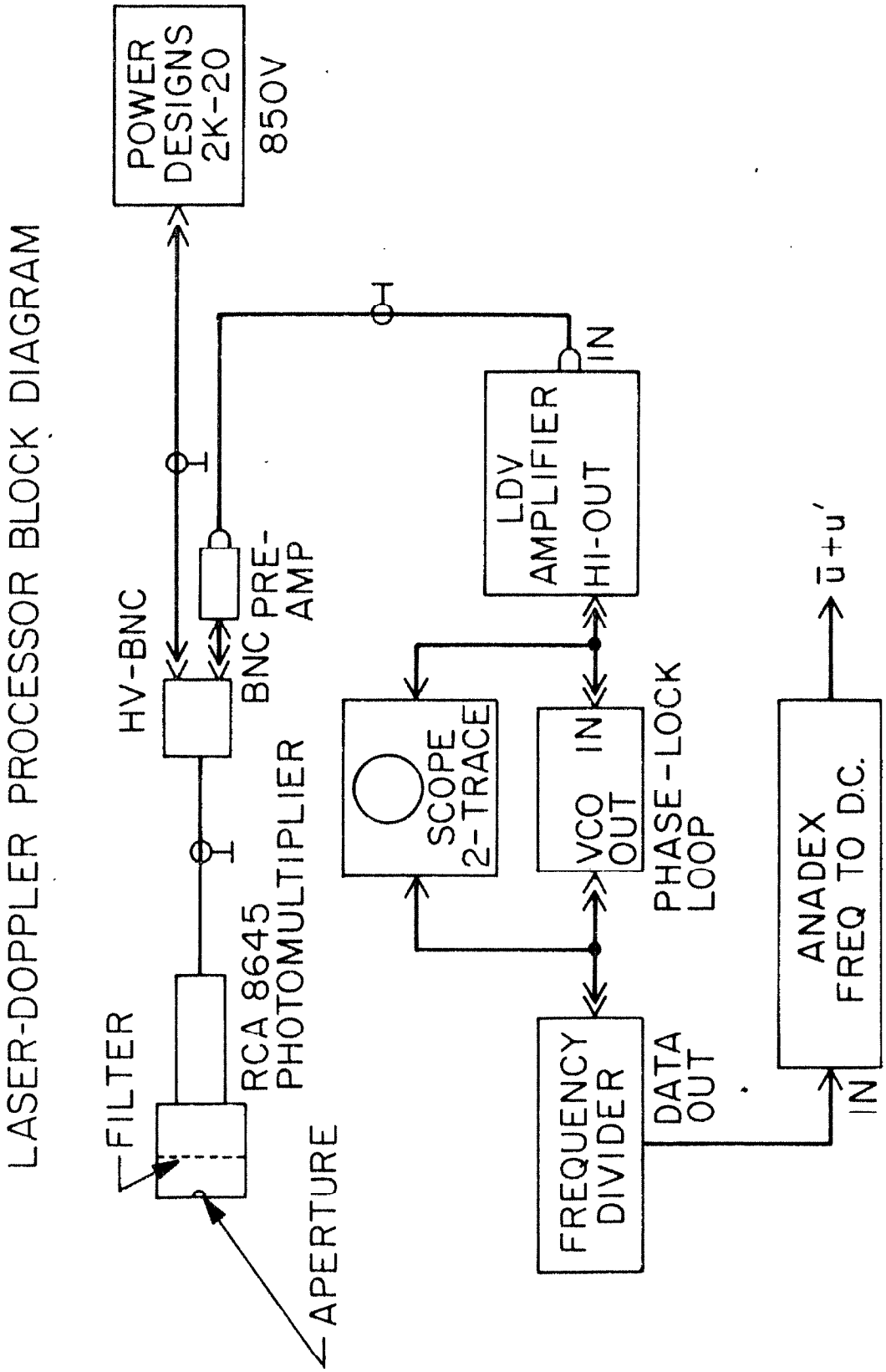

Fig. A1 Schematic for the LDV processor.

APPENDIX B

CALIBRATION OF MASS FLOW MEASUREMENT SYSTEM

In order to truly represent the mass flow rate by the laser doppler velocimeter measurements, it is desirable to minimize the boundary layer in the section where the velocity is measured. The nine-to-one converging nozzle just prior to the measuring station was designed to do this. To assure that we have obtained a good flat velocity profile across the channel, a small Pitot tube was used to traverse the two laser viewing sections to measure the steady velocity profile. It was found that the boundary layer thickness was typically about 10 percent of the radius as shown in Figs. B1 and B2. The slope of the profile was due to the reduced cross sectional area occupied by the Pitot tube. The laminar boundary layer calculation gives a thickness of about 5 percent of the radius at the viewing station. This calculation used the result of a flat plate laminar boundary layer starting from the end of the convertent nozzle. The discrepancy between measured and calculated values is due to the crude assumption made in the calculation.

There is an important issue of whether the oscillating velocity profile has the same shape as the steady velocity profile since the shape affects the basic assumption of mass flow measurement. This was resolved by Acosta (1975) who found that the thickness of oscillating boundary layer had little effect on this type of mass flow measurement.

To evaluate the smoothing chambers, the turbulence level against flow rate was measured. This was accomplished by comparing the rms output of the LDV as measured by a HP 3400 true rms meter

with the dc value. The resultant measurement is actually an inseparable combination of the fluid flow turbulence and the electronic noise of the LDV processor. The result is shown in Fig. B3 which demonstrated that the turbulence level is mostly under 1 percent of the mean flow.

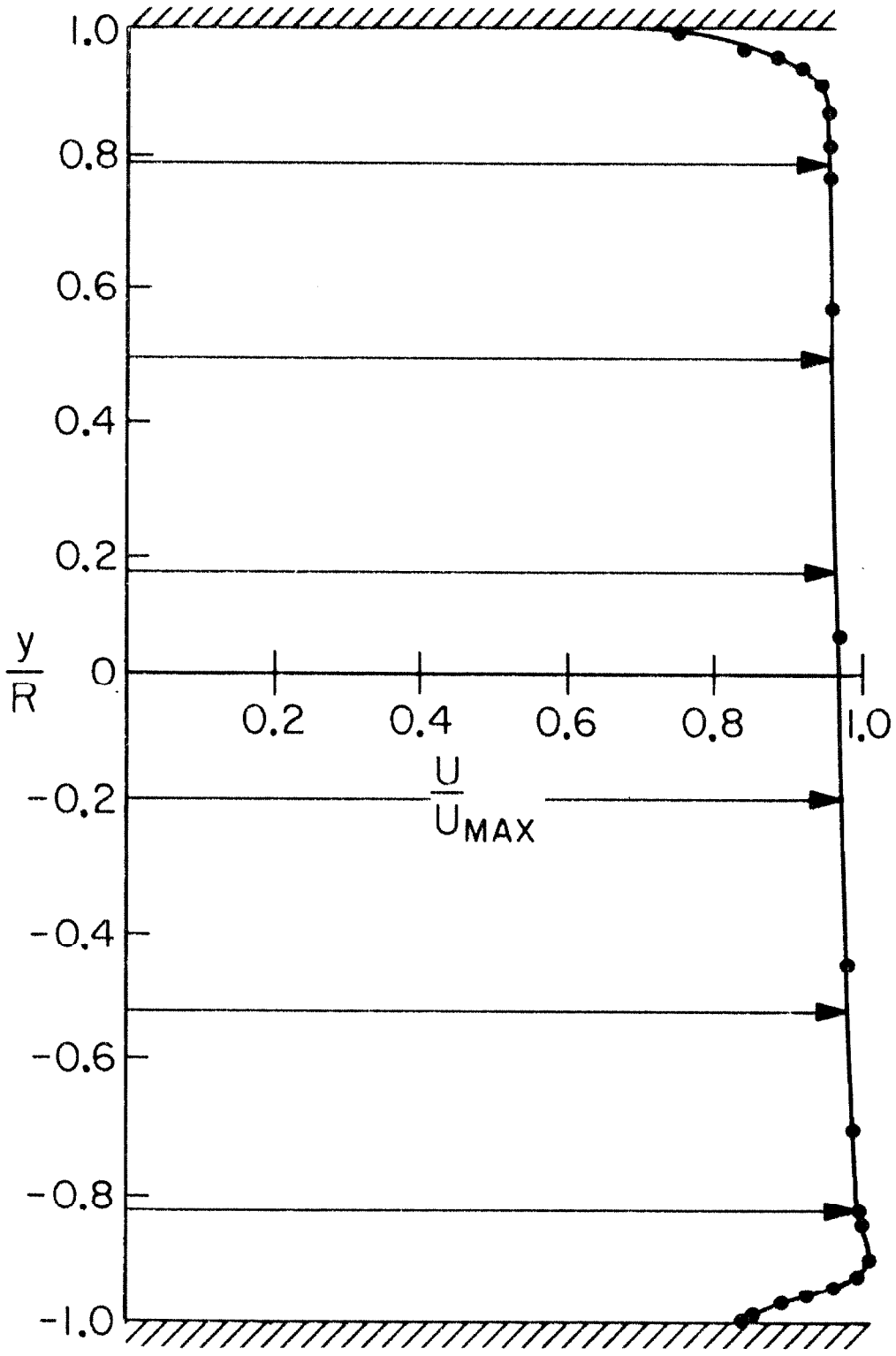

Fig. B1 Steady state velocity profile across the upstream laser doppler velocimeter viewing channel.

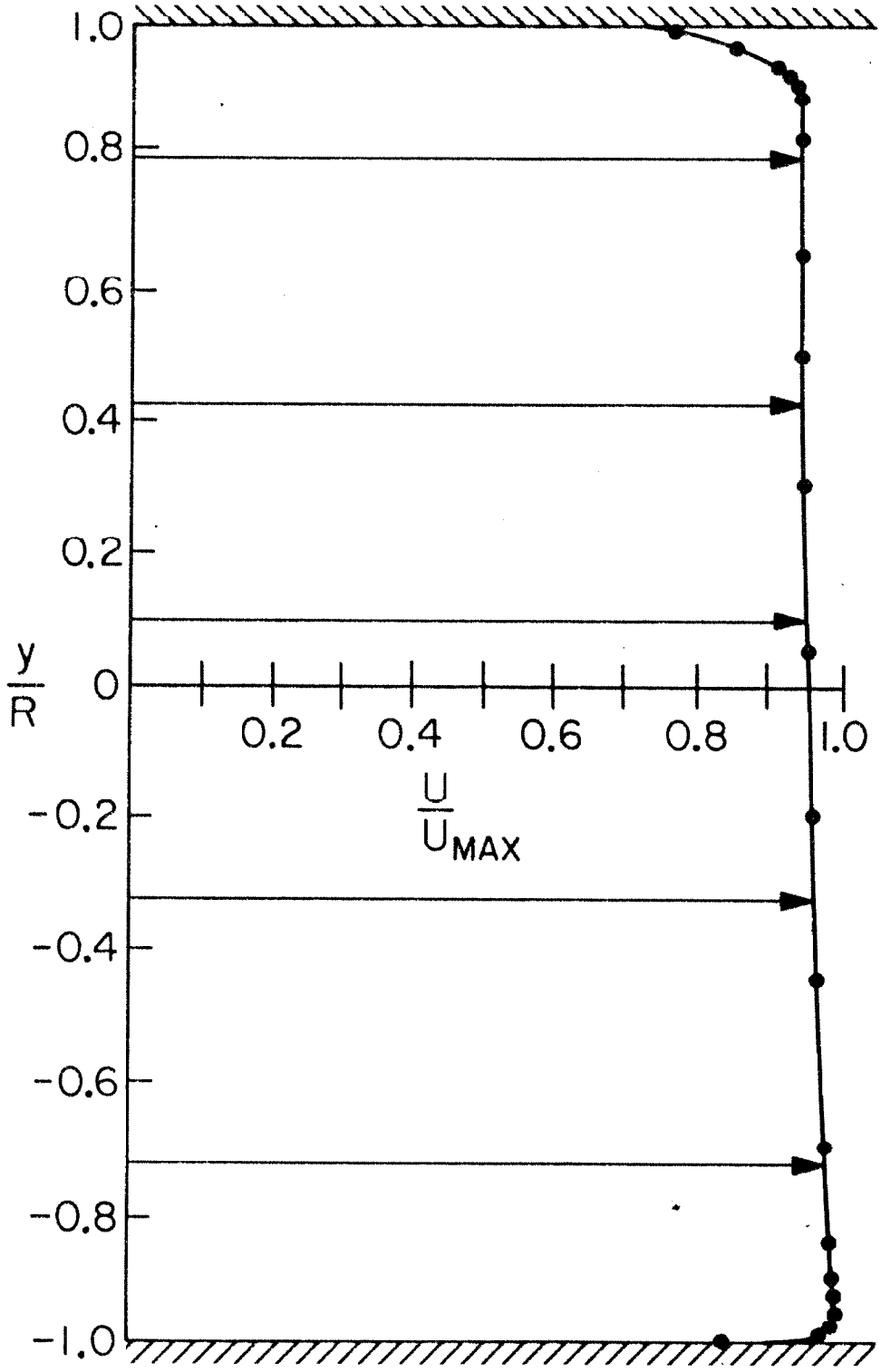

Fig. B2 Steady state velocity profile across the downstream laser doppler velocimeter viewing channel.

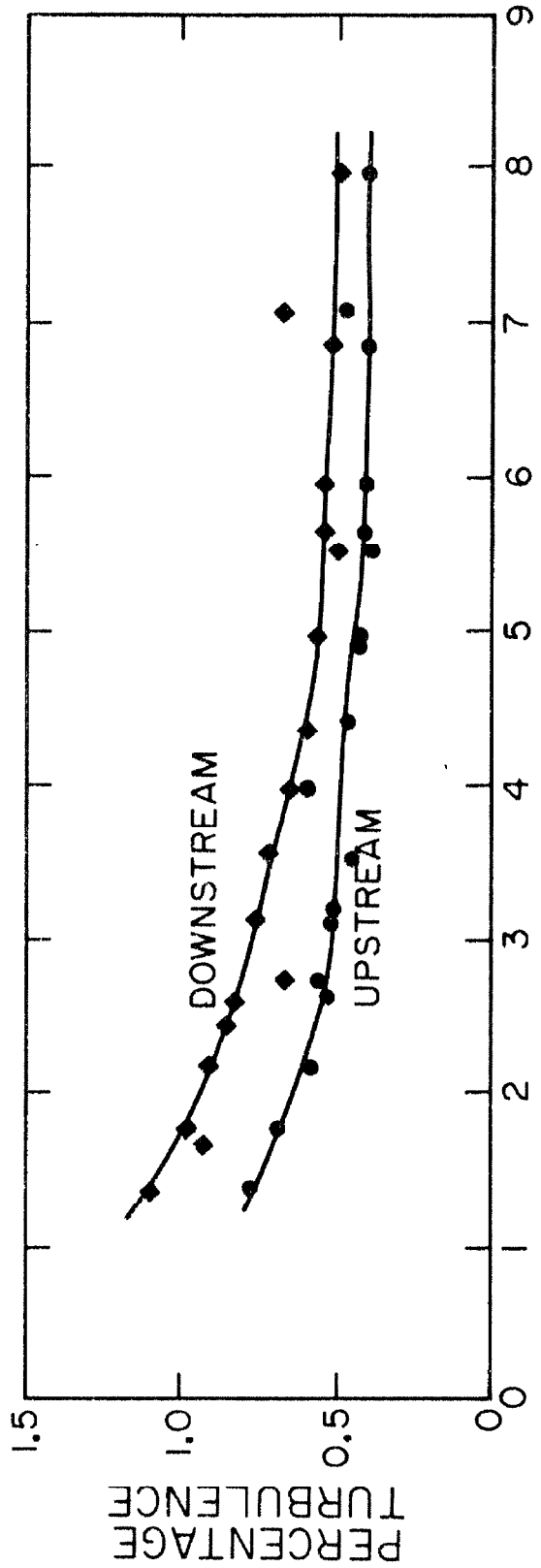

Fig. B3 Turbulence levels as measured by the LDV systems.

APPENDIX C

FLOW CHARTS OF COMPUTER PROGRAMS

The block flow charts of the three programs mentioned in Chapter IV are given here. These are:

(1) RAWDATA

(2) TRANSCO

(3) PUMA

RAWDATA BLOCK FLOW CHART

This program takes the voltage readings from experiment, converts them into the appropriate units and plots them as a function of frequency. It also calculates the required dimensionless groups to be processed by the next program, TRANSO.

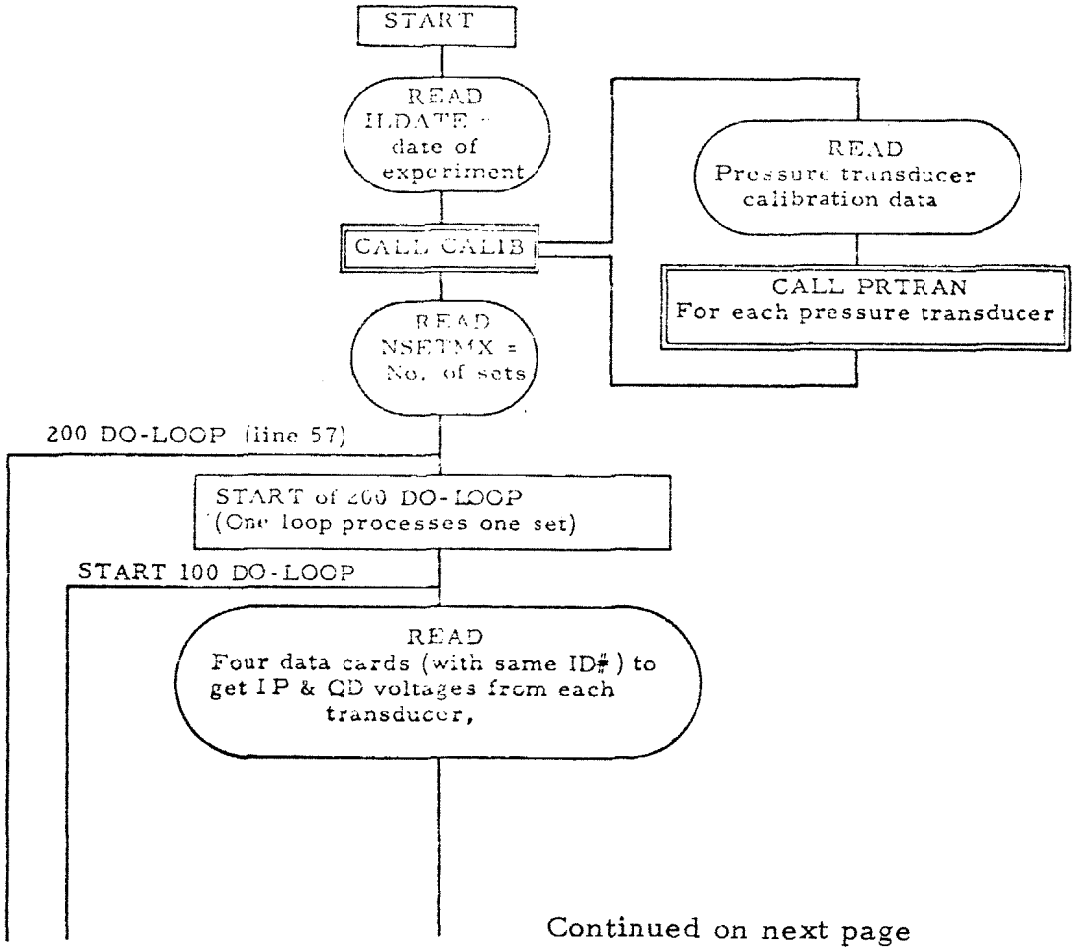

Continued on next page

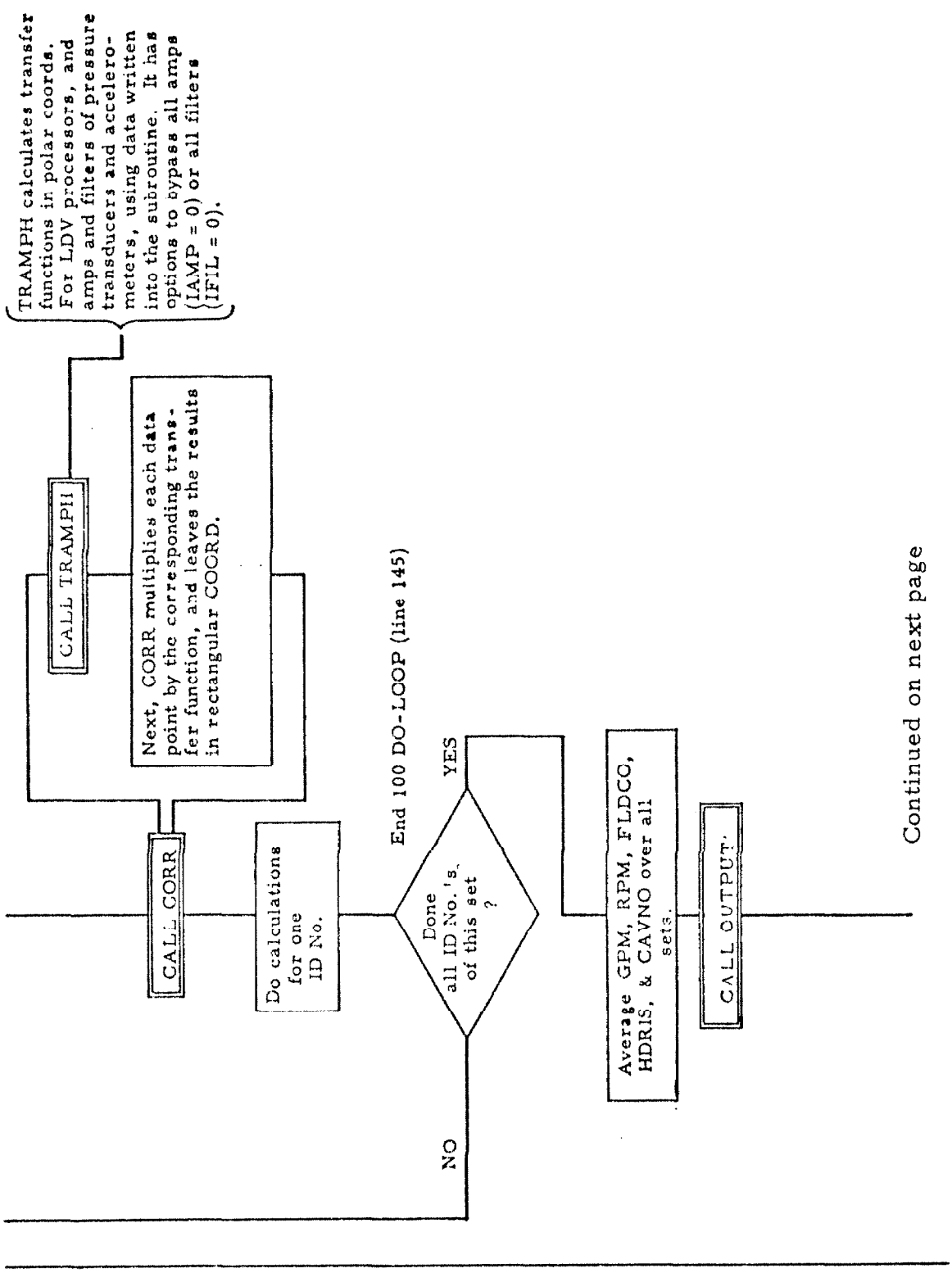
TRAMPH calculates transfer functions in polar coords. For LDV processors, and amps and filters of pressure transducers and accelerometers, using data written into the subroutine. It has options to bypass all amps (IAMP = 0) or all filters (IFIL = 0).
CALL TRAMPH
Next, CORR multiplies each data point by the corresponding transfer function, and leaves the results in rectangular COORD.
CALL CORR
Do calculations for one ID No.
End 100 DO-LOOP (line 145)
Done all ID No.'s. of this set ?
YES
NO
Average GPM, RPM, FLDCO, HDRIS, & CAVNO over all sets.
CALL OUTPUT
Continued on next page

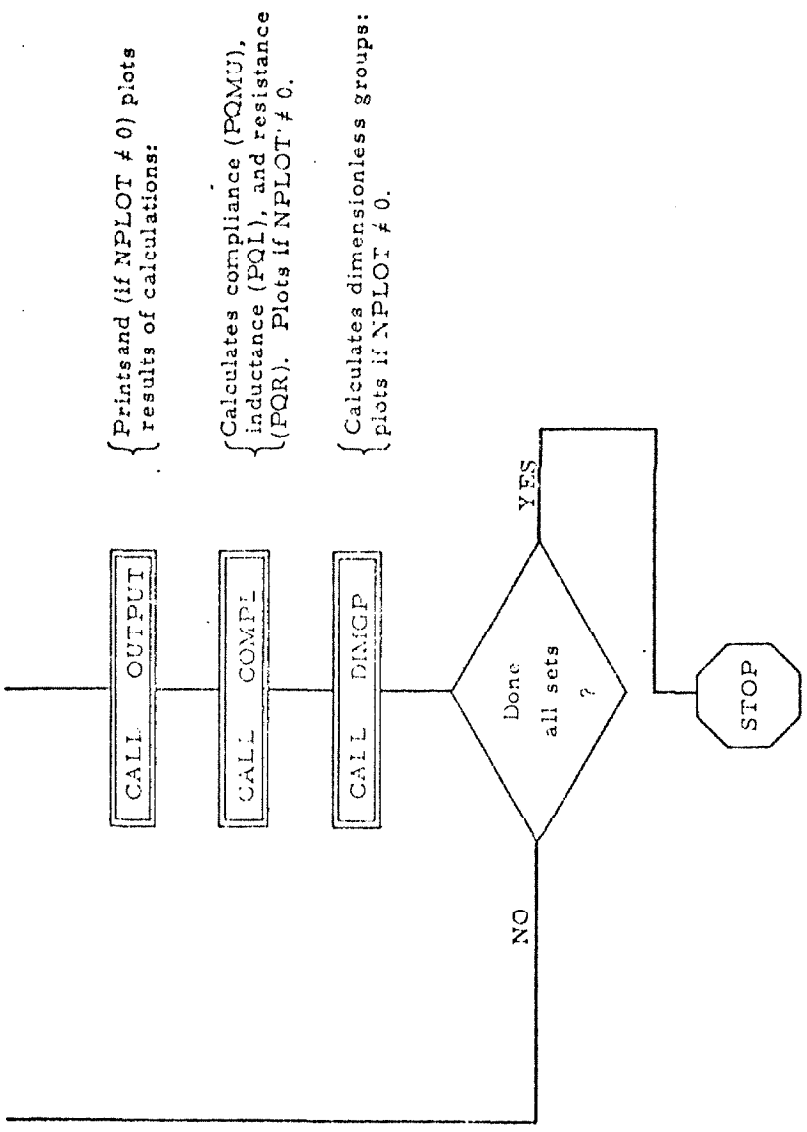
CALL OUTPUT
Prints and (if NPLOT ≠ 0) plots results of calculations:
CALL COMPL
Calculates compliance (PQMU), inductance (PQL), and resistance (PQR). Plots if NPLOT ≠ 0.
CALL DIMGP
Calculates dimensionless groups; plots if NPLOT ≠ 0.
Done all sets ?
YES
NO
STOP

TRANSCO BLOCK FLOW CHART

This program finds the transfer function complex matrix Z, as determined by pressure and mass flow measurements made at the upstream and downstream measuring stations, and provided to the program by data cards. One SET is composed of NUMWAY Z matrices at each of NFREQ frequencies. The program computes and processes one set entirely before it starts on the next set. NSETMX sets form one "bunch" of sets. Bunches of sets are processed until all data cards have been used.

Data cards for one set are grouped by frequency. For each frequency, one card identifies the frequency, and NK (NK ≥ 2) cards follow, each providing a pressure and mass flow at the upstream and at the downstream measuring stations. If NK > 2, the program may compute Z matrices using different combinations (specified in the array NWAY by the user for each set) of the NK data cards.

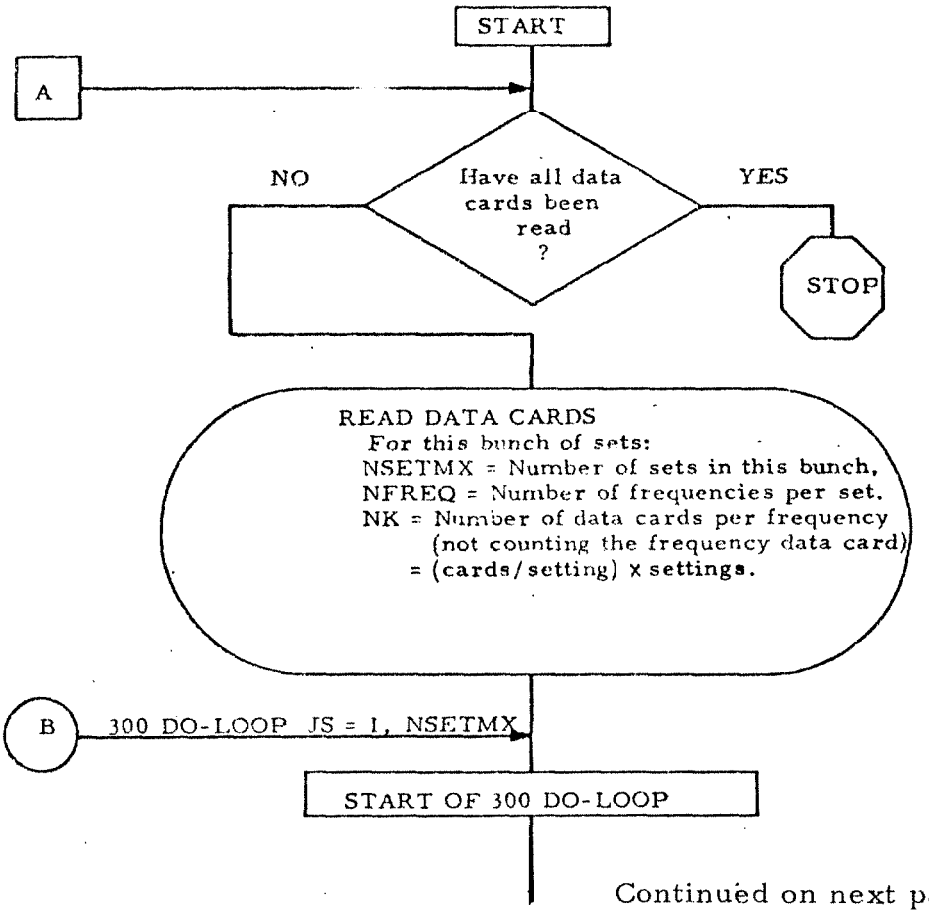

Continued on next page

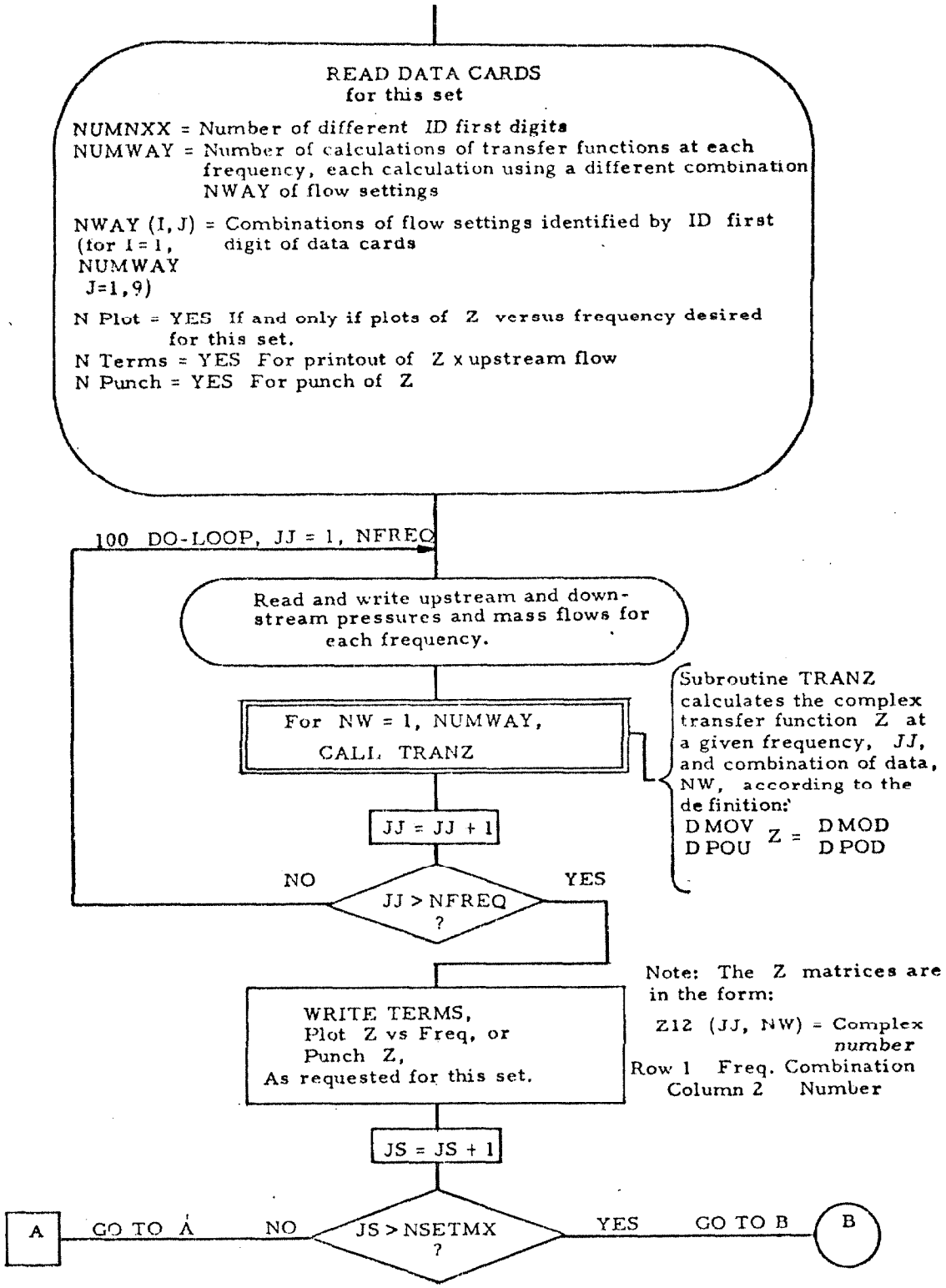
READ DATA CARDS
for this set
NUMNXX = Number of different ID first digits
NUMWAY = Number of calculations of transfer functions at each frequency, each calculation using a different combination NWAY of flow settings
NWAY (I, J) = Combinations of flow settings identified by ID first digit of data cards
(for I = 1, NUMWAY J=1,9)
N Plot = YES If and only if plots of Z versus frequency desired for this set.
N Terms = YES For printout of Z x upstream flow
N Punch = YES For punch of Z
100 DO-LOOP, JJ = 1, NFREQ
Read and write upstream and downstream pressures and mass flows for each frequency.
For NW = 1, NUMWAY,
CALL TRANZ
Subroutine TRANZ calculates the complex transfer function Z at a given frequency, JJ, and combination of data, NW, according to the definition:
DMOV / DPOU Z = DMOD / DPOD
JJ = JJ + 1
NO
JJ > NFREQ ?
YES
WRITE TERMS,
Plot Z vs Freq, or
Punch Z,
As requested for this set.
Note: The Z matrices are in the form:
Z12 (JJ, NW) = Complex number
Row 1 Freq. Combination
Column 2 Number
JS = JS + 1
A
GO TO A
NO
JS > NSETMX ?
YES
GO TO B
B

PUMA BLOCK FLOW CHART

This program finds the pump transfer function complex matrix ZP, given ZU and ZD matrices and a ZT matrix input on data cards. One "set" is completed when NUMWAY ZP matrices at each of NFREQ frequencies is calculated, printed, plotted, and punched. The program repeats this process NSETMX times to complete one "bunch of sets". Bunches of sets will be processed for however many data are in the input deck.

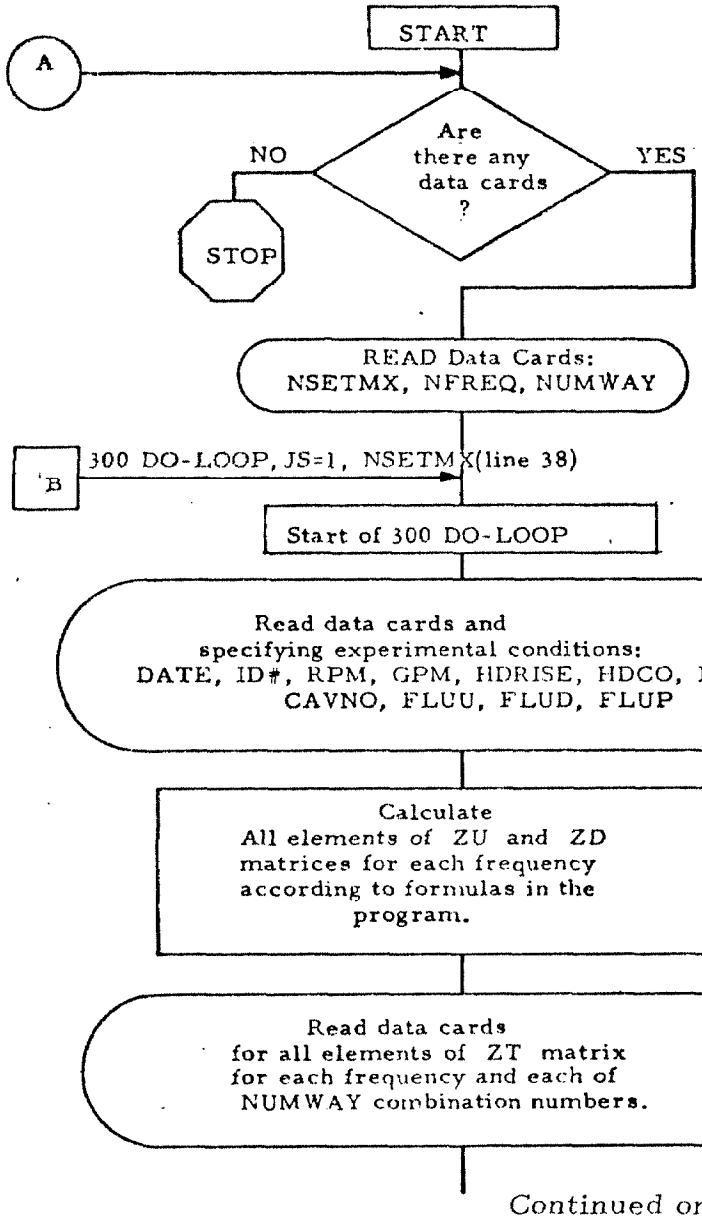

Continued on next page

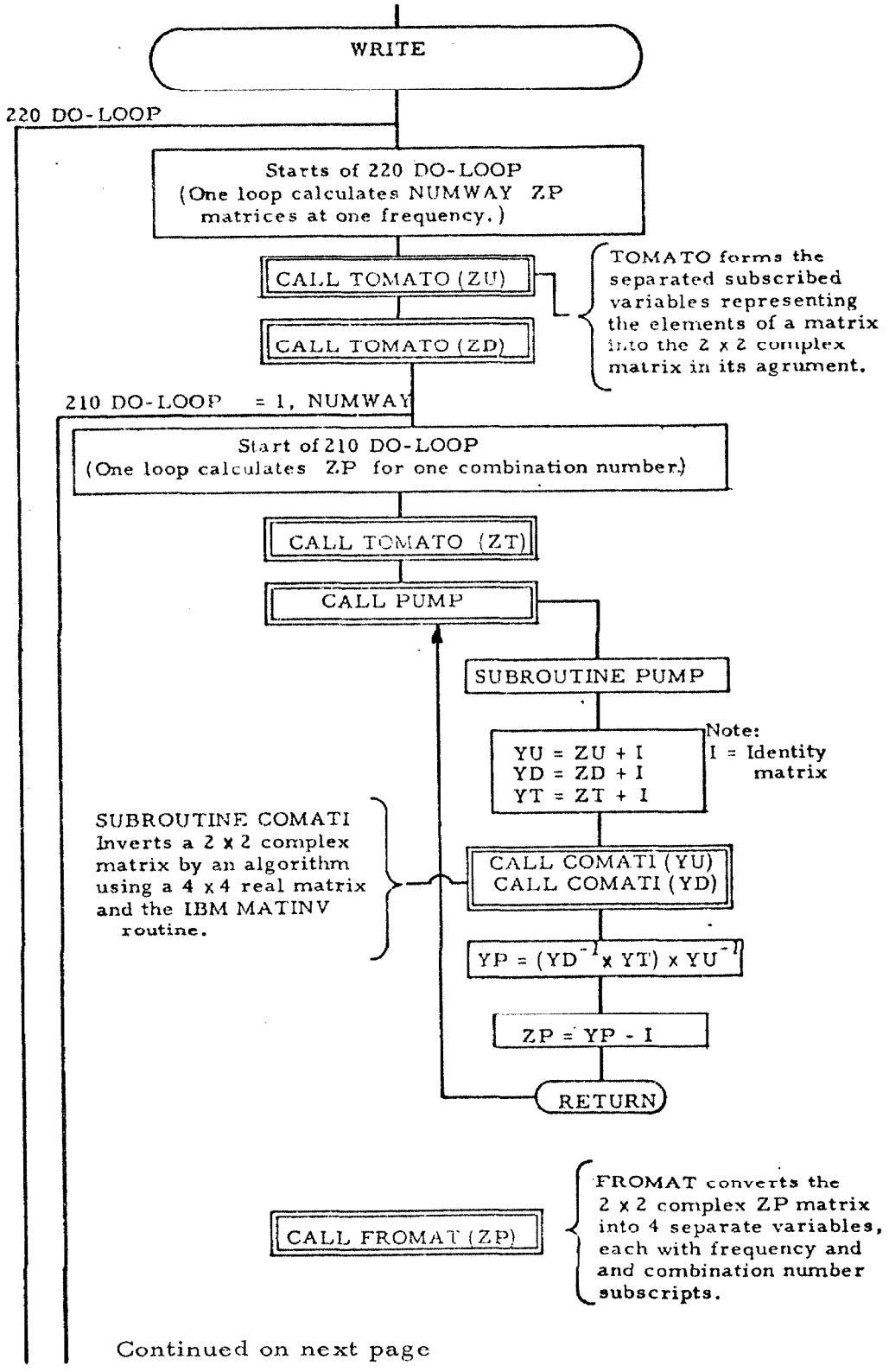

Continued on next page

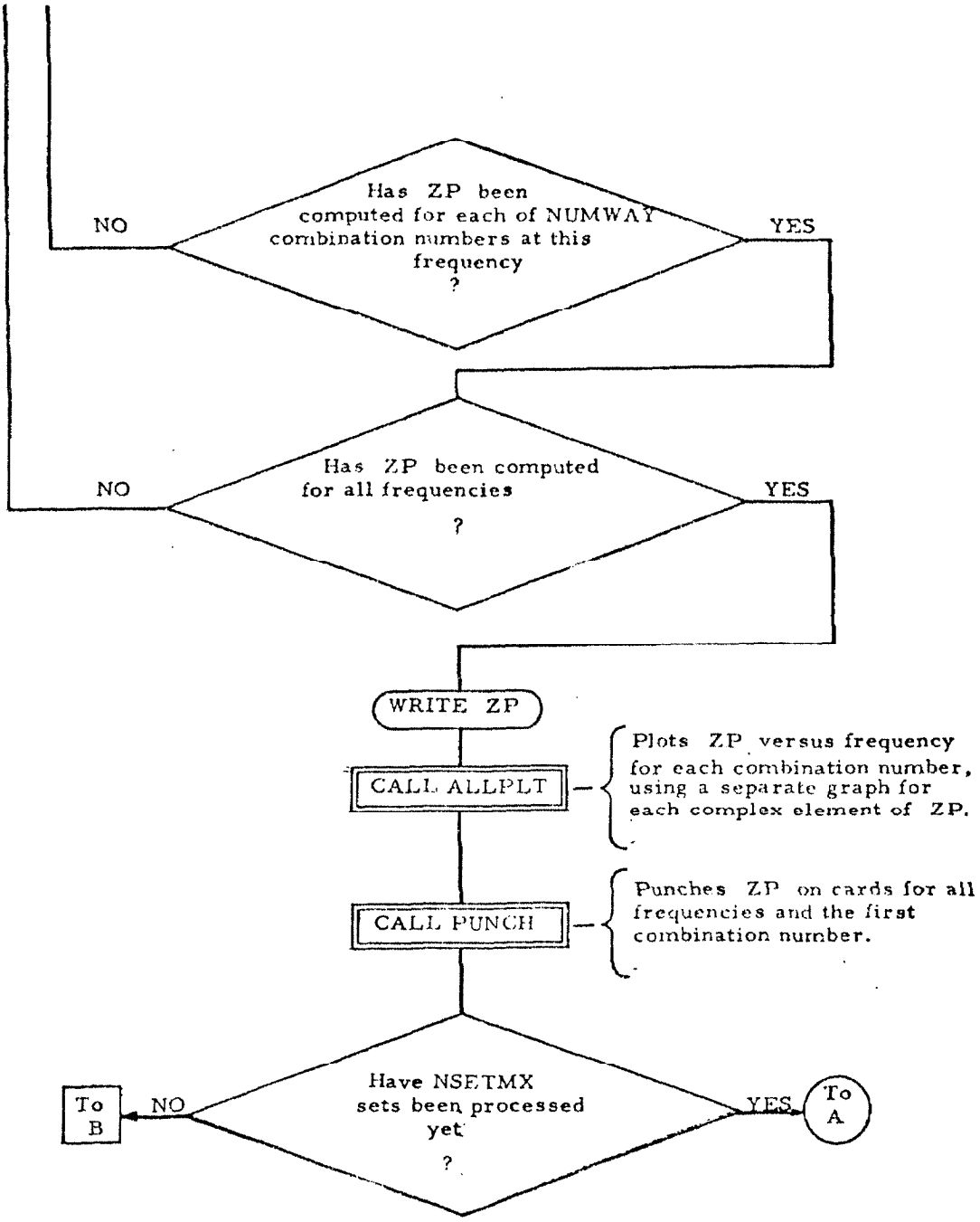
Has ZP been computed for each of NUMWAY combination numbers at this frequency ?
NO
YES
Has ZP been computed for all frequencies ?
NO
YES
WRITE ZP
CALL ALLPLT
Plots ZP versus frequency for each combination number, using a separate graph for each complex element of ZP.
CALL PUNCH
Punches ZP on cards for all frequencies and the first combination number.
Have NSETMX sets been processed yet ?
NO
To B
YES
To A

APPENDIX D

SPECIAL LEAST SQUARE FIT OF THE Z-MATRIX CALCULATION

The formula for the transfer matrix Z is

$$\begin{pmatrix} p_d - p_u \\ m_d - m_u \end{pmatrix} = \begin{pmatrix} Z_{11} & Z_{12} \\ Z_{21} & Z_{23} \end{pmatrix} \begin{pmatrix} p_u \\ m_u \end{pmatrix} \tag{1}$$

where all the elements are complex.

To solve for the Z elements for a given set of mean flow conditions, a minimum of two linearly independent sets of measurements, p_u, p_d, m_u and m_d are needed as mentioned in the introduction. However, in the present experiment more than two data sets were obtained and a least square fit procedure was needed to find the best fit Z-matrix. Denote these sets of experimental data by

$$p_u^i,\ p_d^i,\ m_u^i,\ m_d^i \qquad i = 1, 2 \ . \ . \ . \ I$$

where I is the total number of experimental sets. The procedure substituted these data into Eq. (1) and calculated the two residue values for each experimental set assuming the Z elements were known. Next, the summation of all the square of the amplitudes of the complex residues for each equation of Eq. (1) was calculated separately. The two unknown elements in each equation were varied independently by differentiating to minimize this residue summation. This resulted in two linear equations which were then solved to give the two unknown Z elements. This was repeated for the other equation to give the other two elements.

The results of this calculation are:

$$Z_{11} = \frac{S_5 S_2 - S_3 S_6}{S_1 S_5 - S_3 \overline{S}_3} - 1 \qquad \text{(D3)}$$

$$Z_{12} = \frac{S_1 S_6 - \overline{S}_3 S_2}{S_1 S_5 - S_3 \overline{S}_6} \qquad \text{(D4)}$$

where

$$S_1 = \sum_{i=1}^{I} p_u^i \overline{p_u^i} \qquad \text{(D5)} \qquad S_2 = \sum_{i=1}^{I} p_d^i \overline{p_u^i} \qquad \text{(D6)}$$

$$S_3 = \sum_{i=1}^{I} m_u^i \overline{m_u^i} \qquad \text{(D7)} \qquad S_4 = \sum_{i=1}^{I} m_d^i \overline{p_u^i} \qquad \text{(D8)}$$

$$S_5 = \sum_{i=1}^{I} m_u^i \overline{m_u^i} \qquad \text{(D9)} \qquad S_6 = \sum_{i=1}^{I} p_d^i \overline{m_u^i} \qquad \text{(D10)}$$

and

$$Z_{21} = \frac{S_4 S_5 - S_7 S_3}{S_1 S_5 - S_3 \overline{S}_3} \qquad \text{(D11)}$$

$$Z_{22} = \frac{S_1 S_7 - \overline{S}_3 S_4}{S_1 S_5 - S_3 \overline{S}_3} - 1 \qquad \text{(D12)}$$

where

$$S_7 = \sum_{i=1}^{I} m_d^i \overline{m_u^i} \quad . \qquad \text{(D13)}$$

These equations were used to least square fit the experimental data.